

BIOGEOCHEMICAL CHANGES OF CHEMICAL SIGNALS IN THE GEORGIA
“LAND-TO-OCEAN CONTINUUM”

by

Zhaohui (Aleck) Wang

(Under the Direction of Wei-Jun Cai)

ABSTRACT

Major portion of this dissertation concentrated on interpreting and analyzing temporal and spatial variability of the CO₂ system in the Georgia land-to-ocean continuum, which consists of Georgia marsh-influenced riverine and non-riverine estuaries and their adjacent continental shelf up to the shelf-break.

Chapter 2 described an improved fiber optic *p*CO₂ sensor based on a long pathlength liquid-core waveguide made by Teflon AF 2400. Three pronounced characteristics of the sensor are short response time, high sensitivity and long-time stability.

Chapter 3 discussed the spatial and temporal variability of distributions of nitrogen nutrients in the five Georgia riverine estuaries. Estuarine nitrification and marsh denitrification are likely two major processes that modify spatial distributions of inorganic nitrogen within these estuaries. Seasonality of river discharge and temperature are apparently responsible for observed seasonal changes in distribution patterns of inorganic nitrogen.

Chapter 4 examined CO₂ dynamics in the South Atlantic Bight (SAB). The study found that this shelf region is a strong atmospheric CO₂ source annually and an exporter of inorganic carbon to the open ocean. The carbon budget of the region indicated that the system is net heterotrophic annually. The annual CO₂ source of the system to the atmosphere is likely maintained as a combined result of net heterotrophy, more intensive heating, and high discharge of inorganic carbon from coastal salt marshes.

The research in Chapter 5 was centered on the seasonal variations of the CO₂ system in Georgia estuary-marsh complexes. CO₂ degassing and inorganic carbon export from a marsh-dominated tidal creek, the Duplin River, were quantified on a monthly basis in order to examine seasonality of marsh-estuary interaction. The study concluded that marsh export of inorganic carbon primarily supports CO₂ degassing and inorganic carbon export in the marsh-dominated estuaries. Extrapolation of the Duplin River's result to the entire SAB salt marshes indicated that marsh export of inorganic carbon likely has significant influence on the CO₂ dynamics in the SAB.

As a summary of carbon cycle in the Georgia “land-to-ocean continuum”, a carbon mass balance and transport model and an “extended continental shelf pump” hypothesis were presented in Chapter 6.

INDEX WORDS: *p*CO₂ Sensor, Fiber Optic, Spectrophotometric, Long Pathlength, Liquid-core Waveguide, Inorganic Nitrogen, Nutrients, Nitrogen Fluxes, Carbon Cycle, CO₂, Inorganic Carbon, Biogeochemistry, CO₂ Fluxes, Seasonal, Global Warming, Georgia Estuaries, Salt Marsh, South Atlantic Bight, Southeastern United States

BIOGEOCHEMICAL CHANGES OF CHEMICAL SIGNALS IN THE GEORGIA
“LAND-TO-OCEAN CONTINUUM”

by

Zhaohui (Aleck) Wang

B.S., Xiamen University, P. R. China, 1994

M.S., The University of New Hampshire, 1998

A Dissertation Submitted to the Graduate Faculty of The University of Georgia in Partial
Fulfillment of the Requirements for the Degree

DOCTOR OF PHILOSOPHY

ATHENS, GEORGIA

2003

© 2003

Zhaohui (Aleck) Wang

All Rights Reserved

BIOGEOCHEMICAL CHANGES OF CHEMICAL SIGNALS IN THE GEORGIA
“LAND-TO-OCEAN CONTINUUM”

by

ZHAOHUI (ALECK) WANG

Approved:

Major Professor: Wei-Jun Cai

Committee: William J. Wiebe
Merryl Alber
James T. Hollibaugh
Richard A. Jahnke

Electronic Version Approved:

Maureen Grasso
Dean of the Graduate School
The University of Georgia
May 2003

DEDICATION

This work is dedicated to my beautiful wife, Jing, who has been giving me her selfless support for my study and research all these years.

ACKNOWLEDGMENTS

First of all, I want to thank my major advisor, Dr. Wei-Jun Cai for pushing me all these years, but in the right direction. I want to thank my committee members, who have made many valuable suggestions to this work. Special thanks to Dr. Jahnke for kindly providing us ship-time for the across-shelf survey. It really initialized the study of Chapter 4.

Special thanks to Dr. Larry Pomeroy, who has given many critical suggestions to this work. Thank Dr. James R. Nelson for providing us ship-time.

Thank Julie Amft, Edward Sheppard, and Ken Helm for helping me take and process samples. Thank the crews of R/V Bluefin and R/V Savannah for providing supports for our sampling cruises.

Gratitude to all lab members, Dr. Yongchen Wang, Dr. Hongwei Ji, Guirong Han, Feizhou Chen, and Jian Wang. Special thanks to Dr. Wang, who has been a mentor and a great friend to me along the way.

TABLE OF CONTENTS

	Page
ACKNOWLEDGMENTS	v
CHAPTER	
1. INTRODUCTION	1
2. A LONG PATHLENGTH LIQUID-CORE WAVEGUIDE SENSOR FOR REAL-TIME $p\text{CO}_2$ MEASUREMENTS AT SEA.....	7
3. DISTRIBUTIONS AND FLUXES OF INORGANIC NITROGEN IN THE FIVE GEORGIA RIVER ESTUARIES OF THE SOUTHEASTERN UNITED STATES.....	33
4. INORGANIC CARBON DYNAMICS AND AIR-SEA CO_2 FLUX IN THE SOUTHEASTERN CONTINENTAL SHELF OF THE UNITED STATES	74
5. SEASONAL CHANGES OF THE CO_2 SYSTEM IN MARSH-INFLUENCED COASTAL WATER SYSTEMS OF THE SOUTHEASTERN UNITED STATES.....	117
6. SUMMARY.....	156
REFERENCES	163

CHAPTER 1

INTRODUCTION

Along the Georgia shoreline of the Atlantic Ocean in the southeastern United States, the river-estuary-marsh complexes, near-shore lagoons and sounds, and their adjacent continental shelf up to the 60-m isobath (shelf-break), form a natural “land-to-ocean continuum” (Pomeroy et al., 2000) where water and material experience a series of mixing, exchange, transformation, and transport across several frontal zones.

Except for the off-shore environment on the continental shelf, interaction and exchange between intertidal marshes and adjoining estuaries and between marsh-influenced estuaries and the coastal ocean have been major focuses for numerous ecological and biogeochemical studies of the area over four decades. The related research began as early as 1950's with emphasis of carbon flow inside the intertidal marsh based on observations from one or several closely related marsh-estuary sites (Ragotzkie and Pomeroy, 1957; Teal, 1962; Odum, 1968). Later, “outwelling” hypothesis (Odum, 1968; Odum, 1980) regarding whether the marsh systems serve as a net sink or source of carbon and nutrients to the coastal ocean was proposed and soon generated intensive debates in scientific community (see integrated studies in Nixon, 1980; Dame, 1994; Childers 1994; Childers et al., 2000).

During recent years, the pendulum has swung to more integrated and systematic studies for the Georgia coastal river-marsh-estuary ecosystems, such as Georgia River Land Margin Ecosystem Research (GARLMER) (1994 – 1999): a comparative study of

the transport and transformation of materials from rivers through the land-sea margin, which has generated large number of high-quality research articles, and pushed our understanding of marsh-estuary-coast interaction and exchange to a new level (see detailed references in the webpage <http://lmer.marsci.uga.edu>). On the other hand, the on-going Georgia Coastal Ecosystem – Long-Term Ecological Research (GCE-LTER) project, which began in 2000, emphasizes the effects of natural and anthropogenic variability of terrestrial, oceanic, and atmospheric inputs with different temporal and spatial scales on the ecosystem function at the Georgia land-ocean margin, and the effects of the resulting variation in material flows on processes in the Georgia coastal wetlands (GCE-LTER Proposal, Hollibaugh and Pennings, 1999).

Off the Georgia coast, the adjacent continental shelf, which locates in the central South Atlantic Bight (SAB) of the United States, has also been a research subject for intensive oceanic and ecological studies during the last 20 years or so. In the book entitled “Ocean Processes: U.S. Southeast Continental Shelf”, Menzel (1993) described in detail previous finding in hydrological, biological, and chemical processes for this continental shelf area in the eastern coast of the United States. Two cross-front ocean processes were particularly highlighted in this book: water mixing across the coastal frontal zone between near-shore water and off-shore water, and interaction and exchange between off-shore water and the Gulf Stream water across the shelf break. In the years thereafter, knowledge concerning oceanic processes for this area continued growing, especially in physical modeling (Chen et al., 1999; Atkinson et al., 1996; Kourafalou et al., 1996a and b), and water-column and sediment biological production/respiration (Pomeroy et al., 2000; Jahnke et al., 2000; Nelson et al., 1999; Verity et al., 1993). Most

recently, remote sensing technique was applied to study the movement of water fronts in the Georgia continental shelf (Li et al., 2002).

Major portion of this dissertation concentrated on interpreting and analyzing temporal and spatial variability of sea surface $p\text{CO}_2$ and dissolved inorganic carbon (i.e. the CO_2 system) in this Georgia land-to-ocean continuum defined earlier. Studies on the water-column CO_2 system in the coastal systems of Georgia has been rare, if any, in the past, but CO_2 emission from intertidal marsh has been documented (Giurgevich and Dunn, 1981 and 1982; Morris and Whiting, 1986). Recent CO_2 studies conducted by Cai and co-workers (Cai and Wang, 1998; Cai et al. 1998; Cai et al. 1999; Cai et al. 2000) in the Altamaha and Satilla River estuaries of Georgia demonstrated that the spatial and temporal variability of the CO_2 system in the estuarine water provided us insight knowledge for interpreting biological and chemical signals during the interaction and exchange of material between intertidal marshes and estuarine water.

Given the direct linkage between inorganic carbon system and biological activity, changes of CO_2 -system signals can serve as a net-process indicator for ecosystem metabolism, and thus can be used to trace the system-level carbon (energy) flow if direct measurement of CO_2 system is available (Smith and Hollibaugh, 1993 and 1997; Gattuso et al., 1998). On the other hand, studying CO_2 system in the coastal region has its own irreplaceable role in understanding global and local carbon cycles, and thus the climate change. Our progress made in this field is falling behind while compared to CO_2 study in the open ocean (Tsunogai et al., 1999; DeGrandpre et al., 2002; Frankignoulle and Borges, 2001; Boehme et al., 1998), and until now we still can not say with convincing evidence whether the coastal region around the global is a net source or sink to the

atmospheric CO₂. Quantification of the CO₂ budget in the global land-ocean margin is thus far from realistic. In the Georgia coastal systems, CO₂ study is just initialized, except in the several Georgia estuaries, knowledge concerning CO₂ system in the near-shore systems and on the continental shelf remained blank before this dissertation work.

This dissertation represents 4-year work and consists of four major chapters, each of which has been or will be soon submitted as peer-reviewed journal articles for publication. Each chapter is independent in format, but has inherent linkage in terms of subject focused and spatial coverage in this land-to-ocean continuum.

Chapter 2 described an improved spectrophometric fiber optic *p*CO₂ sensor based on a long pathlength waveguide made by Teflon AF 2400. The first version of this sensor, a bench system, developed two years ago and has been published as the first long pathlength fiber optic *p*CO₂ sensor (Wang et al., 2002a). The sensor presented herein is an improved version and has been successfully applied for monitoring sea surface *p*CO₂ along the Georgia coast (Wang et al., 2002b). Two most pronounced characteristics of the sensor are short response time (the time required to reach the sensor equilibrium) and high sensitivity due to inherent physical and optical features of Teflon AF material.

Chapter 3 discussed the spatial and temporal variability of distributions of nitrogen nutrients in the main channels of the five major Georgia river estuaries based on multiple-year data collected during the GALMER project. A simple estuarine mixing model or box model (Boyle et al., 1974; Liss, 1976; Li and Chan, 1979; Office, 1979; Kaul and Froelich, 1984) was constructed to quantify nitrogen fluxes for the investigated estuaries. Special effort was made to discuss how the river flow, intertidal marsh, and temperature have a net influence on seasonal variations of distributions and fluxes of

nitrogen species in the water column of the main estuarine channels. The chapter generally used a compare-and-contrast format (piedmont river estuaries vs. coastal plain river estuaries) during the course of the discussion in order to emphasize the difference in distributions caused by different biogeochemical scenarios.

The major goal of Chapter 4 was to investigate CO₂ dynamics in the South Atlantic Bight (SAB) using seasonal inorganic carbon data along a cross-shelf transect off Wassaw Sound, Georgia, up to the shelf break. In addition to data analysis and presentation, the discussion was focused on several aspects. First, CO₂ fluxes across the air-sea interface were calculated in order to evaluate the magnitude of CO₂ source/sink relative to the atmosphere in the SAB on an annual basis. Second, export rate of inorganic carbon from the SAB was evaluated based on a one-box steady-state model. Third, a carbon inventory in the SAB was presented in light of new information on inorganic carbon fluxes and water-column respiratory rates measured by a new inorganic carbon method; ecosystem metabolism of the SAB was then discussed. Last, the “continental shelf pump” hypothesis (Tsunogai et al., 1999), which addressed that why and how global continental shelf area is an important sink for atmospheric CO₂, was examined in the SAB.

In Chapter 5, the discussion focus was brought back to near-shore systems (estuaries, oceanic sounds, and marsh systems) of the GCE-LTER site. The research was centered on the seasonal variations of the surface water CO₂ system in this estuary-marsh complex (Altamaha Sound, Doboy Sound, Sapelo Sound, and the Duplin River), where a natural gradient of riverine influence from the Altamaha River is apparent. In addition to presenting results of inorganic carbon data collected from the seasonal GCE-LTER

surveys, estimates of TC export, surface-water CO₂ degassing, and apparent net heterotrophy (see Chapter 5 for definition) in the Duplin River, a marsh-dominated blind tidal river adjacent to Doboy Sound, were made in order to demonstrate intertidal marsh is an important inorganic carbon source, and thus supports apparent net heterotrophy of nearby estuarine and sound water. The study further extrapolated results from the Duplin River to the entire salt marsh system in the South Atlantic Bight, and argued that inorganic carbon export from coastal salt marsh systems make significant contribution to the inorganic carbon budget of the adjacent SAB. The “outwelling” concept (Odum, 1968) was then revisited in light of inorganic carbon export from Georgia intertidal marshes.

To synthesize findings in Chapter 4 and 5 in terms of carbon cycle in the “land-to-ocean continuum” of the southeastern United States, Chapter 6 presented a carbon mass balance and transport model and an “extended continental shelf pump” hypothesis. The carbon model used inorganic carbon fluxes to constrain net ecosystem heterotrophy of the SAB; it also has universal implication for studying ecosystem metabolism. Although “extended continental shelf pump” hypothesis may over-simplify some situations of carbon cycle at certain level, it does provide a conceptual model that generalizes how marsh export of carbon, both organic and inorganic, would play a critical role in shaping temporal and spatial variability of the CO₂ system and ecosystem metabolism in this “land-to-ocean continuum”.

CHAPTER 2

A LONG PATHLENGTH LIQUID-CORE WAVEGUIDE SENSOR FOR REAL-TIME

$p\text{CO}_2$ MEASUREMENTS AT SEA¹

¹ Wang, Z. A., Cai, W. J., Wang, Y. C., and Upchurch, B. L. Submitted to *Marine Chemistry*, 7/20/2002.

Introduction

Our current understanding of relative sources and sinks to atmospheric CO₂ in marine environments is mostly derived from a combination of field data and model analysis (Sarmiento and Sundquist, 1992; Feely et al., 1998; Sarmiento and Gruber, 2002). Validation of model analysis relies on field CO₂ data, which is presently limited by sparse spatial and temporal coverage. Consequently, the need for reliable and easy-to-use CO₂ measuring devices has prompted the development in recent years of a variety of techniques and methods for coastal and oceanic water applications.

"CO₂ gas equilibrators plus detector" (Wanninkhof and Thoning, 1993; Feely et al., 1998), and spectrophotometric measurement using fiber optic sensors (Goyet et al., 1992; DeGrandpre et al., 1993) are two methods for *p*CO₂ measurement in marine environments. The systematic configuration in "equilibrator plus detector" method consists of a gas-water equilibrators and a CO₂ gas analyzer. Showerhead sprinkler, bubbler-filled container, and thin-film equilibrators are three designs used in water-gas equilibrators (Körtzinger et al., 2000). A non-dispersive infrared gas analyzer (NDIR), such as Li-COR[®] Model 6252 or 6262, or gas chromatograph, is used to measure CO₂. Gas-phase samples after equilibrium with sample water are directed into the CO₂ analyzer for detection. Most underway observations of sea surface *p*CO₂ have been made using this method and can achieve a precision as high as 0.3 – 0.4 μatm *p*CO₂ (Feely et al., 1998). This technique needs a large quantity of water sample to reach the gas-water equilibrium state, which is itself a function of temperature. The whole system is often large and complex and not suitable for long-term mooring and unattended monitoring.

The spectrophotometric method has promising features, which include high sensitivity, good stability and selectivity, and simplicity. Over years, investigators have put much effort into developing spectrophotometric $p\text{CO}_2$ sensors to realize these promising features in oceanic $p\text{CO}_2$ monitoring. Currently, spectrophotometric $p\text{CO}_2$ sensors can achieve a precision around $1 \mu\text{atm CO}_2$ (DeGrandpre et al., 1995) and a response time as fast as about 2 minutes (99% of full response) (Wang et al., 2002) for oceanic application. These sensors are mostly compact in size, require low-power, and directly measure water-phase samples. They have been successfully deployed in mooring applications (DeGrandpre et al., 1995; Merlivat and Brault, 1995; Bates et al., 2000).

Spectrophotometric CO_2 measurement generally is based on the same theoretical principle as spectrophotometric pH measurement (Robert-Baldo et al., 1985; Byrne and Breland, 1989; Goyet et al., 1992). For spectrophotometric $p\text{CO}_2$ sensors, a sulfonephthalein indicator (pH sensitive) is enclosed inside a membrane cell, which functions as both a traditional cuvette of a spectrophotometer and a CO_2 equilibrator. $p\text{CO}_2$ changes in samples surrounding the cell are reflected in pH changes of the indicator inside the cell when CO_2 crosses the membrane and reaches equilibrium by diffusion. pH changes of the indicator are detected with optical fibers connected to a spectrophotometer. The membrane material of the cell is mostly made by PTFE or silicone rubber, which is permeable to CO_2 molecules but reduces input light quickly (DeGrandpre et al., 1999). The length of the membrane cell (optical path length) is therefore mostly less than 1 cm in order to increase the signal/noise (S/N) ratio of throughput light.

Wang et al. (2002) presented a long pathlength (10 to 20 cm) $p\text{CO}_2$ fiber optic sensor using a gas-permeable liquid-core waveguide made by a new copolymer of 2,2 bis

trifluoromethyl-4,5 difluoro-1,3 dioxole with tetrafluoroethylene (trademarked as Teflon AF 2400 by DuPont™). At about same time, Byrne et al. (2002) developed a similar Teflon AF sensor to measure total dissolved inorganic carbon (TC) in natural waters using a similar concept. Teflon AF is superior as a membrane material due to its low refractive index (RI) and high permeability to CO₂ molecules. Lower RI relative to indicator solution allows a significant increase in the optical path length of the sensor without sacrificing S/N ratio. High sensitivity (2 – 3 μatm in the *p*CO₂ range of 200 – 500 μatm) was achieved by using long capillary Teflon AF tubes as measuring cells (Wang et al., 2002). High permeability to CO₂ molecules results in a fast response time of 2 minutes (time to reach 99% of full response). The application using Teflon AF as liquid-core waveguides with long optical pathlength was first introduced by Waterbury et al. (1997) for measuring trace concentrations of Fe (II). Thereafter, similar applications have also been presented to measure chromium (VI) and molybdenum (VI) (Yao and Byrne 1999), pH (Kaltenbacher et al., 2000), and nitrite and nitrate (Zhang, 2000; Steimle et al, 2002) in natural waters.

We herein report an underway CO₂ system based on spectrophotometric measurement. The major portion of the system is an improved long pathlength Teflon AF *p*CO₂ fiber optic sensor which used a multi-wavelength technique to detect changes of light signal (Robert-Baldo et al., 1985; Byrne and Breland, 1989; DeGrandpre et al., 1995). Wang et al. (2002) chose relative absorbance at a single wavelength to be the optical detection signal for the *p*CO₂ sensor. A primary disadvantage of using single-wavelength absorbance was the short-time baseline drift that resulted in short-time stability and required frequent calibration. Multi-wavelength measurement used

absorbance at three wavelengths. Two wavelengths assessed the absorbance peaks of acid and base forms of the indicator, while a third wavelength (reference wavelength) measured changes of optical system. Signal changes in the acid and base absorbance peaks resulting from chemical sensing did not affect the third wavelength (Byrne and Breland, 1989; DeGrandpre et al., 1999). A calculated $p\text{CO}_2$ response was derived by using the absorbance ratios at three wavelengths. By this technique, the sensor's stability was significantly improved. Meanwhile, temperature dependence of the sensor response was "dampened" because of the similarity in the temperature dependence of indicator dissolution constant and seawater pH (Byrne and Breland, 1989).

Theory

Most sulfonephthalein indicators used in spectrophotometric $p\text{CO}_2$ sensors produce two-step dissociation in aqueous solution as shown below:



where K_{11} and K_{12} are the first and second dissociation constants of the indicator. Since mostly $pK_{12} - pK_{11} > 6$, these indicators can be treated as simple monoprotic acids (the second step dissociation, K_{12}) in theoretical consideration of the sensor's response for typical seawater $p\text{CO}_2$ measurement (200 – 1000 μatm). The indicator solution is prepared in a $\text{NaHCO}_3/\text{Na}_2\text{CO}_3$ buffer solution in order to obtain sensitive pH/ $p\text{CO}_2$ changes (Jensen and Rechnitz, 1979). After $p\text{CO}_2$ reaches equilibrium across the sensor's membrane, the sensor's optical signal, S_{CO_2} , is linked to pH of the indicator solution by the following equation (Robert-Baldo et al., 1985; Byrne and Breland, 1989; DeGrandpre et al., 1999):

$$S_{CO_2} = -\log\left(\frac{R - \epsilon_{2(HI)}/\epsilon_{1(HI)}}{\epsilon_{2(I)}/\epsilon_{1(HI)} - R \cdot \epsilon_{1(I)}/\epsilon_{1(HI)}}\right) = pK_{I2} - pH \quad (\text{Equation 2.2})$$

where subscripts “1” and “2” represent two wavelengths (λ_1 and λ_2) where acid and base absorbance peaks of the indicator occur; R is the absorbance ratio of the indicator at λ_1 and λ_2 ; $\epsilon_{1(HI)}$ and $\epsilon_{2(HI)}$ are the molar absorptivities of the HI form of the indicator at λ_1 and λ_2 , respectively; $\epsilon_{1(I)}$ and $\epsilon_{2(I)}$ are the molar absorptivities of the I²⁻ (fully unprotonated) at λ_1 and λ_2 , respectively.

For our actual pCO_2 measurements, the direct detection signals were light intensities at three selected wavelengths, and S_{CO_2} was calculated based on the middle part of Equation 2.2 using predetermined molar absorptivities (see later discussion). Calibration of the sensor was made by plotting S_{CO_2} against known pCO_2 values. Since S_{CO_2} is also linked to pK_{I2} and pH by Equation 2.2, theoretical calculation can predict S_{CO_2} from pK_{I2} and pH, and can be used to verify the sensor’s performance as a calibration procedure. pK_{I2} was determined for a given temperature from literature, while pH was related to pCO_2 by the following equation derived from carbonate equilibria of the indicator buffer solution (DeGrandpre, 1993; Wang et al., 2002):

$$[H^+]^3 + ([Na^+] - K_{I2}[I]_T/(K_{I2} + [H^+]))[H^+]^2 - (K_1K_h pCO_2 + K_w)[H^+] - 2K_1K_2K_h pCO_2 = 0 \quad (\text{Equation 2.3})$$

where $[H^+]$ is the hydrogen ion concentration, $[Na^+]$ is the total concentration of sodium ion introduced by Na_2CO_3 used for making indicator buffer solution (i.e. total alkalinity), $[I]_T$ is the total concentration of the indicator, K_w is the water dissociation constant, K_h is the Henry’s law constant ($pCO_2 = K_h [H_2CO_3^*]$, where $[H_2CO_3^*] = [CO_{2(aq)}] + [H_2CO_3]$), K_1 and K_2 are the carbonic acid dissociation constants. Equation 2.3 was solved for pH

($[H^+]$) at given pCO_2 , $[Na^+]$, $[A]_T$, and all constants in a Matlab® program. Theoretical S_{CO_2} is then obtained by subtracting pH from pK_{12} .

Methodology

Teflon AF Sensor and Optimization. The design of the sensor was similar to that by Wang et al., 2002 (Fig. 2.1A). The fiber optic-based spectrophotometer (SpectroPette™, World Precision Instruments, Sarasota, FL) measured the light intensities in the visible spectrum from 400 to 800 nm with a wavelength accuracy of ± 1 nm. Bromothymol blue (BTB) was selected as the indicator in this study (see later discussion). The intensities at three selected wavelengths, 434 (λ_1), 620 (λ_2) and 740 nm, were recorded after the BTB buffer solution and the sample (standard) reached CO_2 equilibrium across the Teflon AF capillary tubing (Fig. 2.1A). Absorbance, R, and S_{CO_2} were subsequently calculated using Equation 2.2. After each measurement cycle, the indicator buffer solution was renewed. To correct light for fluctuations and avoid frequent "blank" determination for absorbance between pCO_2 measurements, "blank constants" K_{λ} s for each of the three wavelengths were determined every a few days (DeGrandpre et al., 1999). The absorbance was calculated between blank measurements by using respective K_{λ} at individual wavelengths. The stray light, which could limit the sensitivity of the sensor, ranged from $\sim 0.25\%$ at 560 – 620 nm to $\sim 1\%$ near 430 nm for the spectrophotometer.

While PhR was used in our previous work (Wang et al., 2002), we changed the indicator to BTB in this study. Laboratory tests demonstrated that BTB exhibited higher sensitivity than did PhR for oceanic pCO_2 measurements (Fig. 2.2). Theoretical

calculation also confirmed such a difference. This is primarily a result of their different pK_{12} values. At 20°C, pK_{12} is ~ 7.3 and 8.0 for BTB and PhR, respectively. Because pK_{12} or color change of BTB [pH = 6.0 (yellow) ~ 7.6 (blue) at 20°C] tailors more closely to the pH change of our indicator buffer solution (total alkalinity 100 to 200 μM) for typical oceanic $p\text{CO}_2$ measurements (200 – 600 μatm), higher sensitivity for BTB is expected. DeGrandpre et al. (1993) also made a similar conclusion based on theoretical calculation of their sensor response for different indicator pK_{12} . Note that the indicator with higher pK_{12} should be used to achieve high sensitivity for lower-level $p\text{CO}_2$ (<200 μatm) measurement.

Given Equations 2.2 and 2.3, optical signal of the sensor is affected by the indicator concentration. Therefore, the buffer effect of the indicator dissociation as shown in Equation 2.1 needs to be considered while optimizing indicator concentration for $p\text{CO}_2$ measurements (Wang et al., 2002). The buffer effect is reflected by lowered sensitivity ($\Delta S_{\text{CO}_2}/\Delta p\text{CO}_2$) with increased indicator concentrations as shown in Fig. 2.3 (the slope of the curve increases with decrease of indicator concentration). For a given light source, significantly reducing indicator concentration to increase the sensor's sensitivity will result in saturation of the detector. Alternately, the optical path length can be increased while reducing the concentration of the indicator. Due to the optical properties of the Teflon AF, these two adjustments were made without suffering from low level of the throughput light. Currently, 5 μM BTB was used as the optimal concentration in our Teflon AF sensor with 21-cm optical pathlength for field applications. By theoretical calculation and laboratory tests, this concentration resulted in negligible buffer effect (Fig. 2.3), and the sensor maintained high sensitivity.

The sensitivity of the sensor varies with different total alkalinity (Na_2CO_3 concentrations) of the indicator solution (Fig. 2.4). Clearly, the indicator solution without Na_2CO_3 is less sensitive to $p\text{CO}_2$ changes than that with Na_2CO_3 (Fig. 2.4). The sensitivity of the sensor reaches a maximum near 0.1 mM Na_2CO_3 and then decreases (Fig. 2.4). Total Na_2CO_3 concentration determines the initial pH of the indicator solution. The most sensitive absorbance change in the pH range of the colorimetric reaction [BTB, pH = 6.0 (yellow) ~ 7.6 (blue) at 20 °C] should be tailored to the measurement range of $p\text{CO}_2$ (Wang et al., 2002). Meanwhile, the S/N ratios of light intensities (detection signals) at selected wavelengths must also be considered while optimizing Na_2CO_3 concentration. Higher Na_2CO_3 concentration with higher initial pH will result in darker color of indicator solution and lower the S/N ratio of throughput light. Based on above results, 0.05 mM Na_2CO_3 was selected for oceanic $p\text{CO}_2$ measurements (200 – 600 μatm). Under optimal conditions of the sensor, the noise levels at three selected wavelengths were better than 0.004 AU for the spectrophotometer used.

Chemicals and Molar Absorptivities. BTB was obtained from SIGMA Chemical Co. Ultrapure Na_2CO_3 (J. T. Baker) was dried for 8 hours in an 110°C oven and kept in a desiccator before use. Indicator buffer solutions were prepared with Milli-Q water and kept in sealed aluminum laminate bags (Pollution Measurement Corporation, Oak Park, IL).

To determine molar absorptivities of HI^- and I^{2-} of BTB at two desired wavelengths (λ_1 and λ_2) (Equation 2.2), two series of BTB solutions with various concentrations (5, 20, 60, 100 μM) were prepared. The pH of each series was adjusted to 4 or 9, such that the majority of the indicator in a solution existed as either HI^- or I^{2-} form.

The absorbance of each solution at 434 (λ_1) and 620 nm (λ_2) was measured with a spectrophotometer (Model UV160U, Shimadzu, Japan) using a 1 cm cuvette cell. Based on Beer's Law, molar absorptivities [$\epsilon_{1(HI)}$, $\epsilon_{2(HI)}$, $\epsilon_{1(I)}$ and $\epsilon_{2(I)}$] were calculated as the slope of the linear regression between absorbance and BTB concentration at 434 and 620 nm. The results ($M^{-1} \text{ cm}^{-1}$) were $\epsilon_{434(HI)} = 14223$, $\epsilon_{434(I)} = 3301$, $\epsilon_{620(HI)} = 39$, $\epsilon_{620(I)} = 29042$, which agreed with values reported by DeGrandpre et al. (1993).

To examine the effect of temperature change on molar absorptivities, the cuvette cell was thermostatically controlled, and molar absorptivities were subsequently determined at different temperature (5, 10, 15, 20, 25, 30°C). The experimental results indicated that molar absorptivities [$\epsilon_{1(HI)}$, $\epsilon_{2(HI)}$, $\epsilon_{1(I)}$ and $\epsilon_{2(I)}$] did not show apparent dependence on temperature, and their relative difference among different temperature was only 1 – 3%, which were close to the detection limit of the spectrophotometer. By experiments, pK_{12} for BTB only varies from 7.27 to 7.37 in the temperature range of 5 – 30°C (Baehr and DeGrandpre, 2002). Since the pH of BTB solutions was adjusted to 4 or 9 for determining molar absorptivities, color change of BTB in its acid or base form was insensitive to temperature change. Therefore, little temperature dependence of these molar absorptivities is expected.

Standards. CO₂ gas standards (0-2000 μatm) were mixed by two GFC17 mass flow controllers (Aalborg Instruments & Controls, Inc. Orangeburg, NY) using certified CO₂ and N₂ gasses (BOC Gasses). Mixed CO₂ gas standards were calibrated using a Li-Cor CO₂/H₂O analyzer (Model 6252) before use.

Water standards were prepared for field calibrations and for determining the sensor's temperature dependence. Preparing gas standards often involve large gas tanks

and power consuming equipments. Water standards, on the other hand, are much easier to be handled in the field. By using water standards, temperature of the system can be readily controlled to reduce uncertainty resulting from temperature discrepancy between indicator solution and standards. Moreover, water standards are necessary for future unattended in-situ mooring. Therefore, preparing and testing water standards is a necessary step toward broader applicability of the sensor.

Water standards ($p\text{CO}_2$ 300 – 2000 μatm) were prepared by adding Na_2CO_3 to borax-HCl buffer solutions with different pH values (Lide, 1994) in 2.5 liter glass bottles at room temperature ($\approx 23^\circ\text{C}$). The buffer solution was used to prevent short-term $p\text{CO}_2$ variation. The bottles were sealed for storage. By laboratory tests, there was no detectable $p\text{CO}_2$ change for a water standard during a 40-day period. To calibrate the water standards, the Teflon AF $p\text{CO}_2$ sensor was first calibrated using gas standards; the water standards were then measured with the sensor to determine $p\text{CO}_2$. We did not use known total CO_2 and pH to calculate $p\text{CO}_2$ of the water standards because thermodynamic calculation of the CO_2 system may be associated with a significant loss in precision as compared to $p\text{CO}_2$ measurements (Körtzinger et al., 2000). In our case, the difference between calculated and measured $p\text{CO}_2$ can be as large as 10 μatm in the $p\text{CO}_2$ range of 300 – 600 μatm , which is larger than the detection limit of the sensor.

The bottles of water standards were kept in a temperature-controlled water bath ($\pm 0.1^\circ\text{C}$) to allow temperature equilibrium before use. For each measurement, a water standard was re-circulated through the sensor using a peristaltic pump. There were no detectable temperature variations when the water standards were pumped through the sensor. The volume of the BTB solution entrapped in the Teflon AF tubing was less than

200 μ l. 3 – 5 minutes were sufficient for the BTB solution to reach temperature equilibrium with surrounding water standards.

Underway System. The underway system for measuring the sea surface $p\text{CO}_2$ with the long pathlength Teflon AF fiber optic sensor is shown in Fig. 2.1B. Seawater samples were pumped in from the bottom of the research vessel R/V Blue Fin using an on-board water pump. Water flowed through an Oceanographic Data Information System (ODIS), which measured real-time surface temperature and salinity. The inlet of the water was about 3 meters below the surface.

The Teflon AF sensor measured $p\text{CO}_2$ at a controlled temperature of 23 °C, and the results were corrected to the field temperature based on thermodynamic calculation of the CO_2 system. Water sample from the ODIS flowed through a thermostated water bath before being pumped into the sensor. Aluminum tubes were used in the water bath to maximize heat transfer in short period of time. All other connection tubes were made from PVC[®] or TYGON[®]. The water flow rate, 50-100 ml/min, was controlled by a peristaltic pump during the measurements, so that the water samples achieved the desired temperature (± 0.1 °C). The Teflon AF was fully calibrated under the controlled temperature in the laboratory before the survey. During the survey, calibration was conducted every 24 hours by using one or two water standards under the same temperature conditions to assure that no drift occurred.

The ODIS was also attached to a “shower head equilibrator plus infrared detector (Li-Cor Model Li-6252)” system to independently measure sea surface $p\text{CO}_2$ with field temperature. The details of the design and configuration of this system are similar to those presented in the literature (Feely et al., 1998; Bates et al., 1998; Körtzinger et al.,

2000). The Li-Cor system was calibrated using gas standards. Through laboratory verification, the precision of the Li-Cor system was estimated to be better than 1 μatm $p\text{CO}_2$.

Underway Survey. As a field test and part of a CO_2 study along Georgia's coast, the underway system was used in a research cruise to measure sea surface $p\text{CO}_2$ along a 60-km cross-shelf transect off Wassaw Sound, GA, on December 6 – 7, 2000 (Fig. 2.5). The out-bound survey was conducted on Dec. 6 2000 in a local flooding tide, and the in-bound measurement was made on Dec. 7 during an ebbing tide.

For temperature correction of the Teflon AF sensor, discrete surface water samples at selected stations (Fig. 2.5) during the underway survey were collected for TC measurements. These samples were taken in 125-ml acid-cleaned glass bottles, and 10- μl saturated HgCl_2 was added for preservation. Samples were stored at 7°C for after-cruise laboratory analysis within 3 days. TC was measured by acid release of CO_2 and subsequent quantification with a non-dispersive infrared CO_2 analyzer (Li-Cor 6252) with a precision of 0.1%.

Results and Discussion

Sensor's Performance. Although the direct detection signal of the sensor was changed from measuring a single-wavelength absorbance (Wang et al., 2002) to light intensities at three wavelengths in this study (absorbance ratios and S_{CO_2} were calculated from the intensities), there was no apparent change in the sensor's response time based on laboratory tests (data not shown). The sensor reached 99% of full equilibrium with water samples ($p\text{CO}_2$ 200 – 1000 μatm) within 2 minutes, which is still the fastest response

reported so far for an optical $p\text{CO}_2$ sensor. This is expected because changing the detection signal will not affect any equilibrating processes between indicator buffer solution and water samples.

Experimental response of the sensor was similar to theoretical prediction (Fig. 2.6). The precision of the sensor, which was calculated by using sensitivity ($\Delta S_{\text{CO}_2}/\Delta p\text{CO}_2$) in Fig. 2.6 and standard deviation of the replicate analysis, was $\pm 2 - 3$ μatm for the $p\text{CO}_2$ range of 200 to 500 μatm , ± 5 μatm in the range 500 to 800 μatm $p\text{CO}_2$, and ± 7 μatm for 800 to 1000 μatm . However, there was a small offset between experimental results and theoretical calculation (Fig. 2.6). This difference may result from the uncertainties in the BTB and CO_2 constants (K_w , K_1 , K_2 , K_h , K_{12} and molar absorptivities) that were either experimentally determined, obtained from literature, and/or other theoretically-unaccounted factors, such as stray light effect. Note that the sensor, in principle, does not need calibration for $p\text{CO}_2$ measurement if theoretical calculation matches experimental response perfectly.

The major improvement of the current design was an increase in stability due to a measurement based on multi-wavelengths. Calibration in the previous developments was conducted as often as twice a day to offset the baseline shift and variation of light source, that both contributed significant errors in absorbance measurement. By carefully protecting chemical reagents from contamination, long-term stability of the sensor was achieved as shown by the response curves in Fig. 2.6. Over a 40-day period (Oct. 19 – Nov. 28, 2000), the standard deviation of S_{CO_2} for a 500- μatm standard CO_2 gas was only 0.004 (equivalent to $\pm 5 - 7$ μatm), which was close to the detection limit of S_{CO_2} , 0.001 – 0.002 (derived from replicate analysis), for the current instrumentation. Note that a new

indicator solution was used on Nov. 29, 2000 (Fig. 2.6). However, the difference in experimental response curves between two indicator solutions was also small (Fig. 2.6). Significant improvement in the sensor's stability resulted from the usage of absorbance ratios at different wavelengths, which greatly reduced the influence from variation of light source and baseline drift. For example, measured light intensities varied between measurements for a given sample or standard, but the calculated absorbance ratios and S_{CO_2} showed little difference. Due to such an improvement, calibration frequency in the field application was greatly reduced.

Temperature Effect. The sensor's response is affected by operational temperature, since equilibrium constants are all temperature-dependent. Equations 2.2 and 2.3, combined the temperature-dependent functions of equilibrium constants obtained from literature, were used to derive the theoretical temperature response of the sensor (Fig. 2.7A). Experimental results of the sensor's temperature dependence were consistent with the theoretical prediction in terms of the general pattern (Fig. 2.7B). For a given pCO_2 , the sensor's response (S_{CO_2}) decreased with an increase in temperature, and higher pCO_2 was more sensitive to changes in temperature. Meanwhile, the sensor behaved more closely to the theoretical calculation in the temperature range of 20 – 30°C than did in 5 – 15°C range (Figs. 2.7A and B).

The experimental curves were apparently more sensitive to temperature changes (Figs. 2.7A and B). The possible causes to the deviation from the theoretical results are likely related to the uncertainties in BTB and CO_2 constants and to the temperature effects on the physical and optical properties of the sensor's materials, which had not been included in the theoretical calculation.

Temperature discrepancy between the calibration of the CO₂ sensors and field measurements greatly affects the data quality because original detection signals rely on the calibration curves, which are temperature sensitive. There are two ways to overcome such temperature discrepancy in the *p*CO₂ measurement. Ideally, temperature-dependent function of calibration curves is derived from rigorous laboratory experiments, such that the detection signals at in-situ temperature can be directly converted to in-situ *p*CO₂ results. This derived function may be sensor specific, such that even two similar sensors could have slightly different temperature-dependent functions. Development of such functions requires many resources and is time-consuming. Alternatively, thermostatic devices can be applied to both calibration standards and field samples to overcome the temperature difference. The results from this practice reflect *p*CO₂ at a constant temperature, and can be adjusted to field temperature through equilibrium calculations of the CO₂ systems if other CO₂ parameters (e.g. pH, TC, total alkalinity) are available. This method will need temperature dependence functions of equilibrium constants of CO₂ systems, which could introduce calculation errors to final *p*CO₂ results. On the other hand, controlling standard and sample temperature in the underway monitoring, such as in this work, is relatively easy to achieve. In field measurements where thermostatic devices are hardly applicable, such as in-situ mooring, temperature dependence of calibration curves of the sensor must be pre-determined.

Data Comparison. Final results of the Teflon AF sensor during the underway monitoring were corrected from measured temperature to field temperature by equilibrium calculation of the carbonate system (Skirrow, 1975) using carbonate constants (K_1 and K_2 , Mehrbach et al., 1973 re-fitted by Dickson and Millero, 1987; K_h ,

Weiss, 1974) and TC data. Since TC was sampled discretely, interpolation between the TC data points using polynomial regression on salinity-TC relationship ($R^2 > 0.98$) was applied whenever temperature correction was needed. For the Li-Cor $p\text{CO}_2$ measurement, the temperature of the seawater was not controlled and the results reflected the $p\text{CO}_2$ with field temperature; its $p\text{CO}_2$ data was corrected to 100% water saturated values. The final results from both the Teflon AF sensor and the Li-Cor analyzer represented $p\text{CO}_2$ with 100% water saturation at field temperature under 1 atmospheric pressure (Fig. 2.8).

Two independent data sets of surface water $p\text{CO}_2$ during the two-day survey (Figs. 2.8A and B) agreed well with a linear correlation coefficient R^2 of 0.9649 ($n = 95$). The average relative difference between two data sets was only 1.2%. The test statistics of paired-data mean was not significant different from 0 ($p > 0.666$). Part of the differences was attributed to temperature correction of Teflon AF sensor's results, which was based on the thermodynamic calculation of the carbonate system. The residual plot (difference between two measurements) (Fig. 2.8C) did not show that the results from the Teflon AF sensor had apparent bias relative to those from the Li-Cor system.

Suitability of the Teflon AF Sensor. The described $p\text{CO}_2$ system based on the Teflon AF sensor provides a good alternative method for underway monitoring of sea surface $p\text{CO}_2$. Compared to traditional “shower head equilibrator plus infrared detector” system, this system is much more compact, less power consuming, and has a comparable precision in $p\text{CO}_2$ measurements. Because the Teflon AF sensor directly measures water-phase samples, the gas-water equilibrator, and thus temperature correction for gas-water equilibration (Feely et al., 1998), is eliminated. With proper engineering, the presented

system can be fully automatic. High resolution of underway measurement can also be achieved due to fast response of the sensor.

Spectrophotometric fiber optic $p\text{CO}_2$ sensors have been successfully applied in atmospheric measurements (Wang et al., 2002), in-situ mooring (DeGrandpre et al., 1999; Hood et al., 1999), and underway mapping (this study). Broad applicability, high sensitivity, and simplicity of this type of sensor are promising in field applications. Specifically, the Teflon AF sensor, in addition to other applications, had been proposed to be able to measure all primary variables (pH, TC, total alkalinity, and $p\text{CO}_2$ or $f\text{CO}_2$) of the CO_2 system (Byrne et al., 2002).

A potential advantage of the Teflon AF $p\text{CO}_2$ sensor is its suitability for CO_2 study on fine spatial and temporal scales, such as CO_2 variation in the upper a few to tens of centimeters of the ocean and even in the sea surface microlayer, because only a few milliliters of sample water is needed for actual CO_2 measurement. The current air-sea CO_2 flux estimation assumes homogeneity of bulk $p\text{CO}_2$ above and below the sea surface microlayer (i.e. the stagnant film) up to several meters, where water is pumped in for underway $p\text{CO}_2$ measurements. There has been no solid evidence to support this assumption either from laboratory or field measurements. However, the vertical temperature gradient in the upper several meters of the ocean and thermal skin effect can have a profound influence on the distribution of $p\text{CO}_2$ (Schluessel et al., 1990; Robertson and Watson, 1992; Bates et al., 1998), which greatly challenges the validation of the above assumption and current CO_2 flux estimation across the air-sea interface. The Teflon AF $p\text{CO}_2$ sensor provides a possible means to prove or disprove this assumption.

Figures

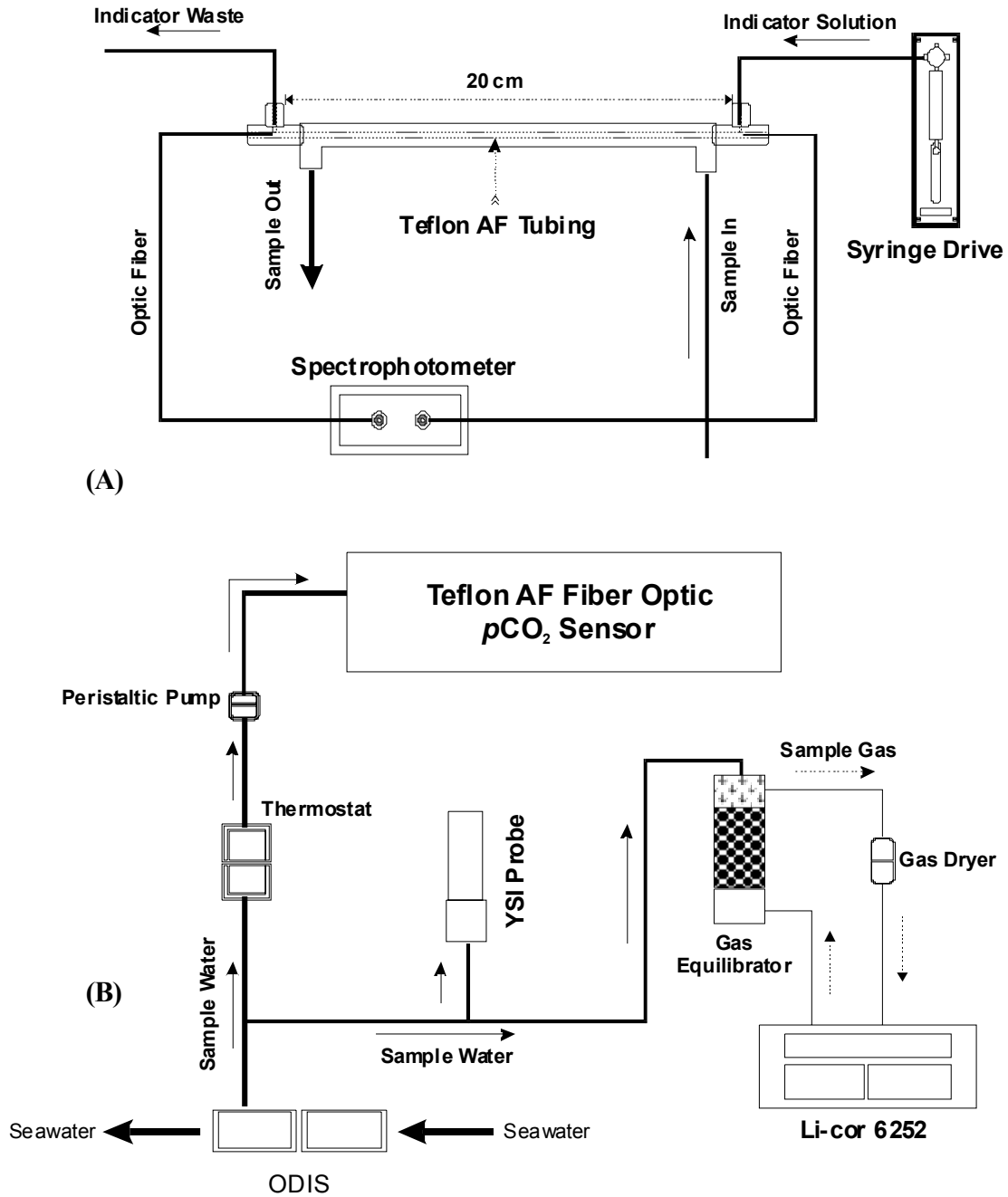


Fig. 2.1. Schematic diagrams of the Teflon AF fiber optic $p\text{CO}_2$ sensor (A) and the on-board underway $p\text{CO}_2$ system (B). The drawing is not proportionate.

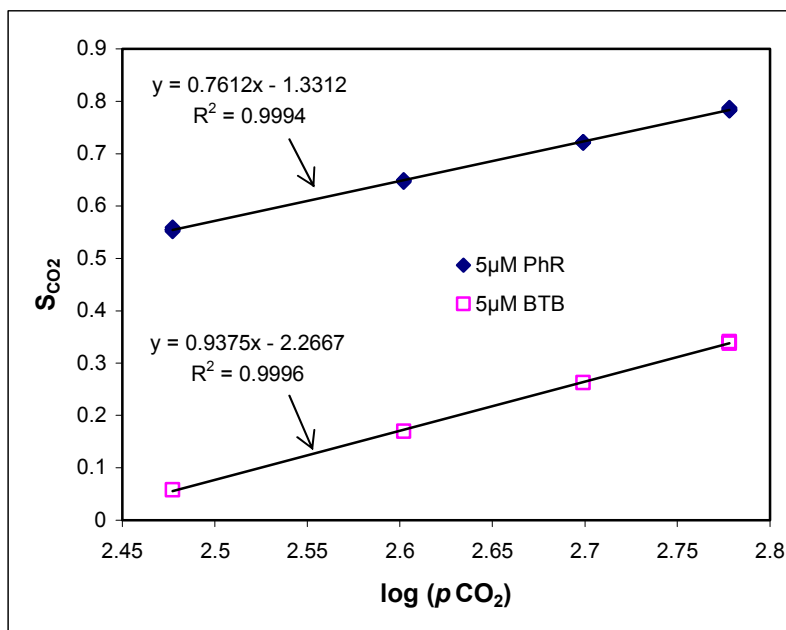


Fig. 2.2. Comparison of experimental responses between PhR and BTB for the Teflon AF 2400 $p\text{CO}_2$ sensor. $p\text{CO}_2$ is in logarithm scale to highlight the slopes of the response curves. For PhR, three selected wavelengths used to calculate absorbance and S_{CO_2} were 431 (λ_1), 558(λ_2), and 730 nm. The PhR molar absorptivities at the selected wavelengths: $\epsilon_{431(\text{HI})} = 19200$, $\epsilon_{431(\text{I})} = 2000$, $\epsilon_{558(\text{HI})} = 200$; $\epsilon_{558(\text{I})} = 56400$. Temperature = 23°C; $[\text{Na}_2\text{CO}_3] = 0.1$ mM; optical pathlength of the sensor was 21 cm. Solid lines are linear best-fits of the data points. Note that larger linear slope for BTB than for PhR indicates higher sensitivity ($\Delta S_{\text{CO}_2}/\Delta p\text{CO}_2$).

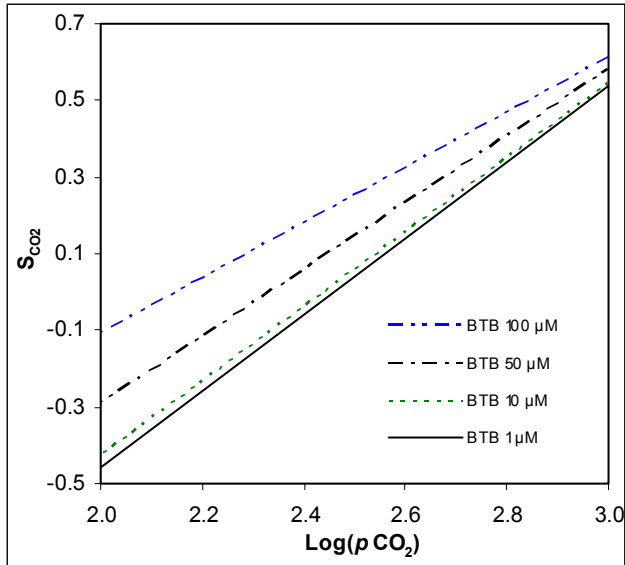


Fig. 2.3. Theoretical responses of the Teflon AF fiber optic CO_2 sensor under different indicator (BTB) concentrations. $p\text{CO}_2$ is in logarithm scale to highlight the slopes of the response curves. The calculation was based on Equations 2.2 and 2.3 with $[\text{Na}_2\text{CO}_3] = 0.05 \text{ mM}$ at temperature of $20 \text{ }^\circ\text{C}$. The constants (K_{12} , K_w , K_1 , K_2 , and K_h) were chosen as following: K_{12} was calculated using the temperature function by Baehr and DeGrandpre (2002); K_w was calculated using the temperature function proposed by Harned and Owen (1958); K_1 and K_2 were calculated using the method by Mook and Koene (1975) and Edmond and Gieskes (1970), respectively; K_h was derived from Weiss (1974).

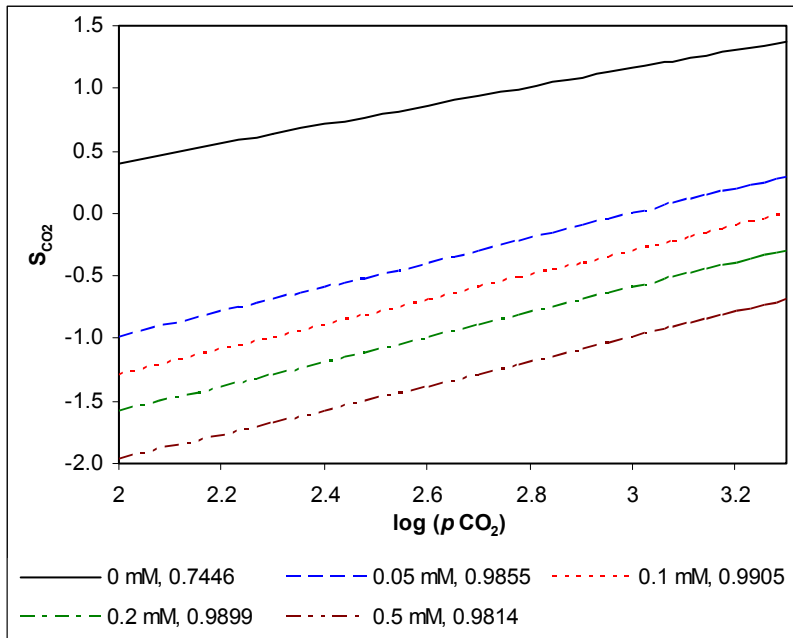


Fig. 2.4. Theoretical responses of the Teflon AF fiber optic CO₂ sensor under different Na₂CO₃ concentrations. $p\text{CO}_2$ is in logarithm scale to highlight the slopes of the response curves. The calculation was based on Equations 2.2 and 2.3 with [BTB] = 5 μM at temperature of 20 °C. The constants were chosen as in Fig. 2.3. The first and second numbers of each legend in the plot denote the concentration of Na₂CO₃ and the slope of linear line, respectively.

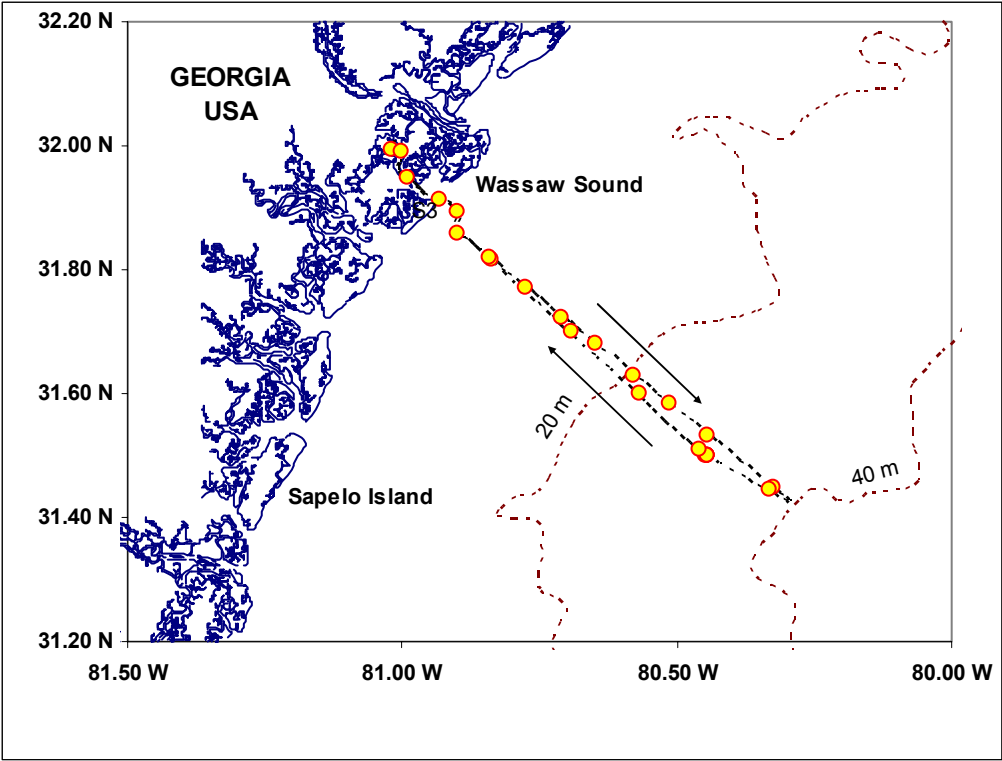


Fig. 2.5. The study area and underway track (dashed line) off Wassaw Sound of Georgia. The arrows indicate the directions of out- and in-bound surveys. Filled circles are discrete sampling stations.

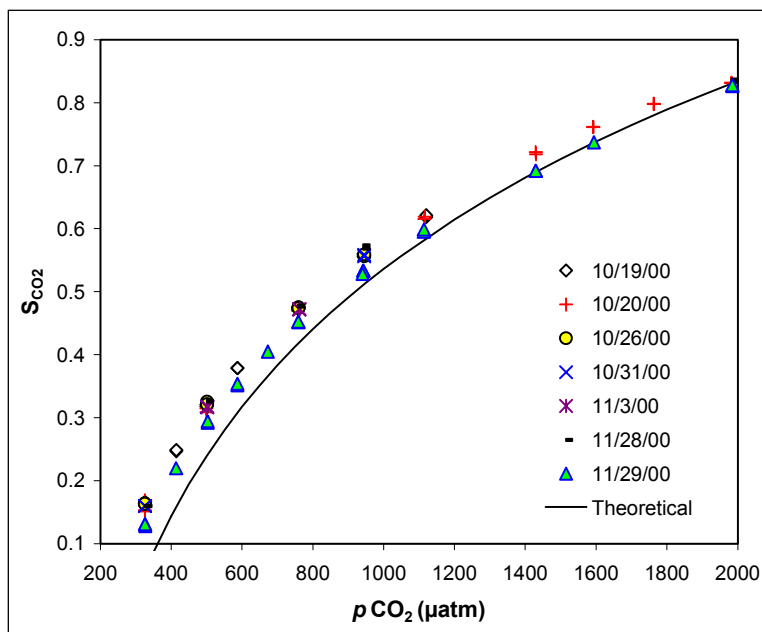


Fig. 2.6. Experimental and theoretical response curves of Teflon AF optic CO_2 sensor. Long-term stability of the sensor's calibration curves are also given here. The temperature was set to be 23°C for both experiment and theoretical calculation. $[\text{BTB}] = 5\ \mu\text{M}$; $[\text{Na}_2\text{CO}_3] = 0.05\ \text{mM}$; optical pathlength of the sensor was 21 cm. K_{a2} , K_w , K_1 , K_2 , and K_h were chosen as in Fig. 2.3. A same indicator buffer solution was used between Oct. 19 and Nov. 28, 2000 for determining experimental response curves. On Nov. 29, 2000, the indicator buffer solution was re-made.

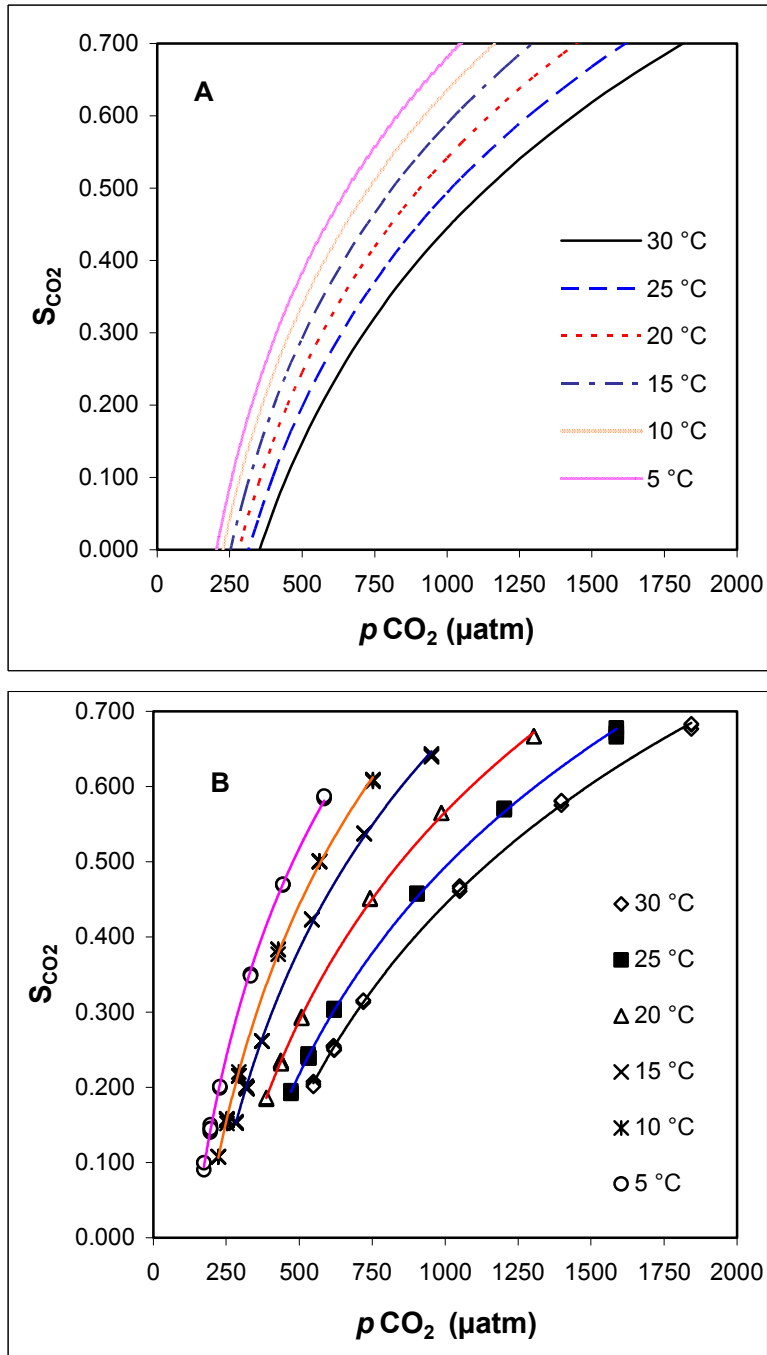


Fig. 2.7. Theoretical (A) and experimental (B) responses of the sensor on temperature variations. All constants were chosen as in Fig. 2.3. The experimental conditions were the same as in Fig. 2.6.

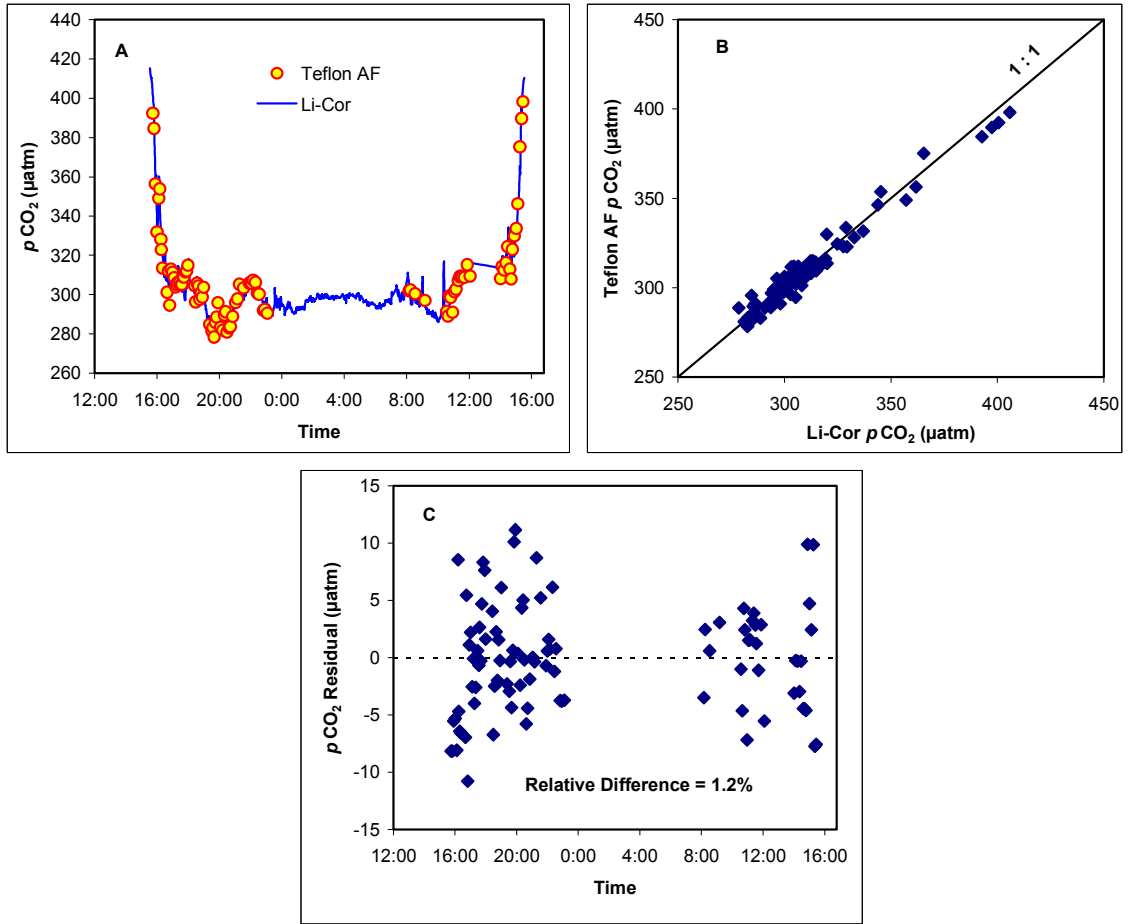


Fig. 2.8. Comparison of sea surface $p\text{CO}_2$ measurements between the “shower-head plus Li-Cor 6262 $\text{CO}_2/\text{H}_2\text{O}$ analyzer” underway system (Li-Cor) and the Teflon AF sensor based underway system (Teflon AF) along a transect off Wassaw Sound, GA. The Teflon sensor conditions were same as in Fig. 2.6. (A) Time series of $p\text{CO}_2$; (B) Teflon AF $p\text{CO}_2$ vs. Li-Cor $p\text{CO}_2$; (C) Time series of residual.

CHAPTER 3

DISTRIBUTIONS AND FLUXES OF INORGANIC NITROGEN IN THE FIVE GEORGIA RIVER ESTUARIES OF THE SOUTHEASTERN UNITED STATES¹

¹ Wang, Z. A., Wiebe, W. J., Cai, W. J., Alber, M. and Sheldon, J. E. To be submitted to *Limnology and Oceanography*.

Introduction

The five major riverine estuaries (Savannah, Ogeechee, Altamaha, Satilla, and St. Marys) along the Atlantic coast of Georgia, USA are characterized by extensive intertidal marshes protected by barrier islands. Studies on biogeochemistry and fluxes of organic and inorganic nutrients in these systems and their adjacent marshes began in the 1950's (Teal, 1962; Odum, 1968) with emphasis on carbon flow between the systems and to the coastal ocean. More complete studies on nutrient distribution and fluxes in these estuaries were reported later (Pomeroy et al., 1972; Beck et al., 1974; Windom et al., 1975; Pomeroy and Wiegert, 1983; Wiebe et al., 1983; Cai et al., 2000). These studies focused either on the interaction of nutrients between the intertidal marshes and the coastal ocean or nutrient biogeochemistry within the intertidal marshes. Studies on long-term and general biogeochemical behaviors of nutrients in the main water channels of these five estuaries have been rare.

Over the years, a major scientific debate, the “outwelling” hypothesis, arose as to whether these marsh-dominated estuaries serve as net sources of carbon and nutrients to the coastal water (Odum, 1968; Pomeroy et al., 1972; Nixon, 1980; Wiegert et al., 1981; Imberger et al., 1983; Chalmers et al., 1985; Hopkinson, 1985; Dame et al., 1986; Hopkinson et al., 1989; Childers et al., 1993). Gradually, tidal ranges, geological ages of a marsh, climatology and morphology of a system, and exogenous environmental forcing have been identified as important factors controlling flux behavior of marsh-dominated systems (Childers, 1994; Dame, 1994; Childers et al., 2000). Therefore, the import/export scenario of different systems is often complex in nature so that the “outwelling”

hypothesis may be viewed as a conceptual stimulus of ideas rather than a strict testable hypothesis (Childers et al., 2000).

For Georgia marsh-estuarine systems, many recent investigators (Griffith and Pomeroy 1995; Cai et al. 1999; Cai et al., 2000; Pomeroy et al. 2000; also see Chapter 5) have concentrated on the subjects of community respiration, system metabolism, inorganic nutrient and carbon fluxes, and CO₂/O₂ biogeochemistry that directly or indirectly link to the outwelling hypothesis in terms of direction and magnitude of the carbon flow between intertidal marshes and their adjacent water systems. The recent argument of nutrient biogeochemistry in these systems is that the Georgia intertidal marshes may serve as a sink of NO₃⁻ and a source of dissolved inorganic carbon (DIC) to adjacent estuaries (Cai et al., 2000).

In 1994, the Georgia Rivers Land-Margin Ecosystem Research (GARLMER) program was launched with the specific focus to investigate the transport and transformation of organic and inorganic materials carried from land to sea by the five major Georgia rivers along the Atlantic coast. Over 6 years of research surveys, GARLMER accumulated a comprehensive data set on various parameters of biogeochemical interest (inorganic nutrients, chlorophyll, respiration, carbon, oxygen, particles, etc.). Part of the GARLMER biogeochemical data set has been reported separately during recent years (e.g. Chen et al., 1997 on phytoplankton; Gonzalez and Moran, 1997 on bacteria; Gao and Zepp, 1998 on dissolved organic carbon; Wiegert et al., 1999 on program review; Blanton et al., 1999 on inorganic particles; Alber and Sheldon, 1999 on river discharge and flushing time; Moran et al., 1999 on biodegradation of dissolved organic matter; Pomeroy et al., 2000 on community respiration).

In this paper, we present the complete inorganic nitrogen data (NO_3^- , NO_2^- and NH_4^+) collected from the GARLMER program. Our emphasis is to compare and contrast the temporal and spatial distributions of inorganic nitrogen between different types of estuaries, and to investigate the primary factors that control their distributions. Estuarine addition/removal and export fluxes of inorganic nitrogen were evaluated by using an estuarine mixing model. To investigate the effect of river flow on the distribution patterns, estuarine addition/removal, and output of inorganic nitrogen, the river discharge and freshwater flushing time were also calculated based on the method proposed by Alber and Sheldon (1999).

Site and Method

Sampling Sites. The five major Georgia Atlantic coast rivers (Fig. 3.1) are almost evenly distributed along a 190-km segment of the Georgia coast, USA. These rivers flow through intertidal freshwater and salt marshes protected on the ocean side by a series of barrier islands. The water and material exchanges between the estuaries and salt marshes are largely tide-driven through tributaries and tidal creeks (Wiegert et al. 1999). Previous studies (Childers et. al., 1993; Childers, 1994; Cai et al., 1999; Pomeroy et al., 2000) have shown that Georgia salt marshes share a common sediment type, biological community, respiratory rate, primary productivity rate, and seasonality, although the rivers themselves differ in origin. Anthropogenic influence is relatively insignificant for all rivers and their estuaries, except for the Savannah River, the drainage area of which encompasses a heavily populated and developed region.

The five rivers can be classified into three categories based on their terrestrial sources. The Altamaha and Savannah rivers originating in the piedmont region are piedmont rivers. The Satilla and St. Marys rivers are coastal plain rivers, and their drainage areas are limited to the coastal plain province. Due to the mixed influence from both the piedmont and coastal plain, the Ogeechee River is a mixed type. The carbonate content and pH are relatively high in the piedmont rivers, while the water transported by the coastal plain rivers is rich in humic acid and has low concentrations of DIC and low pH (Beck et al., 1974; Cai and Wang, 1998; Cai et al., 1998). Although river discharges vary greatly on both seasonal and interannual bases for each of the five rivers, the mean values during the study period were much lower for the two coastal plain rivers (Satilla $34 \text{ m}^3 \text{ s}^{-1}$ and St. Marys $15 \text{ m}^3 \text{ s}^{-1}$) and the Ogeechee River ($61 \text{ m}^3 \text{ s}^{-1}$), than for the piedmont rivers (Savannah $272 \text{ m}^3 \text{ s}^{-1}$ and Altamaha $250 \text{ m}^3 \text{ s}^{-1}$). The high flow rate in the piedmont rivers results in shorter estuarine flushing times of ca. 5 days, compared to the coastal plain (Satilla 67 days and St. Marys 72 days) and mixed-type (Ogeechee 16 days) riverine estuaries. For all rivers, winter and spring are generally high flow seasons, and summer and fall are low flow seasons.

Sampling and Analysis. During the period from April, 1995 to February, 1999, inorganic nitrogen samples (NO_3^- , NO_2^- , NH_4^+) were collected along the main channels of the five Georgia riverine estuaries. The research surveys during the study period are summarized in Table 3.1. The sampling stations for each estuary generally started at the river mouth (some started at 1 – 4 km off the river mouth) and were located every 4 km upstream along the main channel until the salinity reached freshwater. To investigate the effect of the semi-diurnal tidal cycle on the inorganic nitrogen distributions, water

samples were taken every half hour during a 12-hour period at anchor stations on the Satilla River (SL+16 and SL+25.3, where the numbers represent km from the river mouth) and Altamaha River (AL+6.5) during selected surveys (Table 3.1). Except for the anchor stations, water samples were mostly collected during low waters. Due to the non-stratified nature of the water column, only surface water (< 1.5 m from the surface) was collected.

To investigate the effect of intertidal marshes on the distributions of inorganic nitrogen in the main water channels, inorganic nitrogen samples were also collected in June and July, 1996 from White Oak Creek, the largest marsh-dominated tidal creek in the Satilla River estuary (Fig 3.1). The sampling stations started at the creek mouth and continued upstream every 3 – 5 km until 15.7 km. The complete data set from White Oak Creek will be reported elsewhere, as we will use only a small part for discussion.

Water was collected using Niskin bottles, peristaltic pump, impeller pump or directly by opening bottles below the water surface, and stored in acid-washed polyethylene bottles. Samples were vacuum-filtered using either a diaphragm-type electric air pump or a hand pump and polysulfone 47 mm filter towers. At least 125 mL sample water was filtered through an ashed (450 °C for 2 hours) GF/F 47 mm filter and distributed into 50-ml polyethylene bottles. All sample bottles were kept frozen until lab analysis.

The Koroleff method (1983) with modification for colored samples was used for the $\text{NH}_4^+/\text{NH}_3$ analysis: citrate was eliminated, allowing a precipitate (mostly magnesium hydroxide) to form in order to absorb humic substances in the water samples. Freshwater samples (< 5 psu) required an additional hydroxide reagent to form the precipitate. NO_2^-

was analyzed using a Technicon Autoanalyzer (Technicon method No. 158-71W/B), and the results were corrected for the color effect of humic substances. NO_3^- was first reduced to NO_2^- by the spongy cadmium method (Jones, 1984) that involves shaking the buffered sample with small nuggets of spongy cadmium. This procedure used twice the amount of cadmium as suggested by Jones (1984) in order to keep acceptable reduction efficiency in the presence of humic material. The resultant NO_2^- , the total from NO_3^- reduction plus the NO_2^- originally present, was then determined using the NO_2^- analysis method. NO_3^- concentration was calculated by subtraction of the natural NO_2^- .

Estuarine Mixing Model and Flux Estimation. In order to evaluate estuarine production (addition), removal and output of inorganic nitrogen, a continuous estuarine mixing model was constructed. The model used the concepts and assumptions discussed in standard estuarine mixing models (Boyle et al., 1974; Liss, 1976; Li and Chan, 1979; Officer, 1979; Kaul and Froelich, 1984). The basic assumptions were that a dissolved constituent is continuous and maintains a steady state along the salinity gradient of an estuary. The key concept of this model is to use the effective concentration of a constituent (C^*), which represents the concentration at a given salinity that is corrected for the dilution effect or mixing:

$$C^* = C - S \frac{dC}{dS} \quad (\text{Equation 3.1})$$

where C is the concentration of a constituent at salinity S along the estuary. In our version of the mixing model, we divided the salinity gradient into 10 equal salinity intervals (segments). The reason to have only 10 segments was that it maintains useful detailed information on C^* and yet makes the calculation relatively simple. Then infinite derivative dC/dS in Equation 3.1 was replaced by the finite term $\Delta C/\Delta S$, where ΔC and

ΔS were the concentration and salinity change (relative to the previous segment) between two consecutive segments, respectively. S and C in Equation 3.1 were replaced by the average segment salinity S_{seg} , and segment concentration C_{seg} , and C^* were approximated as:

$$C^* \cong C_{\text{seg}} - S_{\text{seg}} \frac{\Delta C}{\Delta S} \quad (\text{Equation 3.2})$$

To calculate C^* of inorganic nitrogen, a concentration – salinity function $C(S)$ was first obtained by regressing the $C - S$ plot with real data. The resulting functions were 2, 3, 4 or 5-degree polynomials that had no physical meaning but were statistically well-fitted (see later discussion). C_{seg} , S_{seg} , ΔC and ΔS could then be calculated from $C(S)$.

We used C_{seg} and S_{seg} to calculate C^* instead of taking a direct derivative of the function $C(S)$ to reduce unreasonably sharp changes in C^* , especially at the sea end-members; this can occur when high-order polynomials are used to describe $C(S)$. The difference between the segment and direct derivative methods was small (about 1%) along the salinity gradient, except at the sea end-members when sharp change in C^* occurs.

After calculating C^* , the net flux, F , passing through each segment of an estuary, can be easily evaluated by:

$$F = RC^* \quad (\text{Equation 3.3})$$

where R is the river discharge. If C^* is estimated for the river and sea end-members, the corresponding fluxes will represent river input and estuarine output, respectively.

This estuarine mixing model was only applied to the distribution of NO_3^- concentrations in the five estuaries. Due to low concentrations and patchiness of NO_2^-

and NH_4^+ in many cases, C(S) functions were statistically difficult to derive and the model was not applied.

Using different order polynomial fits to a C-S plot may generate large differences in estimated C^* at the sea end-members despite using C_{seg} and S_{seg} . The sensitivity of this method to different curve fits suggests that C^* could differ by as much as 50% at the sea end-members (Fig. 3.2). However, different polynomial fits only produce small differences (10% - 20%) in maximum NO_3^- addition (Fig. 3.2A) and removal (Fig. 3.2B), which are prominent features in the coastal plain and piedmont river estuaries, respectively (see later discussion). Moreover, the differences in C^* of NO_3^- at the sea end-members from using different polynomial fits are small compared to this large NO_3^- addition or removal (Fig. 3.2). Therefore, the method is unlikely to bias the major features of NO_3^- distributions and provides reasonable estimates of addition and removal fluxes of NO_3^- . Various versions of this model have been used in recent estuarine studies (e.g. Raymond et al., 2000; Cai et al., 2000).

To further validate this method, several rules were used whenever the model was applied. First, the calculations only included transects that covered an entire estuary (0 salinity to the mouth), except for the Altamaha, where coverage up to 4 km off the mouth was required in order to give reasonable salinity coverage due to its high river flow. Second, polynomial fits of the original data must have an $R^2 \geq 0.90$. Third, if the data did not give reasonable coverage of the salinity gradient (i.e. two data observations were far away from each other in the salinity plots or only a few stations were sampled), then the calculation was not performed, because different polynomial fits could greatly and bias the trends of the data.

River Discharge and Freshwater Flushing Time. Discharge data for the five rivers were obtained from the U.S. Geological Survey (Alhadeff et al. 1999). "Date-specific" freshwater flushing times were estimated according to the method of Alber and Sheldon (1999), which requires information about discharge, estuary volume, and salinity. Estuarine volumes at low and high tide were based on measurements from National Oceanic and Atmospheric Administration (NOAA) charts and calculated as described in Alber and Sheldon (1999). Vertical salinity profiles were obtained from CTD casts (Sea-Bird Electronics SBE-19 or SBE-25) taken along the main axes of the estuaries on the dates of nutrient sampling. Salinity and estuarine volume data were then used in combination to estimate freshwater volume at mid-tide (see details in Alber and Sheldon 1999).

Results

Average Inorganic Nitrogen Concentrations. The river-end average concentrations of NO_3^- in the two piedmont river estuaries (Altamaha and Savannah) were several times higher than the coastal plain (Satilla and St. Marys) and mixed-type estuaries (Ogeechee) (Fig. 3.3A); their estuarine averages fell between their river-end and the sea-end averages but were still significantly higher than the other two types of estuaries (Fig. 3.3A). Contrarily, the estuarine averages for the coastal plain river estuaries were higher than both their river-end and sea-end averages (Fig. 3.3A), indicating a net NO_3^- production within these estuaries. The lowest estuarine average NO_3^- concentrations ($\leq 1.6 \mu\text{M}$) occurred in the St. Marys River estuary. Although the Ogeechee had average NO_3^- concentrations similar to those of the coastal plain rivers, its

estuarine average fell between its river-end and sea-end averages, which resembles the pattern of the piedmont rivers (Fig. 3.3A).

The average NO_2^- contents at the river end-members for all five estuaries were lower than the estuarine averages (Fig. 3.3B). Their estuarine averages during the study period were also uniformly low ($< 0.6 \mu\text{M}$), except in the St. Marys where its average concentration reached $1.6 \mu\text{M}$ (Fig. 3.3B). In the St. Marys River estuary, NO_2^- was a major species of dissolved inorganic nitrogen ($\text{DIN} = \text{NO}_3^- + \text{NO}_2^- + \text{NH}_4^+$) and accounted for 32% of the total. However, NO_2^- was less than 8% of DIN in the other estuaries.

All averages of NH_4^+ concentrations were uniformly low ($< 1.5 \mu\text{M}$) for all estuaries, except for the Savannah (Fig. 3.3C), where the estuarine and sea end member averages nearly doubled.

Inorganic Nitrogen Distribution.

(1) Coastal plain river estuaries – The NO_3^- distribution along the salinity gradient in the coastal plain river estuaries (Satilla and St Marys) always had a maximum in the mid-salinity zone (5 to 15 psu), with the exception of April 8, 1995 in the Satilla (Fig. 3.4 and Fig. 3.5). After NO_3^- peaked, the concentrations dropped quickly to near zero at the sea end-member during most surveys. This pattern did not vary seasonally, although the salinity where the peak NO_3^- occurred changed between surveys. However, the surveys conducted from July to October generally showed higher average concentrations of NO_3^- than in February and April, which corresponded to low and high flow seasons, respectively (Fig. 3.4 and Fig. 3.5).

Similar to NO_3^- , average NO_2^- concentrations from July to October were much higher than those in February and April (Fig. 3.4 and Fig. 3.5). A NO_2^- peak mostly downstream of the NO_3^- maximum (around 20 – 30 psu) during July - October was also prominent in the two coastal plain river estuaries (Fig. 3.4 and Fig. 3.5). This suggests a net accumulation zone of NO_2^- existed within the estuaries.

Contrary to the seasonal patterns of NO_3^- and NO_2^- , NH_4^+ exhibited near-zero concentrations (close to or below detection limit) along the salinity gradient from July to October, except for some cases at the sea end-members, and high concentrations in February and April, when a bell shape (a concentration peak at the mid-salinity) was clear (Fig. 3.4 and Fig. 3.5). The seasonal progression of NH_4^+ distribution can be clearly seen in the Satilla River estuary where more surveys were conducted (Fig. 3.4).

(2) Piedmont river estuaries – The distribution patterns of inorganic nitrogen in the piedmont river estuaries differed significantly from those of the coastal plain river estuaries. Among all surveys of the Altamaha and the Savannah, NO_3^- concentrations did not show mid-salinity maxima or net accumulation; the maximum concentrations occurred at or near the river end-members (Fig. 3.6 and Fig. 3.7). Instead, NO_3^- distributions showed prominent removal within these estuaries (Fig. 3.6 and Fig. 3.7). Seasonal change in average NO_3^- concentrations in the piedmont river estuaries was not as prominent as in the coastal plain river estuaries (Fig. 3.6 and Fig. 3.7). However, the seasonal pattern was clear for NO_2^- , with high average concentrations occurring from July to October and low in February and April. Whenever NO_2^- peaks (bell-shape) occurred in these estuaries, their locations were further upstream (≤ 15 psu of salinity) than in the coastal plain river estuaries (Fig. 3.6 and Fig. 3.7).

Similar to the coastal plain river estuaries, distribution of NH_4^+ in the Altamaha also oscillated between the low-concentration stage in summer and fall and the high-concentration stage in winter and spring. The bell shape distribution (mid-salinity peak) of NH_4^+ was clear in February and April, while in summer NH_4^+ concentrations did not drop to near 0, as was observed in the coastal plain river estuaries (Fig. 3.4, Fig. 3.5 and Fig. 3.6). On the other hand, the NH_4^+ distribution in the Savannah was consistent and less patchy during all of the surveys (Fig. 3.7) where a NH_4^+ peak with maximum concentration of about 6 – 7 μM always occurred near 8-km from the mouth. Such a consistent pattern in the Savannah may have resulted from a point source of anthropogenic contamination near the location.

(3) Mixed-type river estuary – The distribution patterns of NO_3^- in the Ogeechee River estuary (Fig. 3.8) showed mixed characteristics of both coastal plain and piedmont river estuaries. During the survey in April, 1995, NO_3^- showed clear removal within the estuary, while prominent NO_3^- addition in the upper estuary occurred in February, 1999 and October, 1995. However, the seasonal difference in NO_3^- concentrations was not clear. The NO_2^- and NH_4^+ distributions in the Ogeechee showed either patchiness or a bell shape, and seasonal variations were also less apparent than those observed in the other two types of estuaries.

Anchor Station. Noticeable production and removal processes of inorganic nitrogen were observed along the salinity gradients of the Georgia river estuaries (Figs. 3.4 – 3.8). However, the data from anchor stations in the Satilla and Altamaha river estuaries suggest these processes occurred on a time-scale longer than a single tidal cycle (Fig. 3.9 and Fig. 3.10). The major notable feature of the time series plots in Fig. 3.9 and

Fig. 3.10 (upper half) is the prominent “mirror image” property of the inorganic nitrogen concentrations, where the concentrations at a given salinity during ebb tides were virtually identical to those during flood tides. Although the concentration-salinity plots (lower half in Fig. 3.9 and Fig. 3.10) showed evident curvature, the water masses at any given salinity did not change in concentration; they simply oscillated back and forth across the anchor stations. This indicates that the curvature of the salinity plots of inorganic nitrogen, or the net result of the production and removal processes in the Georgia river estuaries, resulted from processes occurring on a time-scale significantly longer than one tidal cycle.

Model Results. Consistent with the general pattern of NO_3^- distribution in the coastal plain river estuaries, effective NO_3^- concentration ($[\text{NO}_3^-]^*$) showed that a pronounced net addition zone existed at intermediate salinities (5 – 15 psu) for most of the surveys (Fig. 3.4 and Fig. 3.5). Large NO_3^- addition generally occurred in summer and fall. Despite the possibly large uncertainty of C^* at the sea end-members, it is still indisputable to say in some cases (e.g. Satilla in July, 1996 and August, 1998) that the majority of upper-estuarine produced plus riverine input NO_3^- was removed in the lower estuaries, which resulted in little export of NO_3^- to the coastal ocean (Fig. 3.4, Fig. 3.5 and Table 3.2). The definite NO_3^- removal in the lower estuaries always occurred in summer and fall (Table 3.2). Of all surveys, the export fluxes of NO_3^- from the coastal plain rivers were below $6 \times 10^7 \text{ mmol d}^{-1}$ (Table 3.2).

In contrast to the coastal plain rivers, the piedmont river estuaries, which have much faster flow rates (Table 3.2), mostly did not have net NO_3^- addition zones, but net removal zones usually existed within the estuaries (see $[\text{NO}_3^-]^*$ in Fig. 3.6 and Fig. 3.7).

Once again, large NO_3^- removal tended to occur in summer and fall. The export fluxes of NO_3^- for piedmont river estuaries (mostly $> 20 \times 10^7 \text{ mmol d}^{-1}$, Table 3.2), despite net removal, were higher than those of the coastal plain rivers. This is a primary result of the higher flow rates and higher NO_3^- concentrations in the piedmont rivers. For the Ogeechee, the estuarine mixing model was only applied to the data from February, 1999, which had a result similar to the coastal plain river estuaries.

Discussion

Estuarine Processes and Marsh Effect. The NO_3^- salinity plots and C^* estimation all indicate a net NO_3^- production zone in the upper estuaries of the coastal plain rivers, with only a few exceptions (Fig. 3.4 and Fig. 3.5). Such a net addition was mostly prominent in summer and fall under low-flow condition. Since these estuaries generally show a mid-estuary maximum of Chl a concentration (Otero et al., 2000), biological uptake of NO_3^- probably works against this accumulation. The interaction of water between the main estuarine channels and adjacent marshes could not have resulted in NO_3^- accumulation in the system because the marsh acts as a sink for NO_3^- (Childers et al., 1993; Childers, 1994; Cai et al., 2000). Anthropogenic contamination is unlikely an explanation to this accumulation, since these estuaries are relatively pristine. There has been no report suggesting significant groundwater intrusion in the two coastal plain river estuaries. Given these arguments, the NO_3^- maxima and net addition at the intermediate salinities of the coastal plain river estuaries may indicate intensive nitrification in the water column and/or in the sediment within the main channels.

Two important factors provide further evidence for estuarine nitrification. First, the regions of lowest dissolved oxygen (DO) concentrations and saturation states (50 – 60%) are in the 0 – 15 psu salinity range (Cai et al., 1999), almost overlapping the NO_3^- production zone. Second, usually in summer and fall under low-flow condition (except for February, 1999 when a slow flow condition occurred in an expected high flow season) when a large NO_3^- accumulation occurred, NH_4^+ concentrations were always near 0 (close to or below detection limit) at the intermediate salinities (Fig. 3.4 and Fig. 3.5). This was a sign of NH_4^+ -fueled nitrification. Part of the required NH_4^+ for nitrification likely came from the marshes, as indicated by the higher concentrations of NH_4^+ in the marsh-dominated White Oak Creek adjacent to the Satilla River (July, 1996 in Fig. 3.4). Other NH_4^+ sources may include NH_4^+ released from the riverbed (Cai et al., 2000) and breakdown of particulate organic nitrogen (PON) via ammonification within the water column of the main channel (Balls et al., 1996).

The upper estuary NO_3^- maximum in the coastal plain river estuaries reflects a net production of nitrification over denitrification. Cai et al. (2000) calculated that the NO_3^- concentrations in the main channel of the Satilla River estuary would be over 10 times higher than observed if only nitrification took place. After NO_3^- reached the mid-salinity peak, it was either diluted by sea water with low NO_3^- concentration or showed apparent removal in the lower estuaries. Such a removal was mostly clear in the Satilla in summer and fall when river flow was minimal (Fig. 3.4). Apparently, estuarine nitrification declined or simply stopped at certain steps in the lower estuaries. On the other hand, marsh denitrification, mostly in the marsh sediment, must be responsible for the lower-estuarine NO_3^- removal mostly occurring in summer and fall when marsh respiration was

high (Cai et al., 2000). Tidal action in the lower estuary probably brings the main channel water, enriched with NO_3^- , into the marsh to fuel denitrification, leaving the outflow water with little NO_3^- (Cai et al., 2000). This can also be seen from the lower NO_3^- concentrations inside White Oak Creek (July, 1996 in Fig. 3.4). Such a removing process occurred under low-flow condition and often resulted in little estuarine NO_3^- export to the coastal ocean (Table 3.2). When river discharge was high, NO_3^- in the main channel of the lower estuaries was forced by flow to mix with sea water, leaving unclear sign of removal in the C^* plots (Fig. 3.4 and Fig. 3.5). Often accompanied with NO_3^- removal, NO_2^- was accumulated in the lower estuaries of the coastal plain rivers (Fig. 3.4 and Fig. 3.5) probably due to oxidation of NH_4^+ and/or marsh denitrification as indicated by higher NO_2^- concentration in the marsh creek (July, 1996 in Fig. 3.4).

Contrary to the coastal plain river estuaries, the field data and C^* estimation for the piedmont river estuaries (Altamaha and Savannah) showed that generally no NO_3^- accumulated in the mid-salinity region (Fig. 3.6 and Fig. 3.7); in fact a net removal occurred throughout these estuaries during most surveys. Large NO_3^- removal usually occurred in summer and fall under low-flow condition, which resembled the situation of NO_3^- addition in the coastal plain river estuaries. The difference in the distribution pattern of NO_3^- between the coastal plain and piedmont river estuaries was likely related to differences in river discharge and estuarine flushing time (see later discussion). Note that even the lowest river discharge in the piedmont rivers was among the highest flow in the coastal plain rivers (Table 3.2). Due to faster flow, thus the short flushing time, of the piedmont river estuaries, significant amounts of NO_3^- could not be accumulated. A similar proposition was presented by Balls et al. (1996) for the upper Forth Estuary,

Scotland. Despite the different origins, the coastal plain and piedmont river estuaries are similar in the characteristics of their climates, biological activities, and marsh-related processes (Childers et al., 1993; Childers, 1994; Cai et al., 1999; Pomeroy et al., 2000). Therefore, marsh denitrification may still be the major mechanism of the NO_3^- removal in the piedmont river estuaries. The difference of the addition/removal scenario between the coastal plain and piedmont river estuaries may in fact support the argument that nitrification is mainly an estuarine process and may greatly rely on the time that allows it to proceed, while denitrification is mainly a marsh process, and is less influenced by river discharge. The piedmont river estuaries did not show elevated Chl a concentration compared to the coastal plain river estuaries (Otero et al., 2000); thus water-column NO_3^- uptake by primary producers (phytoplankton) was probably not responsible for major removal of NO_3^- . Consistent with the denitrifying scenario in the piedmont river estuaries, NH_4^+ depletion was not observed along the salinity gradient during the sampling period (Fig. 3.6 and Fig. 3.7).

The proposed denitrification/nitrification scenario is further consistent with observed seasonal variations of inorganic nitrogen. In February and April, NO_3^- peaks in the coastal plain river estuaries were relatively small and net removal processes were not prominent (Fig. 3.4 and Fig. 3.5), suggesting that rates of nitrification and denitrification were depressed probably due to combined effects of fast river flow and low temperature; thus NH_4^+ accumulated and had a bell shape distribution along the salinity gradient (Fig. 3.4 and Fig. 3.5). From July to October, net NO_3^- accumulation at the intermediate salinity of the coastal plain river estuaries increased and net NO_3^- removal was noticeable in the lower estuaries, suggesting both nitrification and denitrification proceeded to a

greater extent; NH_4^+ concentrations were thus low. In the piedmont river estuaries, estuarine nitrification rarely dominated at any portion of the estuaries even in summer and fall. Consistently, NH_4^+ concentrations never dropped to the values that were close to detection limit all year-round (Fig. 3.6 and Fig. 3.7). However, net NO_3^- removal within these estuaries still showed a similar seasonal pattern with large removal in summer and fall and small removal or no removal in winter and spring (Fig. 3.6 and Fig. 3.7).

River Flow and Temperature Controls. The temporal and spatial variations of inorganic nitrogen in estuaries are controlled by the biogeochemical processes and factors which are usually interweaved and are complicated in nature. Despite of complexity of the five Georgia riverine systems, many features of inorganic nitrogen distributions described, such as addition/removal of NO_3^- , are remarkably repeatable over the period of the investigation. The seasonal changes in inorganic nitrogen concentrations and addition/removal patterns imply that temperature may be an important controlling factor. On the other hand, seasonality of river flow also seems to be related to the observed addition/removal scenario as discussed earlier. We hererin discuss these two controlling factors that seem to be most significant and have apparent control to the distribution patterns of inorganic nitrogen in these estuaries.

Cai et al. (2000) implied that river flow may play a key role in controlling the distributions and fluxes of inorganic nitrogen in Georgia estuaries. The estimation of C^* from the estuarine mixing model also indicate that net NO_3^- production in the Satilla River estuary is associated with river flow: low flow rates correspond to larger $[\text{NO}_3^-]^*$ peaks or larger net addition, while high flow rates correspond to smaller $[\text{NO}_3^-]^*$ peaks or smaller addition (Fig. 3.4). The prominent net removal of NO_3^- in the lower estuary of the

Satilla River in summer and fall also corresponds to low-flow condition. Due to limited surveys and C^* estimation in the St. Marys River estuary, this pattern can not be examined (Fig. 3.5). The river flow rate or discharge inversely corresponds to the estuarine freshwater flushing time, τ , in an estuary (Dyer, 1973):

$$\tau = \frac{\text{Freshwater Volume } V}{\text{River Discharge } R} \quad (\text{Equation 3.4})$$

The physical meaning of the flushing time is the average amount of time fresh water spends within a system (Alber and Sheldon, 1999). Variations of river discharges can thus have significant, direct effects on the flushing time, and thus on the time-scale over which the biogeochemical processes can occur during mixing within an estuary.

Therefore, larger production/removal of NO_3^- may occur in the coastal plain river estuaries whenever flushing time is long, simply because denitrification and nitrification has longer processing time within the estuaries. Due to much shorter flushing time in the piedmont river estuaries (5 days on average) (Table 3.2), estuarine nitrification may be lack of time to proceed before the estuarine water is forced into the coastal ocean by high river flow. This results in no NO_3^- accumulation within the estuaries most times of the year. However, NO_3^- is still being removed by denitrification while estuarine water enters the marsh via tidal exchange. This process may be less directly influenced by the river flow or flushing time.

River flow control on NO_3^- production/removal can be further demonstrated in Figs. 3.11A and B. A significant linear relationship existed between the maximum NO_3^- addition (calculated by the difference between maximum C^* and C^* at the river end-member) and $1/R$ for the Satilla River estuary (Fig. 3.11A). River discharge therefore largely has a “dilution” effect on the NO_3^- accumulation in this estuary. In other words,

the increase of discharge will decrease the concentration of NO_3^- being accumulated. Based on Fig. 3.11A, one may predict from a river discharge how high the $[\text{NO}_3^-]^*$ peak can be or how much NO_3^- is accumulated at the intermediate salinity of the Satilla River. This may be an over-simplified quantification for observed net addition of NO_3^- in the upper estuary of the Satilla River, because other biogeochemical processes may also have accumulative effects on the distribution of NO_3^- . Nevertheless, Fig. 3.11A at least demonstrates that the river flow plays an important role that regulates inorganic nitrogen distributions in the Satilla River. Because of limited model results from the St. Marys and Ogeechee, such a relationship was not clear (Fig. 3. 11A). Similarly, the plot of maximum NO_3^- removal (in concentration unit) vs. $1/R$ in the Altamaha and Savannah shows that the data points from warm (February and April) and cold seasons (July – October) fall onto two separate lines (Fig. 3. 11B), suggesting that river discharge, thus flushing time, also regulates the amount of NO_3^- being removed in the piedmont river estuaries, but that such a control may vary with seasons.

Temperature is another primary controlling factor to the production/removal scenarios of inorganic nitrogen in these estuaries, in that biogeochemical processes are all temperature dependent. Seasonal variations of inorganic nitrogen concentrations and seasonal patterns of the net production/removal scenario in the five Georgia riverine estuaries are all related to temperature changes. Furthermore, temperature has been recognized to be an important factor that regulates the community respiration and system metabolism in Georgia estuaries and coastal waters (Hopkinson, 1985; Griffith and Pomeroy, 1995; Pomeroy et al., 2000). To examine the temperature effect, maximum NO_3^- addition and removal (in concentration unit) in these estuaries are also plotted

against average cruise temperature in Figs. 3.11C and D. Except for the maximum NO_3^- removal during cold months in the Altamaha and Savannah, these correlations are generally more scattered than the relationships between NO_3^- addition/removal and river flow (Figs. 3. 11A and B). However, these temperature dependences are all positive, implying that higher temperature generally favors net accumulation and removal of NO_3^- in the coastal plain and piedmont river estuaries, respectively. It is difficult to separate the river flow control and temperature effects in these estuaries because they are inherently correlated (e.g. high flow, cold seasons; low flow, warm seasons). The difference is that river flow mainly affects the time-scale that biogeochemical processes can proceed within an estuary, while temperature effects are reflected in most biogeochemical processes and their complex interactions. Consequently, the discussion on temperature effects is difficult to be carried on in depth with our current data set. Furthermore, other controlling factors may further complicate the situation, as indicated by scatter in the relationships in Fig. 3.11 and data points apparently away from the correlations (e.g. the Altamaha in August, 1998).

River flow control on net production/removal of inorganic nitrogen in the estuaries of the Georgia rivers supports the idea that the extent to which each nutrient is modified in estuaries largely depends on the flushing time or residence time, as reported for other estuaries (Delaware Bay, Church, 1986; Neuse River Estuary, Christian et al., 1991; nine Scottish east coast rivers, Balls et al., 1994; Richmond River Estuary, Eyre and Twigg, 1997). Although the details tend to be different for the individual systems in terms of biological activity, seasonality, physical mixing and chemical signals, such a notion seems to be a fundamental characteristic of small to mid-size estuaries and coastal

systems. For very large rivers (e.g. Mississippi and Amazon), which have river discharge greater than $3000 \text{ m}^3 \text{ s}^{-1}$, fresh and salt water mixing is pushed onto the continental shelf (Nixon et al., 1996); thus the flow control of the biogeochemical processes within the estuarine boundaries may be different from our case. The finding that the net NO_3^- production in an upper estuary of the Satilla River is a function of river flow (Fig. 3.11) is consistent with the qualitative description of NO_3^- production in the Upper Forth Estuary (Scotland) (Balls et al., 1996). Positive dependence of net removal or denitrification on the flushing time (or residence time) has also been recognized for many different coastal and estuarine systems (Nixon et al., 1996). In freshwater lakes, such a relationship has also been documented (Andersen, 1974; Kelly et al., 1987).

NO₃⁻ Output Fluxes. Due to apparent NO_3^- removal within the lower portion of the Satilla River in summer and fall (Fig. 3.4 and Fig. 3.5), the output fluxes (into the ocean) are in many cases less than 50% of the total input (riverine plus estuarine produced NO_3^-) (Table 3.2), and sometimes there is no net NO_3^- output at all (e.g. July 1996, Satilla River; also see Cai et. al. 2000). For the Satilla River, the average river input plus mean NO_3^- production in the upper estuary during the study period was $5.4 \times 10^7 \text{ mmol d}^{-1}$, while the average output NO_3^- flux was only $1.7 \times 10^7 \text{ mmol d}^{-1}$ (Table 3.2), which suggests on average ca. 70% of the total NO_3^- input was removed within the estuary and only 30% exported to the coast. With limited model estimates (Table 3.2), the average NO_3^- output for the St Marys River was $0.4 \times 10^7 \text{ mmol d}^{-1}$ over the study period. Much smaller output flux of NO_3^- compared to the Satilla was a result of low NO_3^- concentration and small river discharge (Table 3.2). The St. Marys had the lowest average concentrations among all five estuaries (Fig. 3.1); this was consistent with a large

marsh area in the estuary where marsh denitrification probably kept NO_3^- concentration low most of the time.

The average NO_3^- outputs from the Altamaha and Savannah rivers were similar, with the Altamaha exporting $25.7 \times 10^7 \text{ mmol d}^{-1}$ and the Savannah $33.8 \times 10^7 \text{ mmol d}^{-1}$ (Table 3.2). The average removal within these estuaries accounted for 53% and 33% of the riverine input NO_3^- fluxes in the Altamaha and Savannah rivers, respectively. The piedmont river estuaries exported NO_3^- one order of magnitude higher than the coastal plain river estuaries due to the higher riverine NO_3^- content and river discharge. Because the model estimate was only applied to one survey in the Ogeechee (Table 3.2), further flux discussion is excluded.

We attribute the NO_3^- loss in the five Georgia estuaries to net denitrification over nitrification, which on average accounts for about 33 – 70% of the total NO_3^- input (Table 3.2). Seitzinger (1987 and 1988) and Seitzinger and Giblin (1995) concluded that a largely constant 45% of the DIN input was removed through denitrification in estuaries, although there appear to be exceptions (e.g. Norsminde Fjord, Denmark, Nielsen et al., 1995). In Chesapeake Bay, Boynton et al. (1995) found that about 26% of total input inorganic nitrogen was denitrified within the system, while denitrification accounts for about 43% - 54% of total inorganic nitrogen inputs in Delaware Bay and 13% - 27% in Narragansett Bay (Nixon et al. 1995 and Nixon et al. 1996). Although the Georgia river estuaries have large marsh areas where intensive denitrification occurs, our estimation of the relative NO_3^- removal generally falls within the range listed above.

After scaling all the NO_3^- output fluxes in Table 3.2 to percentages of total NO_3^- inputs, we displayed the results against estuarine flushing time (Fig. 3.12). The relative

output of NO_3^- fell into two distinct groups. For the piedmont river estuaries, relative NO_3^- output decreased quickly as increase of flushing time (Fig. 3.12). This was consistent with net NO_3^- removal scene in these estuaries: the longer the flushing time, more NO_3^- was denitrified and less NO_3^- was exported to the ocean. For the coastal plain river estuaries, the relationship seemed to be less clear. This was probably due to the relatively complex scenario where both net NO_3^- production and removal occurred at different portion of the estuaries super-imposed by seasonal variation. Nixon et al. (1996) summarized the total nitrogen output in various estuaries, coastal and freshwater-lake systems around the North Atlantic Ocean, and found an inverse linear relationship between the logarithm scale of mean water residence time and the net fractional transport of nitrogen to the continental shelf. Dettmann (2001) took one step further from the Nixon's finding and concluded that the fraction of nitrogen that is exported or denitrified within an estuary can be predicted from the freshwater residence time through a simple model. These conclusions strongly support our interpretation of the data, although we only included NO_3^- in our flux estimation.

Summary. Both the original data and C^* estimation indicated that a net NO_3^- production zone occurred in the upper estuaries of the coastal plain rivers, mostly due to net nitrification over denitrification. NO_3^- accumulation was larger during warm months when river discharge was low. Especially in summer and fall, the NO_3^- was then partially or completely removed within the lower estuaries by denitrification that most likely occurred over the marsh through tidal excursion. In the piedmont river estuaries, the net NO_3^- production zone was not seen, and net removal existed along the salinity gradient. Accompanied with large NO_3^- removal in summer and fall, NO_2^- accumulated in the main

channel water of five Georgia estuaries. The data analysis demonstrated that both estuarine (nitrification) and marsh (denitrification) processes and their associated seasonal variations were critical to shaping the distribution patterns of inorganic nitrogen along the main channel of these estuaries.

Distributions of NO_3^- and NO_2^- in all estuaries showed distinct seasonal patterns with higher average concentrations during warm months than during cold months. NH_4^+ distribution exhibited an opposite seasonal pattern. These seasonal patterns are consistent with our explanation in which estuarine nitrification and marsh denitrification are primarily responsible for accumulation/removal of inorganic nitrogen in the main channel of the estuaries.

Depending on how a nutrient species is modified, the corresponding output flux to the coastal ocean differs in relationship to the flushing time or residence time. Such a correlation is negative with respect to NO_3^- output for the piedmont river estuaries, while it is scatter for the coastal plain river estuaries. This difference is consistent with their respective NO_3^- production/removal scenarios.

River flow along with temperature, marsh and estuarine processes seems to play a major role in regulating the observed distribution patterns and production/removal scenarios of inorganic nitrogen along the salinity gradient of these estuaries. Our interpretation of the data provides support for the notion that the extent to which nutrients are modified within an estuary is a function of river flow or flushing time.

Figures

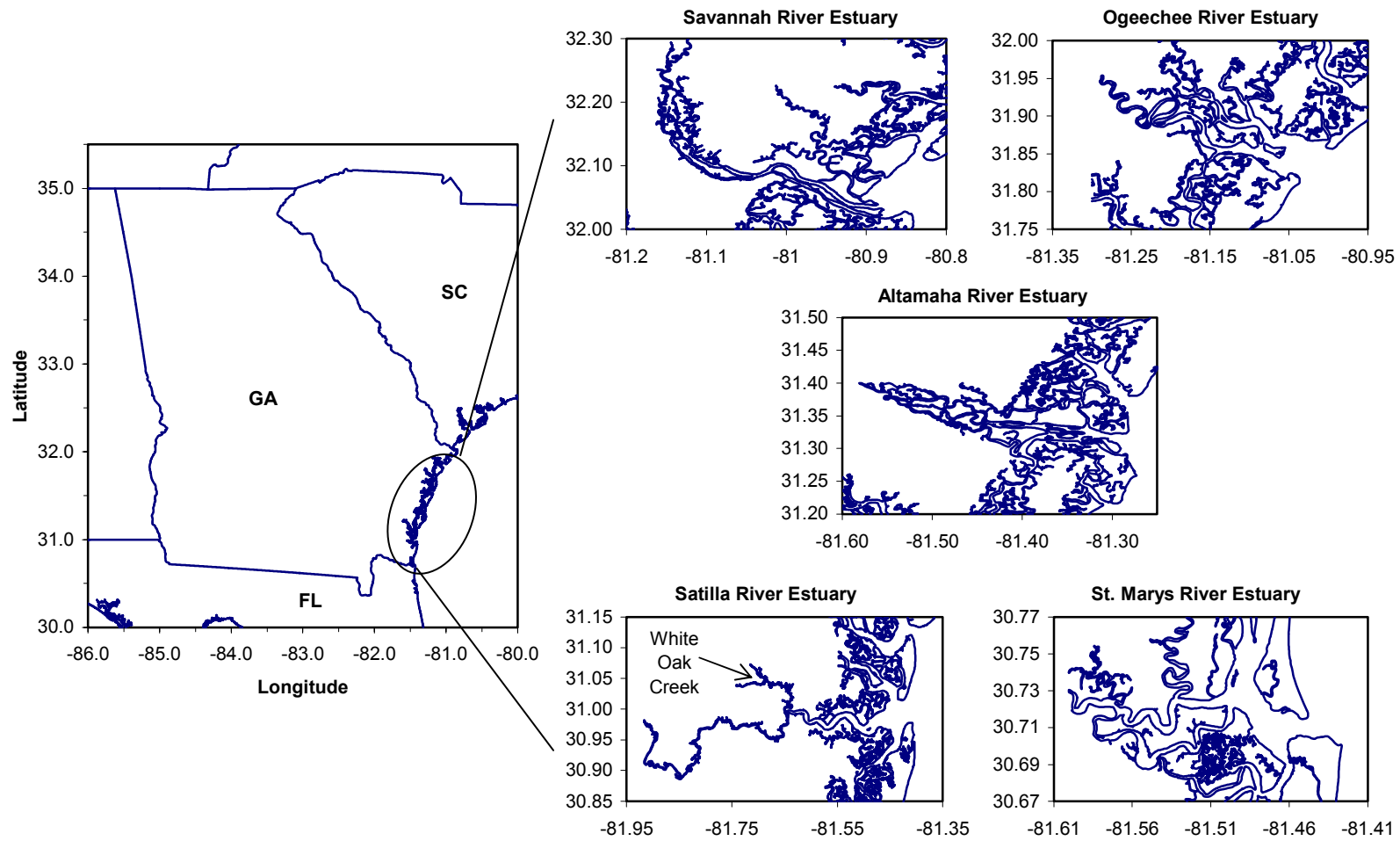


Fig. 3.1. Georgia coast and five major riverine estuaries.

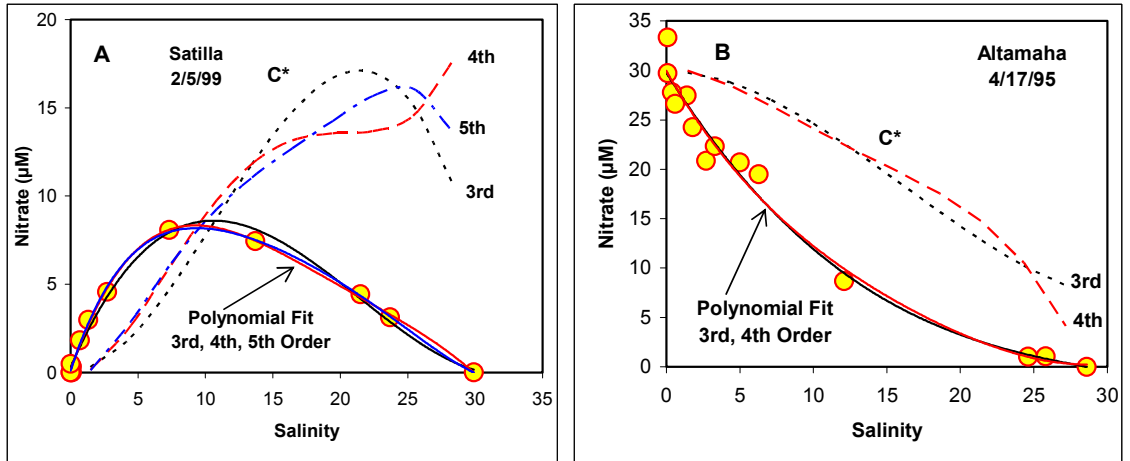


Fig. 3.2. Sensitivity of C^* to different orders of polynomial regressions of NO_3^- -salinity distributions. A. Satilla on Feb. 5, 1999; B. Altamaha on Apr. 17, 1995. The solid lines are 3rd, 4th and 5th order of polynomial fits of the data points. Dotted and broken lines are effective concentrations of NO_3^- (C^*) calculated from different orders of polynomial regressions.

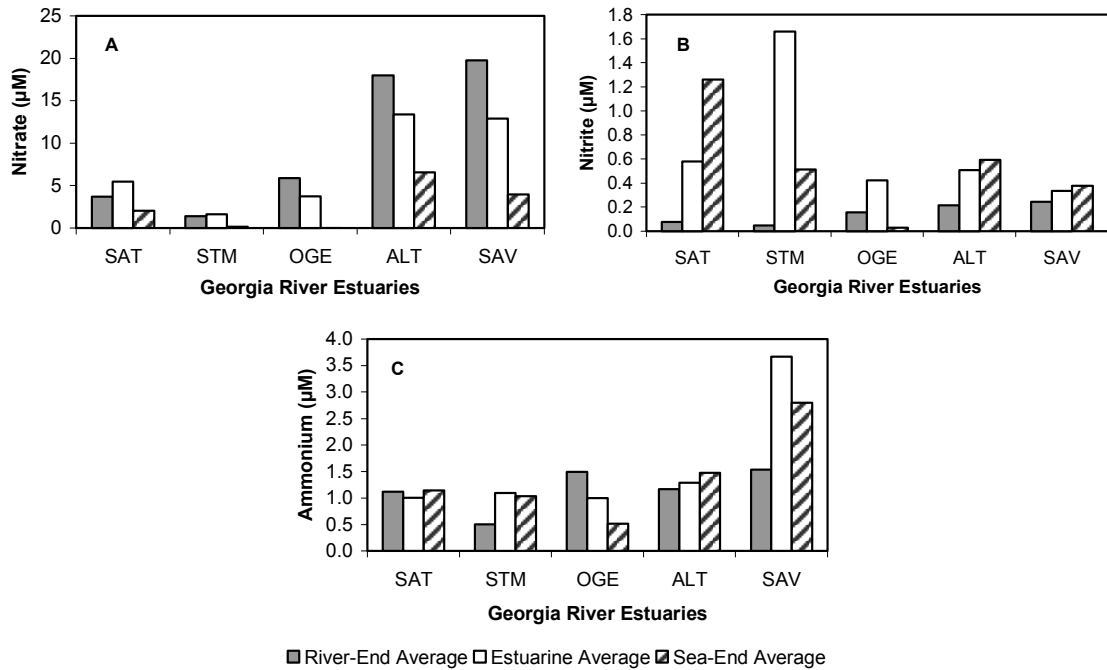


Fig. 3.3. Comparison of average concentrations of NO_3^- , NO_2^- and NH_4^+ in the five Georgia river estuaries. A. NO_3^- ; B. NO_2^- ; C. NH_4^+ . The estuarine average was calculated by using all survey data for each estuary; the river-end average was calculated by using the data with salinity ≤ 0.1 of each estuary; the sea-end average was calculated by using the data collected at and beyond the mouth of each estuary.

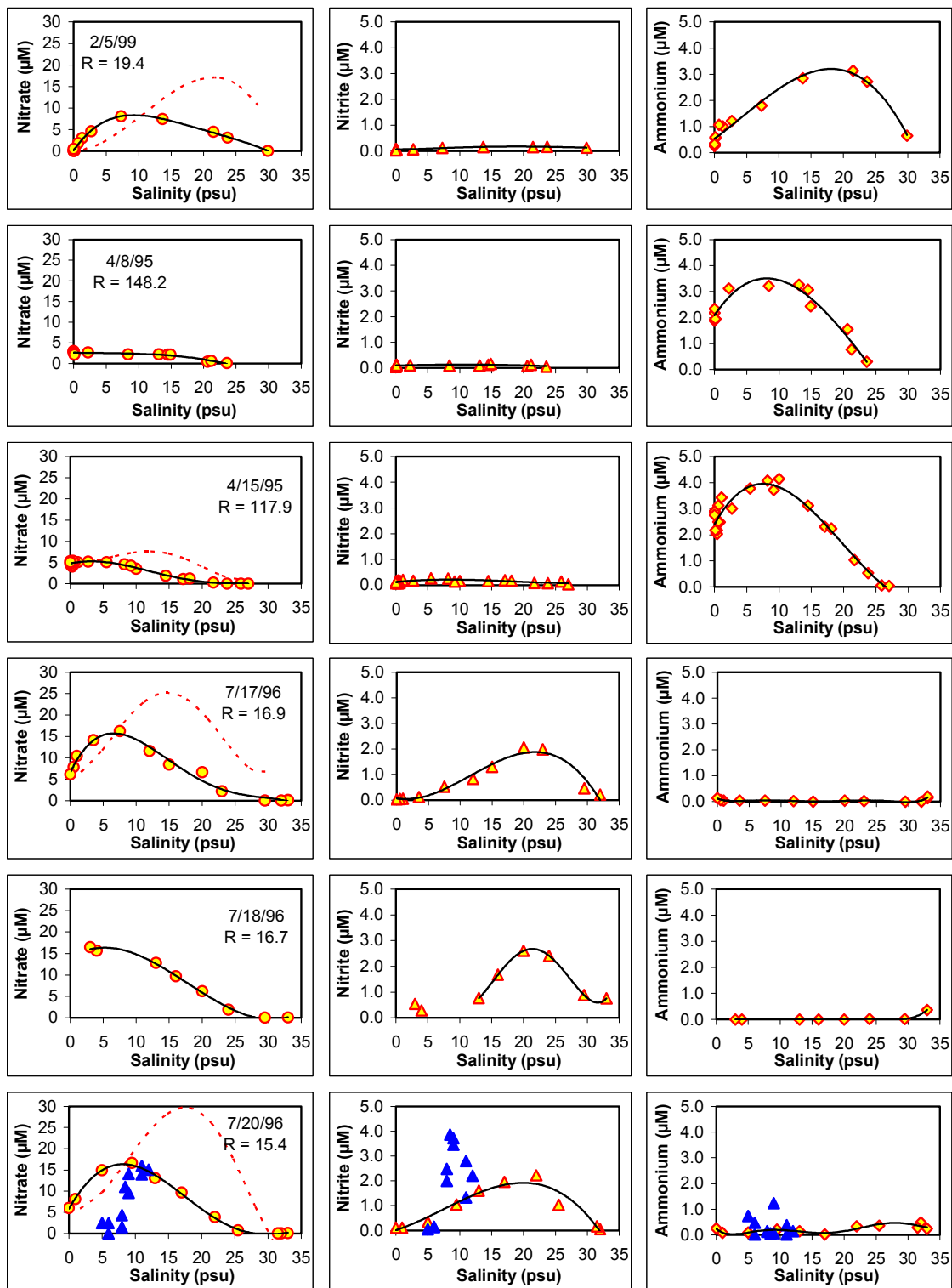


Fig. 3.4

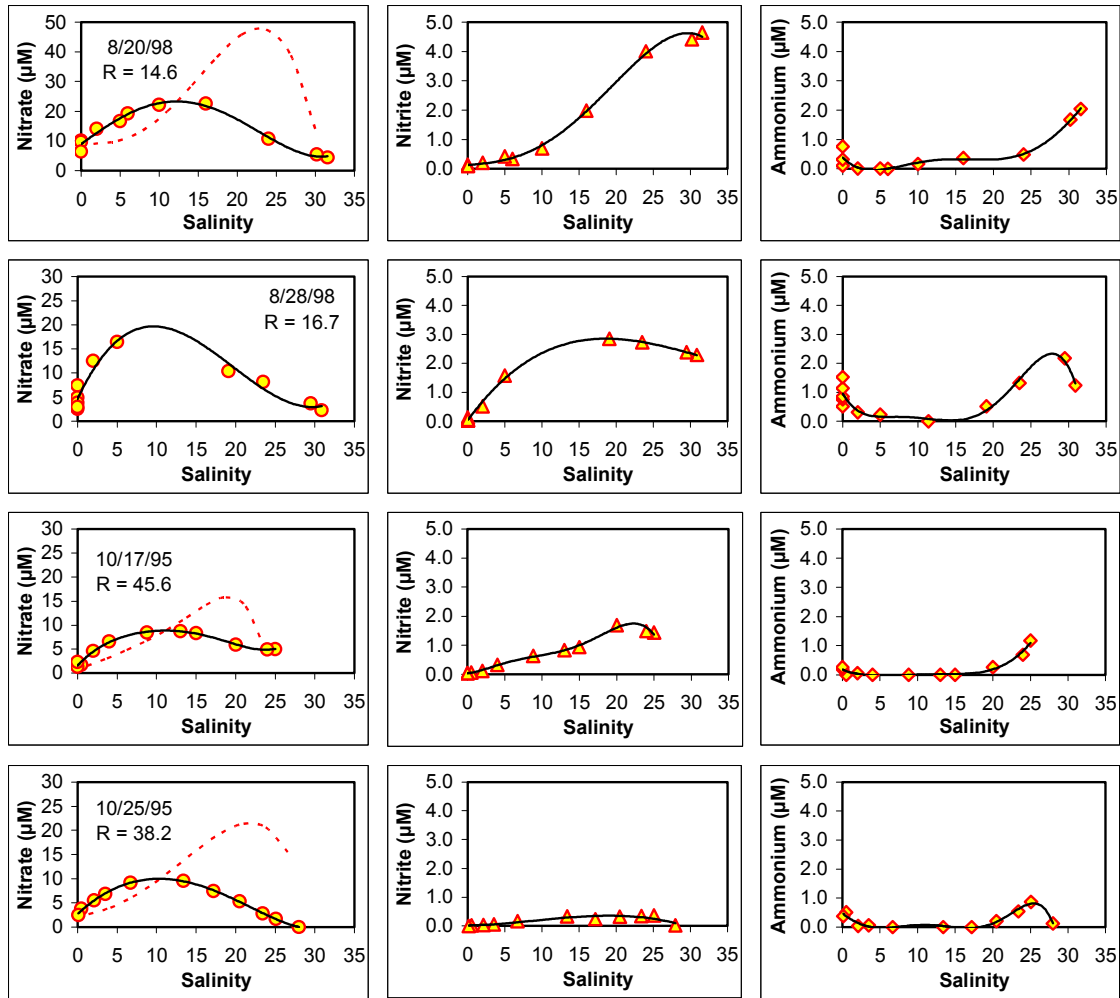


Fig. 3.4 (continued). Concentrations of NO_3^- , NO_2^- and NH_4^+ along the salinity gradient in the Satilla River estuary. The sequence of each figure reflects the progression over a year (Feb. to Oct.) rather than the real time of the surveys. The three plots in the same row are the data from the same survey, with the cruise date and the river discharge ($\text{m}^3 \text{s}^{-1}$), R , listed in the NO_3^- plots. Solid lines are the multiple-order regression fits of the data; the dashed lines in the NO_3^- plots are the effective NO_3^- concentration ($[\text{NO}_3^-]^*$) calculated by using the continuous estuarine mixing model. Filled triangles in the plots of July 20, 1996 are the data collected on July 21, 1996 from White Oak Creek.

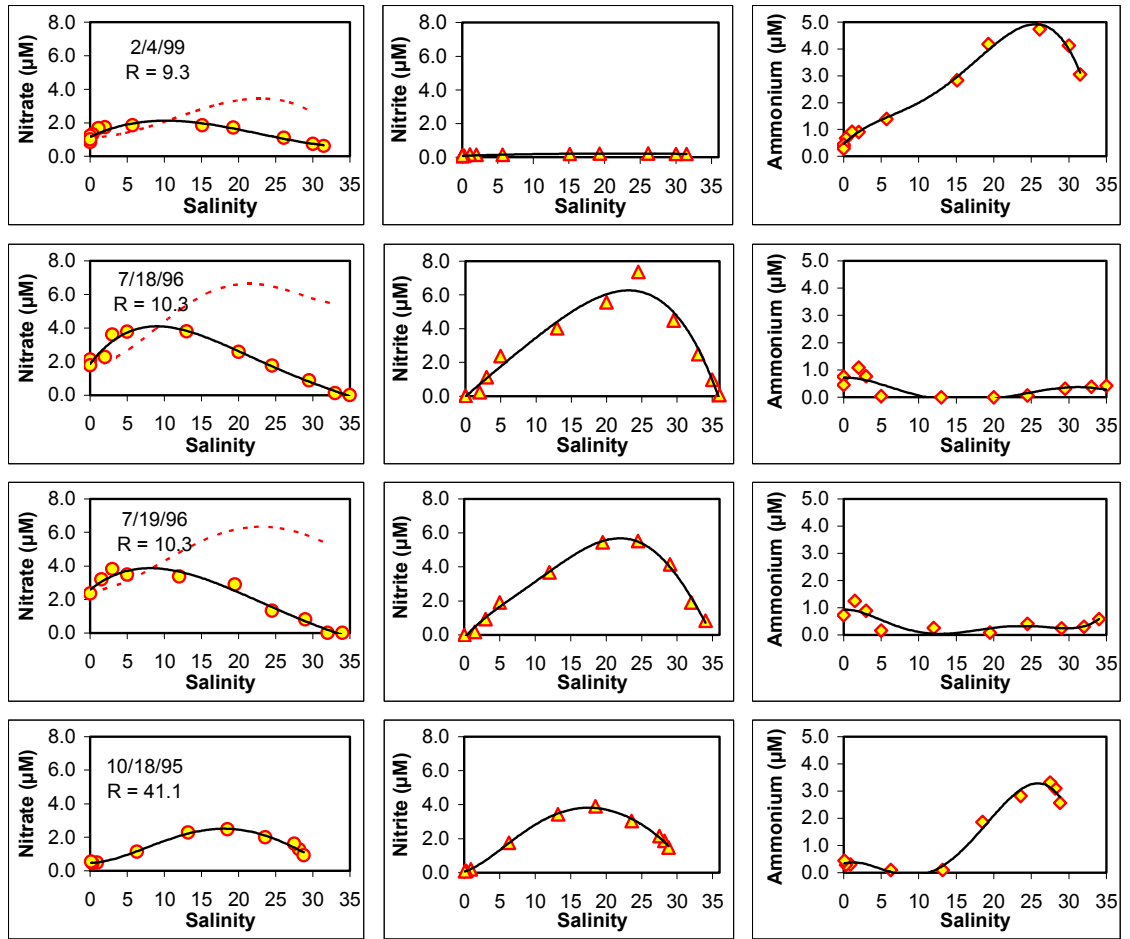


Fig. 3.5. Concentrations of NO_3^- , NO_2^- and NH_4^+ along the salinity gradient in the St. Marys River estuary. See the caption of Fig. 3.4 for legends and explanations.

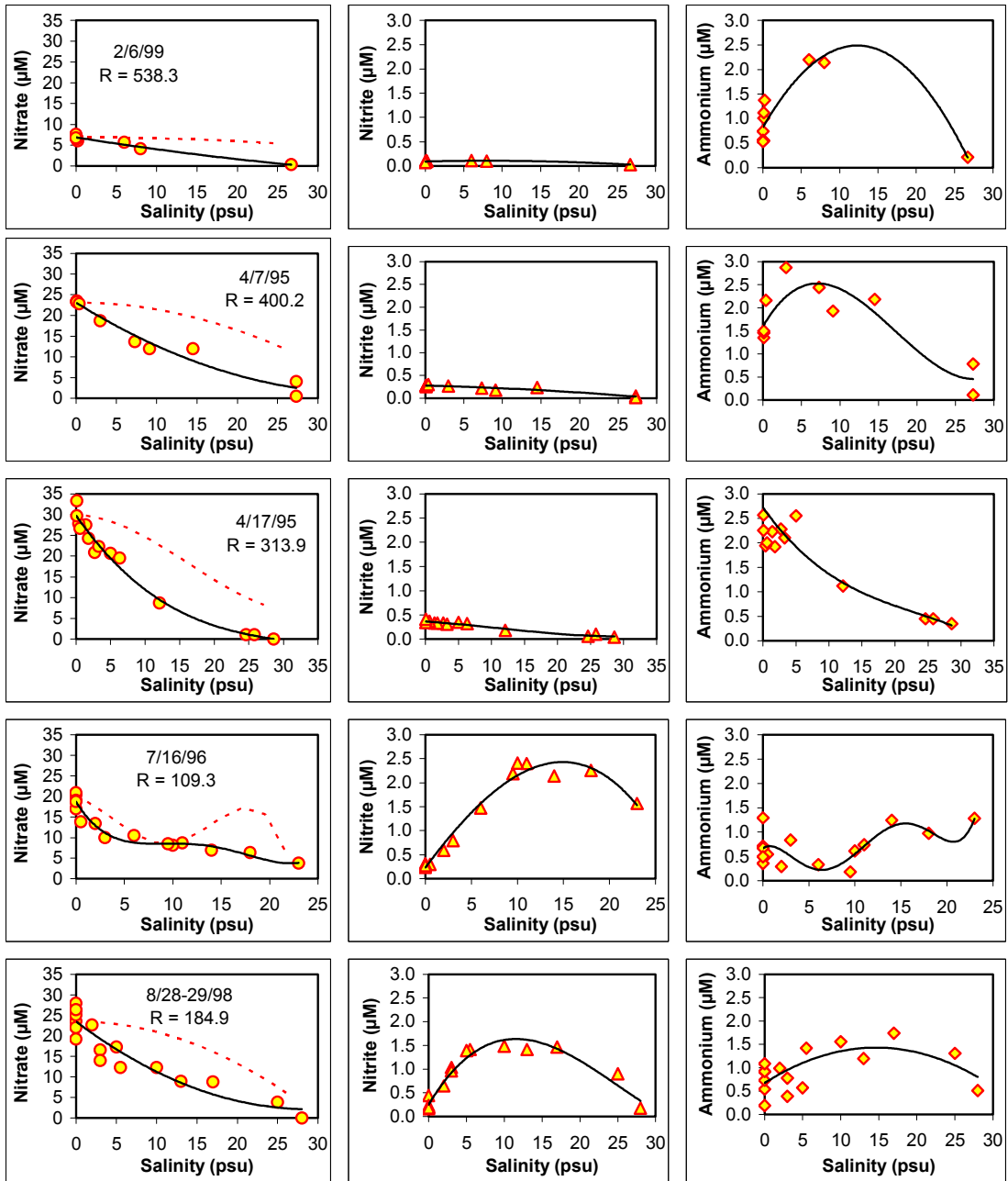


Fig. 3.6

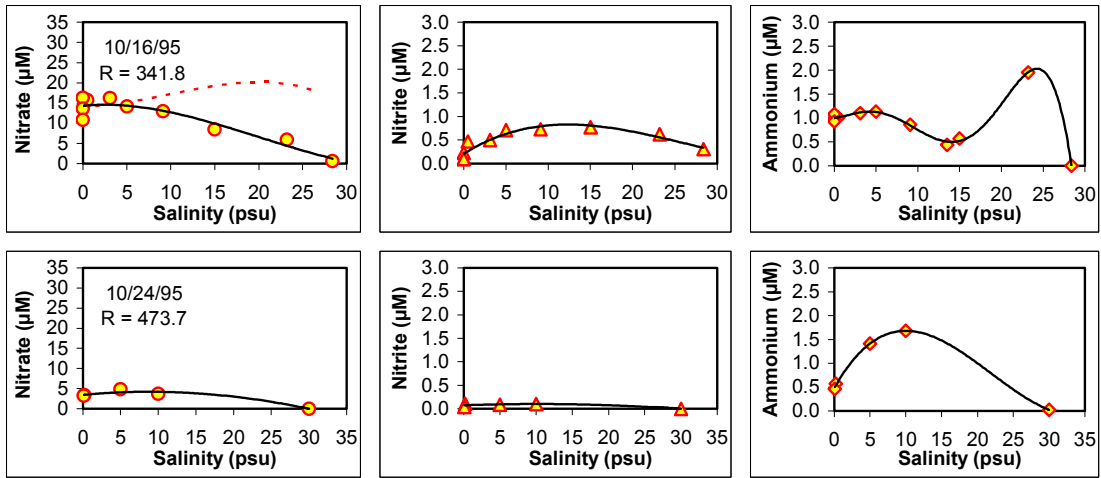


Fig. 3.6 (continued). Concentrations of NO_3^- , NO_2^- and NH_4^+ along the salinity gradient in the Altamaha River estuary. See the caption of Fig. 3.4 for legends and explanations.

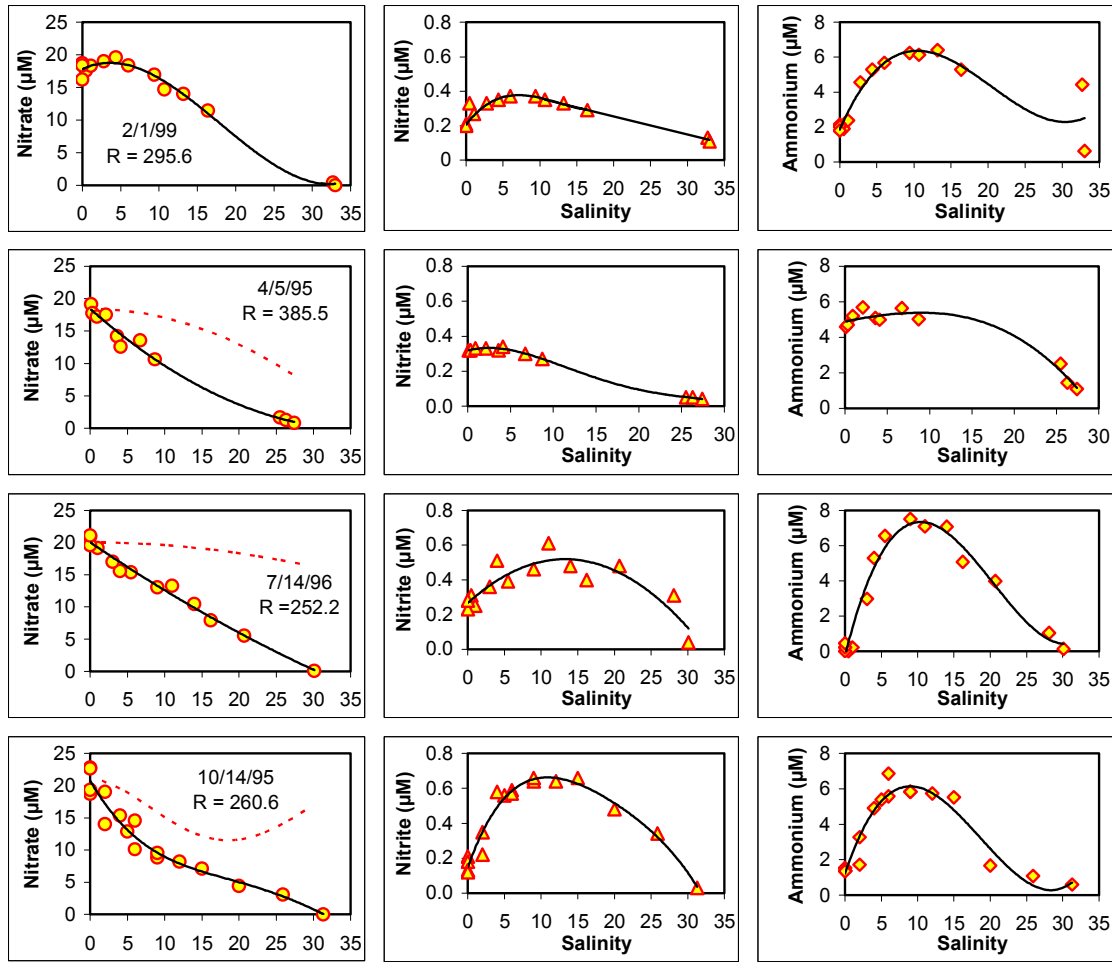


Fig. 3.7. Concentrations of NO_3^- , NO_2^- and NH_4^+ along the salinity gradient in the Savannah River estuary. See the caption of Fig. 3.4 for legends and explanations.

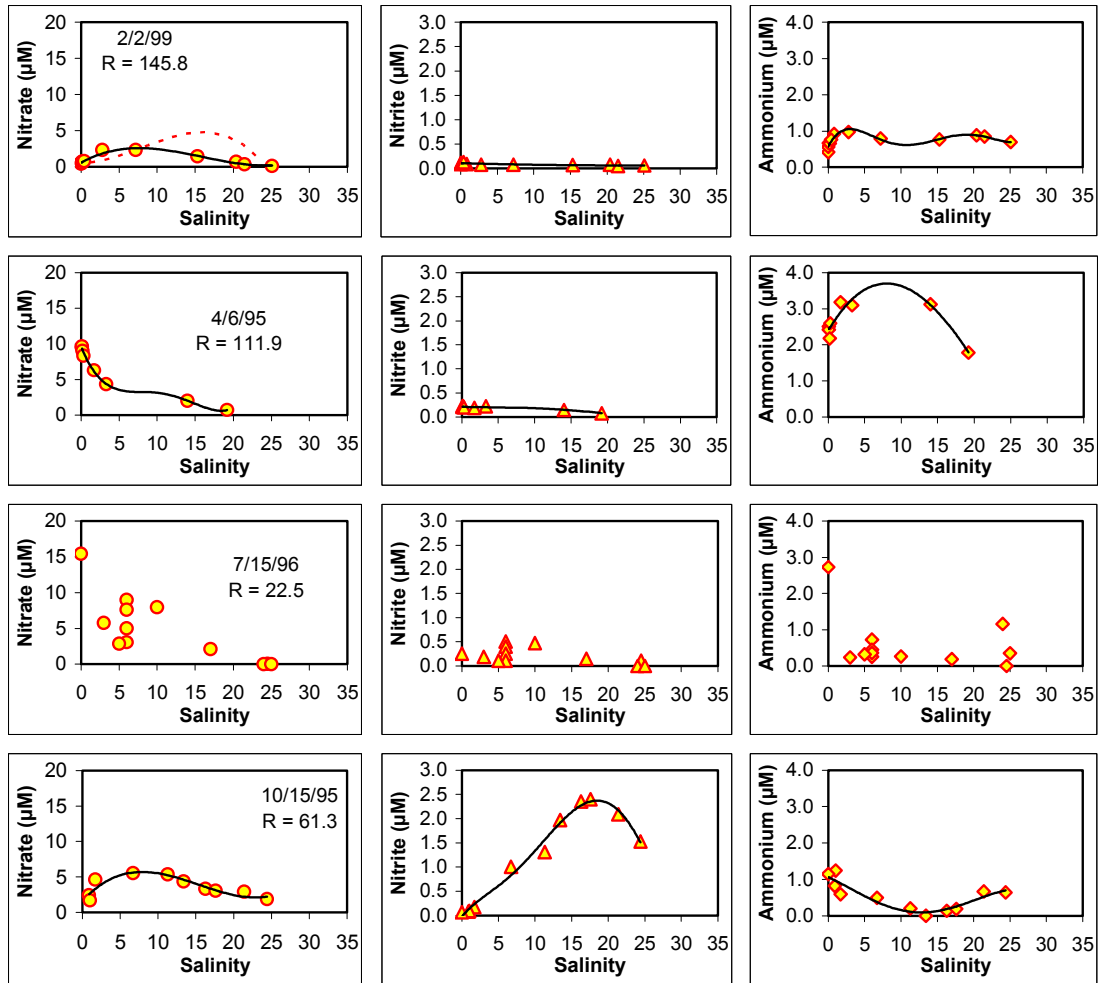


Fig. 3.8. Concentrations of NO_3^- , NO_2^- and NH_4^+ along the salinity gradient in the Ogeechee River estuary. See the caption of Fig. 3.4 for legends and explanations.

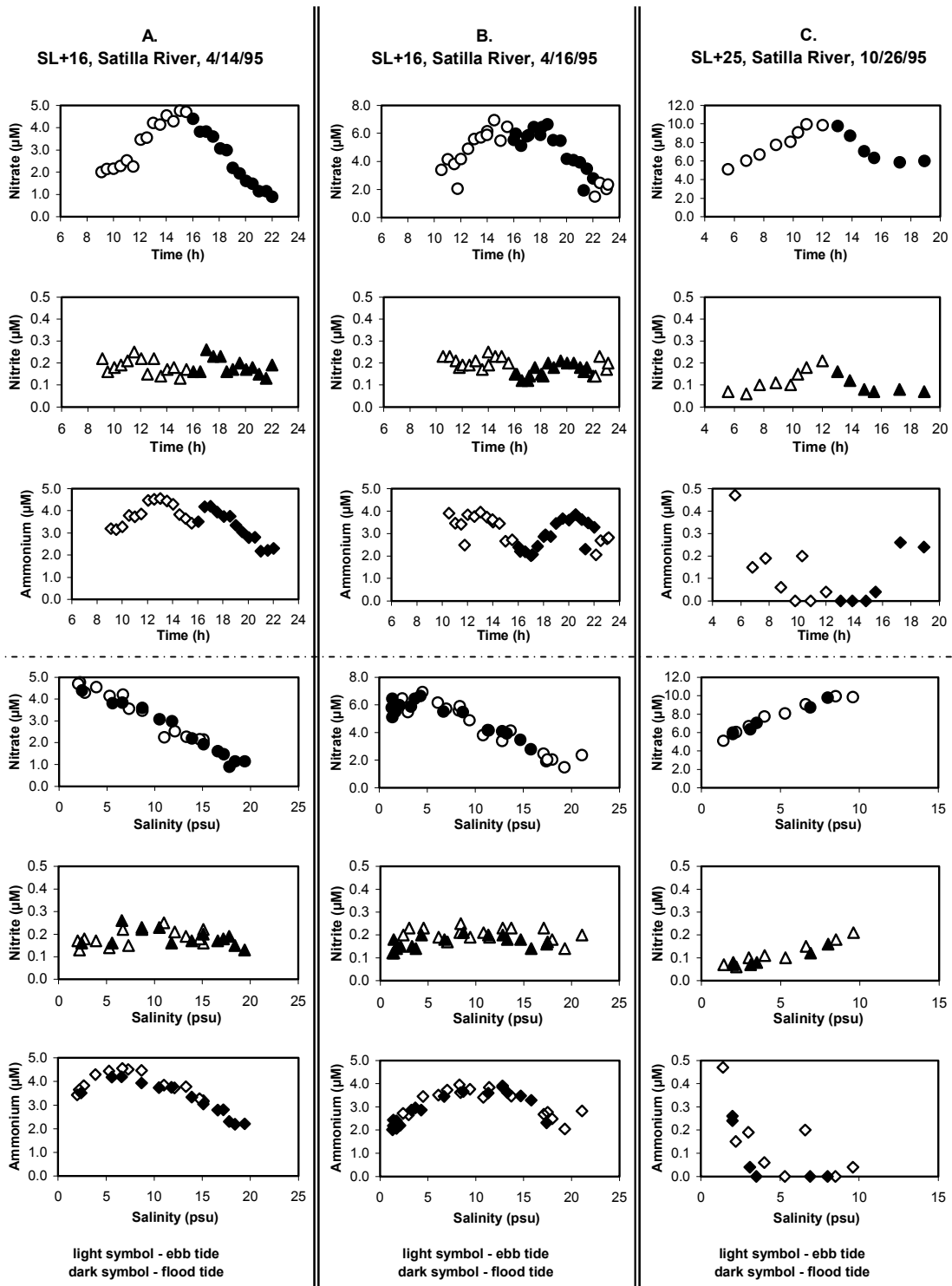


Fig. 3.9. Time and salinity series of NO_3^- , NO_2^- , and NH_4^+ concentrations during anchor stations in the Satilla River estuary. A. Anchor Station SL+16 (16 km upstream from the mouth), April 14 1995; B. Anchor Station SL+16, April 16 1995; C. Anchor Station SL+25 (25 km upstream from the mouth), October 26 1995.

AL+6.5, Altamaha River, 10/27/95

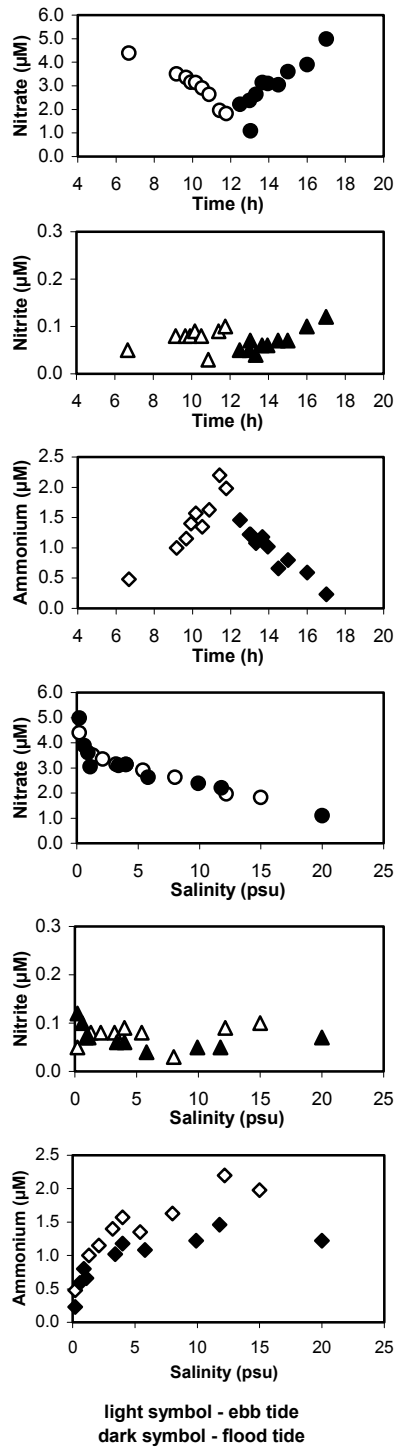


Fig. 3.10. Time and salinity series of NO_3^- , NO_2^- , and NH_4^+ concentrations during an anchor station at AL+6.5 (6.5 km upstream from the mouth) in the Altamaha River estuary, October 27 1995.

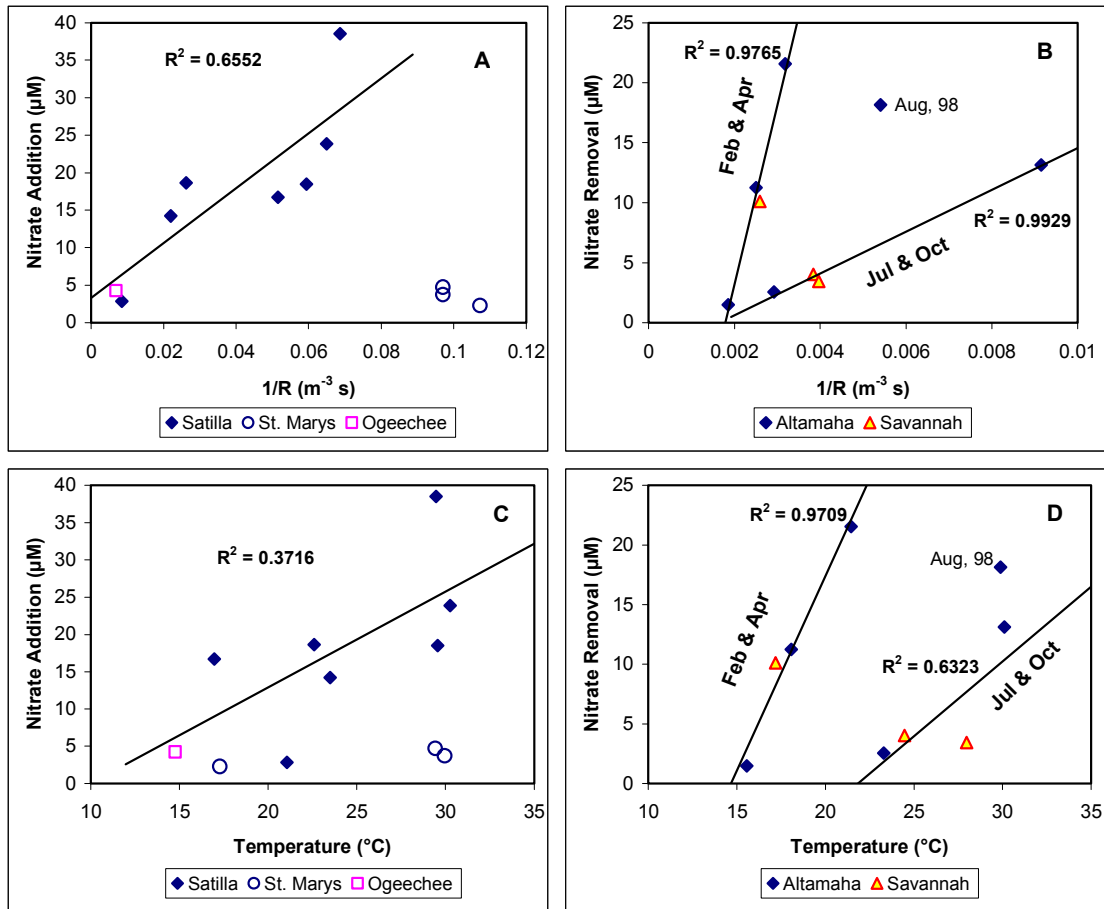


Fig. 3.11. Maximum estuarine NO_3^- addition or removal as a function of river discharge (R) and average temperature. A. Maximum NO_3^- addition vs. $1/R$ for Satilla, St. Marys and Ogeechee; B. Maximum NO_3^- removal vs. $1/R$ for Altamaha and Savannah; C. Maximum NO_3^- addition vs. temperature for Satilla, St. Marys and Ogeechee; D. Maximum NO_3^- removal vs. temperature for Altamaha and Savannah. Maximum NO_3^- addition in the coastal plain river estuaries was calculated by $C_{\text{max}}^* - C_{\text{river}}^*$. Maximum NO_3^- removal in the piedmont river estuaries was calculated by $C_{\text{max}}^* - C_{\text{sea}}^*$. In A and C, the solid lines are the linear best-fit of the data from the Satilla River estuary. In B and D, the data from the cold (Feb. and Apr) and warm months (Jul. and Oct.) are fit separately; the data point of Aug., 1998 is excluded from the linear fitting (see text).

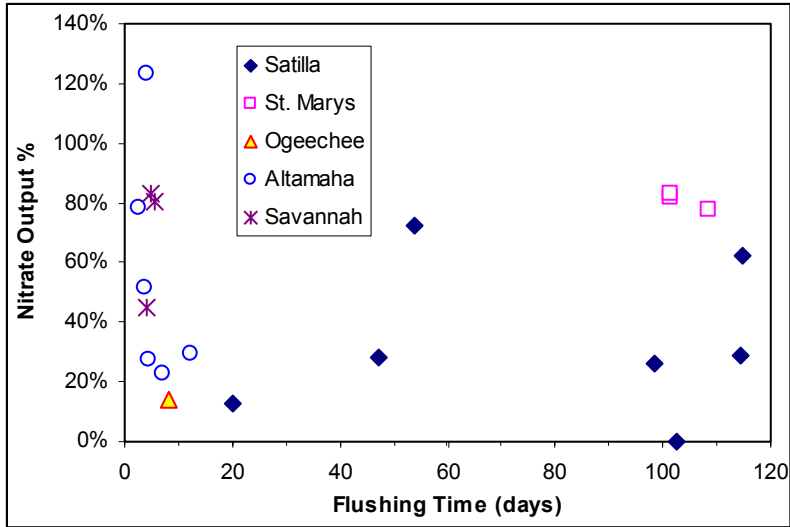


Fig. 3.12. Estuarine NO_3^- output as a percentage of the total input vs. estuarine flushing time. The total input for the coastal plain river estuaries was the sum of riverine input and estuarine addition; the total input for the piedmont river estuaries only included riverine input.

Tables

Table 3.1. Dates of research cruises conducted during the GARLMER project.

Satilla	St. Marys	Ogeechee	Altamaha	Savannah
4/8/1995		4/6/1995	4/7/1995	4/5/1995
4/14/95*			4/17/1995	
4/15/1995				
4/16/95*				
10/17/1995	10/18/1995	10/15/1995	10/16/1995	10/14/1995
10/25/1995			10/24/1995	
10/26/95†			10/27/95‡	
7/17/1996	7/18/1996	7/15/1996	7/16/1996	7/14/1996
7/18/1996	7/19/1996			
7/20/1996				
8/20/1998			8/29/1998	
8/28/1998				
2/5/1999	2/4/1999	2/2/1999	2/6/1999	2/1/1999

* Anchor SL+16 (SL is the abbreviation of the estuary, and +16 denotes the station is 16 km upstream from the mouth); † Anchor SL+25; ‡ Anchor AL+6.5

Table 3.2. Summary of NO_3^- fluxes calculated from the continuous estuarine mixing model. The river input flux is calculated as $C^*_{\text{river}} \times R$, where C^*_{river} is the effective concentration at the river end-member, and R is the river discharge. The addition flux is calculated as $(C^*_{\text{max}} - C^*_{\text{river}}) \times R$, where C^*_{max} is the maximum effective concentration along the salinity gradient. The removal flux is calculated as $(C^*_{\text{max}} - C^*_{\text{sea}}) \times R$, where C^*_{sea} is the effective concentration at the sea end-member. The estuarine output flux is calculated as $C^*_{\text{sea}} \times R$. All fluxes are in the unit 10^7 mmol d^{-1} .

Estuary	Cruise Date	Average Temperature (°C)	Discharge ($\text{m}^3 \text{ s}^{-1}$)	Flushing Time (d)	River Input	Addition (+) or Removal (-)	Estuarine Output
Satilla	4/15/95	21.1	117.9	20.2	4.84	2.91	1.00
	10/17/95	23.5	45.6	47.0	0.62	5.60	1.76
	10/25/95	22.6	38.2	53.9	0.88	6.16	5.11
	7/17/96	29.6	16.9	98.4	0.97	2.69	0.97
	7/20/96	30.3	15.4	102.4	0.77	3.17	-0.47
	8/20/98	29.5	14.6	114.5	1.12	4.85	1.74
	2/5/99	17.0	19.4	114.7	0.05	2.80	1.77
St. Marys	7/18/96	29.4	10.3	101.3	0.17	0.42	0.48
	7/19/96	30.0	10.3	101.3	0.23	0.33	0.47
	2/4/99	17.3	9.3	108.7	0.09	0.18	0.21
Ogeechee	2/2/99	14.8	145.8	8.1	0.70	5.35	0.84
Altamaha	4/7/95	18.1	400.2	3.7	79.95	-38.90	41.05
	4/17/95	21.5	313.9	4.6	80.77	-58.45	22.32
	10/16/95	23.3	341.8	3.9	42.25	-7.52	52.13
	7/16/96	30.1	109.3	12.2	17.62	-12.41	5.21
	8/29/98	29.9	184.9	7.2	37.54	-28.98	8.56
	2/6/99	15.6	538.2	2.7	31.98	-6.90	25.08
Savannah	4/5/95	17.2	385.5	4.1	61.29	-33.69	27.60
	10/14/95	24.5	260.6	5.6	46.76	-9.09	37.67
	7/14/96	28.0	252.2	4.8	43.64	-7.48	36.16

CHAPTER 4
INORGANIC CARBON DYNAMICS AND AIR-SEA CO₂ FLUX IN THE
SOUTHEASTERN CONTINENTAL SHELF OF THE UNITED STATES

Introduction

The coastal ocean, only 7% of the global ocean surface area, generates as much as 15-30% of oceanic primary production (Walsh, 1988; Wollast, 1993; Longhurst et al., 1995; Gattuso et al., 1998). The coastal ocean also accounts for 80% of organic matter burial, 90% of sedimentary mineralization and ca. 50% of calcium carbonate deposition (Mantoura et al., 1991; Pernetta and Milliman, 1995; Gattuso et al., 1998). In the past 30 years, an important scientific issue concerning the role of coastal oceans is whether these systems are net autotrophic or net heterotrophic (Smith and Hollibaugh, 1993; Gattuso et al., 1998; Mackenzie et al., 2000). It now appears that some continental shelf systems are autotrophic while estuaries and other nearshore systems are mostly heterotrophic (Gattuso et al., 1998). A similar but more directly testable question is whether the world's continental shelf acts as a source or a sink of CO₂ for the atmosphere. Walsh (1981; 1988) proposed that "biological export of shelf [organic] carbon [to the slope] is a sink of the global CO₂ cycle." The hypothesis has been evaluated on many ocean margins from the perspective of nutrient and organic matter biogeochemistry, particle flux measurements, and benthic recycling (Falkowski et al., 1988; Rowe et al., 1988; Smith et al., 1992; Reimers et al., 1992). While much has been learned, the issue is still controversial.

Continental shelves are the sites of intensive physical and biological processes from which large air-sea CO₂ gradients are expected (Mackenzie, 1991). Recent measurements of large CO₂ flux ($\sim 35 \text{ gC m}^{-2} \text{ yr}^{-1}$) into the East China Sea (ECS) over nearly all seasons allowed Tsunogai et al. (1999) to propose that the world continental shelf may act as a "continental shelf pump", which transfers about 1 Gt (10^{15} g) C yr⁻¹ of atmospheric CO₂ into the open ocean assuming that the other shelves behave similarly to

the ECS (also see Wang et al., 2000 and Chen et al., 2001 with a value of 0.3-1.0 Gt C yr⁻¹). The simulation of a general circulation model that parameterizes transport processes from the shelf to the deep ocean shows a smaller pump of 0.6 Gt C yr⁻¹ (Yool and Fasham, 2001). These values represent 20 – 50% of current oceanic uptake of anthropogenic CO₂ (Sarmiento and Gruber, 2002) and thus is significant in global carbon cycling. This shelf pump hypothesis is supported by earlier observation in the North Sea (Kempe and Pegler, 1991) and recent studies in the European Atlantic shelf (Frankignoulle and Borges, 2001) where the air-sea CO₂ gradient and annual flux are similar to the ECS. However, CO₂ fluxes measured in the U.S. Middle Atlantic Bight (MAB) suggested a much smaller pump (5 – 10 gC m⁻² yr⁻¹, Boehme et al., 1998; DeGrandpre et al., 2002).

Recent global oceanic monitoring and research projects such as Joint Global Ocean Flux Study (JGOFS) and World Ocean Circulation Experiment (WOCE) have established wide coverage and good quality of data for studying the CO₂ system in open oceans. Both observational and modeling strategies have been substantially improved during the 1990's, providing better understanding of the global carbon cycling and its linkage to the global warming issue, although problems such as uncertainty of the model prediction and simulation remain a challenge (Sarmiento et al., 2000; Sarmiento and Gruber, 2002). Compared to the studies of CO₂ systems in open oceans, CO₂ dynamics in coastal regions and continental shelves only received more attention in recent years (Frankignoulle et al., 1996a; Boehme et al., 1998; Van Geen et al., 2000; DeGrandpre et al., 2002; Wang et al., 2002b). Based on research conducted so far, coastal waters are almost exclusively characterized by large spatial and temporal variations of surface water

$p\text{CO}_2$ with values ranging from as high as a few thousand μatm to slightly lower than atmospheric level. In spite of the recent finding of large CO_2 sinks in the ECS and European Atlantic continental shelf, the fundamental question, how much the land margin area contributes to the global CO_2 budget, remains uncertain. One major challenge for studying the carbon cycling of coastal areas results from the complexity of the systems. The complex hydrographic setting in the coastal region is often a combined result of multiple river inputs, tidal mixing, coastal currents, upwelling, off-shore water intrusion, and sediment inputs.

To improve our understanding of the carbon cycling on the continental shelf and to test “continental shelf pump” hypothesis (Tsunogai et al., 1999), we initialized a seasonal CO_2 study along a cross-shelf transect in the central portion of the South Atlantic Bight (SAB), a subtropical continental shelf system off the southeastern United States. Much has been learned in terms of hydrology, ecology, biology, and sedimentology in the SAB through numerous studies during the last 30 years (Atkinson et al., 1996; Chen et al., 1999; Lee et al., 1991; Verity et al., 1993; Menzel, 1993; Pomeroy et al. 2000; Jahnke et al., 2000; Nelson et al., 1999; Moore, 1999; Moran et al., 1991). Studies concerning the CO_2 system in the SAB, however, were few.

In addition to the data presentation, the discussion of this study will focus on a few aspects of the carbon dynamics in the SAB. First, the annual CO_2 flux in the SAB will be estimated using seasonal measurement of sea surface CO_2 and daily wind record. Second, inorganic carbon export from the SAB to the open ocean will be evaluated based on a one-box steady-state model. Third, the SAB carbon budget will be discussed in the light of the new information obtained from TC-based respiratory rates, air-sea CO_2 flux,

and inorganic carbon export. Last, the “continental shelf pump” concept and governing mechanisms on the CO₂ flux in the SAB will be examined.

Study Site and Methods

Study Site. The study area (Fig. 4.1) is located in the central section of the South Atlantic Bight (SAB), which extends from West Palm Beach, FL, at 27 °N to Cape Hatteras, NC, at 35°N. The Gulf Stream, a major oceanic western boundary current, runs along its shelf break while a series of barrier islands and extensive salt marshes between the barrier islands and shoreline are major characteristics on its land side. Numerous small non-riverine embayments, blind tidal rivers, and riverine estuaries interacting through connecting waterways form a complex hydrology near shore. The SAB is traditionally divided into three regions extending from the coastline to the shelf break: the inner- (water depth < 20 m), mid- (water depth 20 – 40 m), and outer- (water depth 40 – 60 m) shelves. A coastal frontal zone (CFZ) usually forms between the 10 and 20 m isobaths (Menzel 1993; Pomeroy et al., 2000; Jahnke et al., 2000) (Fig. 4.1). Within the CFZ, near-shore water is turbid and contains accumulated discharge of the rivers and water exchanged with intertidal marshes (Pomeroy et al., 2000). Circulation and hydrology within the CFZ are strongly controlled by winds, semidiurnal tides, and freshwater inputs (Menzel, 1993). On the mid-shelf, influence of river discharge decreases while sub-surface water intrusion from the Gulf Stream occurs occasionally in summer (Menzel, 1993; Pomeroy et al., 2000; Atkinson et al., 1996). While entering the outer-shelf, the meanders and eddies created by the Gulf Stream primarily control the fluctuations of the circulation with a frequency of 2 to 14 days (Menzel, 1993).

Upwelling or water intrusion may occur at any time of the year and bring sub-surface water of the Gulf Stream onto the outer-shelf of the SAB (Atkinson et al., 1987; Lee et al., 1991; Menzel, 1993). In general, the advection in the SAB is in the north-south direction, especially for near-shore water.

Transects and Stations. The cross-shelf transect, which is located in the central part of the SAB, crosses the continental shelf off Wassaw Sound, Georgia, to the 60-m isobath close to the shelf break (Fig. 4.1). Four cross-shelf cruises were conducted on December 6 – 7, 2000, April 29, 2002, June 17, 2002, and October 2 – 3, 2002, corresponding to winter, spring, summer, and fall conditions, respectively. During the December and April cruises, the research vessel (R/V Blue Fin or R/V Savannah) only reached S13 and S14 (about 35-m isobath), respectively. There were 13 sampling stations (S01 – S13) during the December cruise, 15 stations (S01 – S14, plus S12a; Fig. 4.1) in April, and 17 stations (S01 – S17) in June and October. S02 – S08, S09 – S14, and S15 – S17 are inner-shelf, mid-shelf, and outer-shelf stations, respectively. The data between S01 and S02 is excluded from the discussion for the SAB since these sites are dominated by the marsh signal. To investigate the along-shore gradient of the CO₂ system, an underway survey with 6 sampling stations was also conducted on May 1, 2002 along the 10-m isobath from outside Dobby Sound to Wassaw Sound (Fig. 4.1).

Underway Measurements and Discrete Sampling. Surface sea water was continuously pumped on-board from the bottom of the research vessel (2.6 m below sea surface) and was measured for *p*CO₂, dissolved oxygen (DO), relative fluorescence, temperature, and salinity during each survey. *p*CO₂ was measured by an automated system that consists of a shower-head and laminated-flow equilibrator and an infrared

analyzer (Li-Cor Model Li-6252)” system (see technical details in Chapter 2). All $p\text{CO}_2$ measurements were corrected for water vapor pressure, and final results reflected $p\text{CO}_2$ under 1 atmospheric pressure with 100% saturation of water vapor at *in-situ* temperature. DO was measured with a YSI 6000UPG Multi-Parameter Water Quality Monitor (Yellow Spring inc., CO). The YSI sensor was calibrated every six hours on board. Precision for DO was $\pm 6.3 \mu\text{mol O}_2 \text{ kg}^{-1}$ or 2% in saturation state. During the October cruise, a WTW Oxi340 DO electrode (WTW inc., FL) was used to replace the YSI sensor for DO underway measurements with a precision of $\pm 3 \mu\text{mol O}_2 \text{ kg}^{-1}$. Relative fluorescence, temperature, and salinity were measured by a flow-through SEABIRD CTD (SEABIRD Inc., WA). The fluorescence sensor was not calibrated. The climatological (e.g. wind speed) and navigational (e.g. GPS and ship track) data were available through ship’s log. All underway data were averaged to one-minute interval for presentation and flux calculation.

Discrete sea surface water samples for total dissolved inorganic carbon (TC), total alkalinity (TA), and nutrients (ammonium, nitrate + nitrite, phosphate, and silicate) were collected at each station along the cross-shelf and the along-shore transects (Fig. 4.1) through an inlet of the on-board pumping system. Nutrient samples were not taken during the December cruise. TC and TA samples were taken in 125 ml acid-cleaned glass bottles, and 10 μl of saturated HgCl_2 solution was added for preservation. These samples were stored at 7°C until laboratory analysis within 1 – 3 weeks. The sampling bottles for TC and TA were allowed to overflow for at least twice their volumes to allow only minimal contact of water with the air. The nutrient samples taken by plastic syringes were immediately filtered into 25 ml PVC bottles through 0.45 μm syringe filters. 2 – 3 drops

of chloroform were added to each bottle, and the samples were stored at $-4\text{ }^{\circ}\text{C}$ until laboratory analysis.

In addition to the underway measurements and surface water sampling, hydrographic stations (S04, S08, S14, S17) were chosen along the cross-shelf transect. CTD profiles were taken at these stations during the April, June and October cruises. Discrete water samples for TC, TA, and nutrients were also taken with Niskin bottles at various depths based on the CTD profiles. The sampling procedures were the same as the surface sampling.

Respiration Incubation. During the April cruise, incubations were conducted on board with sea surface waters from two stations, S04 and W27 (Fig. 4.1), to measure respiratory rates for the inner- and mid-shelf regions of the SAB. For the June cruise, the incubation stations were at S04 and WL01 (Fig. 4.1). WL01 was located to the south of the cross-shelf transect at the mid-shelf region. S04 and S14 were chosen to be the inner- and mid-shelf incubation stations for the October cruise. In the December, 2002, a supplementary off-shore cruise was conducted to measure respiratory rates at SS0 (inner-shelf) and S10 (mid-shelf) (Fig. 4.1).

The respiratory rates were measured from changes in TC concentrations over the time of incubation. The method involved on-board incubation in the dark, which consisted of 2 groups of treatments. Seawater was collected into a 50 liter carboy and mixed well. The water was subsequently overflowed into 6 1-L opaque glass bottles, to three of which were added 200- μl of saturated HgCl_2 solution to stop biological activity and to document initial conditions of the incubation. The other three bottles served to measure changes during the incubation. Each bottle was wrapped with black plastic bag

and placed inside an opaque ice chest flowed with running surface seawater. The incubation lasted 24 to 36 hours. Immediately after termination of the incubation, temperature and salinity were measured with the YSI probe. TC and TA samples were collected for later analysis.

Sample Analysis. TC was measured through an automated TC analyzer developed by Dr. Cai's group, and a technical note describing the details of the analyzer is available upon request. The system was calibrated using certified reference material (CRM) from A. G. Dickson at Scripps Institution of Oceanography, La Jolla, CA. The automated TC analyzer used small-volume (0.1-1.0 ml) samples, and had rapid (less than 5 minutes per analysis) measuring time with a precision of 0.1 – 0.15%. The system consisted of a non-dispersive infrared CO₂ analyzer (Li-Cor 6252), a precision digital syringe pump, a gas flow controller, and a CO₂ stripping reactor. The pumping system was used to pump the sample (normally 0.5 ml) and acid (1 ml of 10 % H₃PO₄) into the reactor after all of the solution in the reactor left from previous analysis was purged. The CO₂ extraction system consisted of a gas flow line, the reactor, and a gas-drying unit. The reactor was designed to strip CO₂ efficiently from a small volume of sample. The body of the reactor was wrapped by an electronic cooling system which was set below ~3°C, and thus a low water vapor pressure was maintained in the reactor. The carrier gas was further dried through a Mg(ClO₄)₂ plug (about 10 ml). Several solenoid valves were used to direct the gas flow. The infrared CO₂ detector and its internal integrator were used to measure CO₂ gas concentration. The detector measured dry gas samples and had a baseline noise of < 0.3 µatm at the flow rate we used. Finally, TC was calculated by integrating the area

under the CO₂ curve over time (< 2 mins). The entire procedure was controlled by a computer via RS232 (Cai unpub.).

TA was determined in a 50-ml sample by Gran titration (Gran 1952) to an endpoint pH of 3.2 using HCl solution. The titrations were carried out by an automatic device using a Kloehe digital syringe and drive modules (Kloehe, Las Vegas, Nevada). The HCl standard solution was calibrated with CRM from A. G. Dickson. The precision of the titration was 0.1 – 0.15%. The results reported in $\mu\text{mol kg}^{-1}$ instead of $\mu\text{eq kg}^{-1}$, which one may read as $\mu\text{mol HCl}$ used for titration of 1 kg of sample solution.

Nutrient samples were measured by Virginia Institute of Marine Sciences Analytical Service Center (<http://www.vims.edu/admin/asc/>) based on standard colorimetric methods. Detailed analytical principles and procedures can be obtained by contacting Carol Pollard (pollard@vims.edu) or through the webpage list above. The analytical precisions were 0.1, 0.02, 0.06, 0.02, 0.9 μM for ammonium, nitrite, nitrate + nitrite, phosphate, and silicate, respectively.

Air-sea CO₂ Flux. The CO₂ fluxes across the air-sea interface were calculated by the following widely used one-dimensional stagnant-film model:

$$\text{CO}_2 \text{ Flux} = k\beta(p\text{CO}_{2w} - p\text{CO}_{2a}) \quad (\text{Equation 4.1})$$

where k is the gas transfer velocity; β (Bunsen coefficient) is the solubility of CO₂ at given temperature and salinity (Weiss 1974); $p\text{CO}_{2w}$ and $p\text{CO}_{2a}$ represent the partial pressure of CO₂ in surface water and overlaying air, respectively. Most uncertainty in this calculation results from estimation of gas transfer velocity (k) which is empirically derived from sea surface wind speed. Two sets of most frequently used “ k vs. wind speed” relationships (Wanninkhof, 1992; Liss and Merlivat, 1986) were applied for this

study. We hereinafter use W and LM to refer to the k parameterizations by Wanninkhof (1992) and Liss and Merlivat (1986), respectively. Gas transfer velocity estimated from LM (k_{LM}) is lower than that from W (k_W), particularly for lower to intermediate wind speeds ($0 - 6 \text{ m s}^{-1}$). At higher wind speed, k_{LM} and k_W are similar. The two estimates likely give the bound on the CO_2 fluxes, and were used for most of the recent CO_2 studies (Boehme et al., 1998; Frankignoulle and Borges, 2001; DeGrandpre et al., 2002).

Results

Cross-shelf Underway Results. Sea surface $p\text{CO}_2$ for all seasons exhibited a large cross-shelf gradient within the coastal frontal zone (Fig. 4.2), and relatively small changes occurred at mid- to outer-shelf. Underway measurements of DO and relative fluorescence also confirmed that there was a hydrographic front near shore all the time, while its exact location varied (Fig. 4.2). Strong temperature- $p\text{CO}_2$ correlation has often been observed in the open ocean (Tans et al., 1990; Goyet et al., 1991; Takahashi et al., 1993; Hood et al., 1999; Bates et al., 2000.), while some coastal studies have noted a strong correlation between $p\text{CO}_2$ (or $f\text{CO}_2$) and DO (DeGrandpre et al., 1996, 1997; Boehme et al., 1998). Regression analyses for our data set revealed that both $p\text{CO}_2$ -temperature and $p\text{CO}_2$ -DO relationships were highly variable in space (across shelf) and with time (four seasons) for the SAB. One exception occurred during the June cruise when DO negatively co-varied with sea surface $p\text{CO}_2$ across the entire shelf of the SAB (Fig. 4.2). Non-consistency of the two relationships suggests that sea surface $p\text{CO}_2$ across the shelf water in the SAB is likely controlled by multiple processes with different spatial and temporal scales.

A seasonal progression of sea surface $p\text{CO}_2$ was clearly seen in Fig. 4.2. Although a small portion of near-shore surface water (inside Wassaw Sound) in winter was over-saturated with $p\text{CO}_2$ (as high as $500 \mu\text{atm}$) relative to the atmosphere ($370 \pm 10 \mu\text{atm}$), under-saturation dominated all three regions of the SAB (Table 4.1). The area-weighted mean $p\text{CO}_2$ during the winter cruise was only $300 \mu\text{atm}$ with a mean air-sea $p\text{CO}_2$ gradient of $-70 \mu\text{atm}$ (Table 4.1), indicating that the SAB acted as a strong CO_2 sink in this season. During the April cruise, sea surface $p\text{CO}_2$ became over-saturated along the entire cross-shelf transect with a $p\text{CO}_2$ range of $424 - 800 \mu\text{atm}$ and a mean air-sea gradient of $137 \mu\text{atm}$ (Fig. 4.2 and Table 4.1). In June, sea surface $p\text{CO}_2$ ranged from 414 to $1200 \mu\text{atm}$, and its over-saturation enhanced. Mean sea surface $p\text{CO}_2$ declined from $550 \mu\text{atm}$ in June to $450 \mu\text{atm}$ in October while over-saturation still prevailed (Fig. 4.2 and Table 4.1).

For all seasons sampled, the maximum sea surface $p\text{CO}_2$ always occurred inside Wassaw Sound (Fig. 4.1), while the minimum were observed at the mid to outer-shelf. Super-saturated $p\text{CO}_2$ of surface water has often been observed along the coast and within the estuaries (Frankignoulle et al., 1996a and b; Kemp et al., 1997; Smith and Hollibaugh 1997; Cai et al., 2000; Raymond et al., 2000). The Georgia coastal systems are generally surrounded by extensive intertidal marshes. The ebbing water, after it has flooded the marsh area, usually brings a high $p\text{CO}_2/\text{TC}$ signal into the coastal water, even during winter (Cai and Wang, 1998; Cai et al., 1999; Chapter 5). The seasonal pattern of sea surface $p\text{CO}_2$ in the SAB (low in winter and high in summer) is, however, opposite to the observation in the European Atlantic shelf (Kemp et al., 1997; Frankignoulle and Borges, 2001) and in the East China Sea (Tsunogai et al., 1997 and 1999; Wang et al.,

2000). On the other hand, the Middle Atlantic Bight (MAB), to the north of the SAB, behaves somewhat in between (Boehme et al., 1998; DeGrandpre et al., 2002), and its over-saturation during warm months is much lower than that of the SAB.

TC, TA and Nutrients. Except for October, 2002, cross-shelf TA-salinity distributions (Fig. 4.3) showed conservative or near-conservative mixing between in-shore water and off-shore water during all other cruises. The causes of apparent non-conservative mixing behavior of TA in October may be multiple. The primary processes that affect alkalinity are calcium carbonate dissolution/precipitation, anaerobic respiration, and water mixing. Aerobic respiration and photosynthesis are known to have little effect on alkalinity (Brewer and Goldman, 1976). The water-column conditions did not seem to favor anaerobic processes, since all near-shore water had DO above 80%. Carbonate dissolution/precipitation and mixing with another near-shore water mass seemed to be equally possible for explaining this apparent bending from the two end-member mixing curve. Meanwhile, this small event occurred inside Wassaw Sound where elevated export of TA from the salt marsh in fall (Chapter 5) may also have influence on the TA mixing. TA at the off-shore end-member was maintained at ca. 2400 $\mu\text{mol/kg}$ with a salinity of 36.2 to 36.5; it showed little seasonal change although the summer and fall cruises reached stations much further off-shore than did the winter and spring cruises. The in-shore end-member of TA exhibited seasonal variability at a similar salinity (S) (e.g. S = 31.6, TA = 2170 $\mu\text{mol kg}^{-1}$ in December; S = 31.7, TA = 2246 $\mu\text{mol kg}^{-1}$ in April; S = 31.1, TA = 2157 $\mu\text{mol kg}^{-1}$ in October).

TC-salinity plots (Fig. 4.3) suggested that significant difference existed between seasons. TC seemed to mix conservatively during the winter cruise, while apparent

removal/addition occurred in other seasons. Conservative (or near-conservative) behavior of TA and non-conservative behavior of TC during mixing (in three out of four seasons) indicated that calcium carbonate dissolution/precipitation is negligible most time of the year because this process changes TA and TC in a ratio of 2:1 (Takahashi et al., 1993; Boehme et al., 1998; Ternon et al., 2000). Similar to TA, TC at the off-shore end-member did not show noticeable seasonal changes, and averaged at $2052 \pm 20 \mu\text{mol/kg}$ with a salinity of 36.2 to 36.5. Contrarily, in-shore TC showed large variability among seasons. For example, TC varied from $1974 \mu\text{mol kg}^{-1}$ at $S = 31.6$ in December to $2151 \mu\text{mol/kg}$ at $S = 31.7$ in June. This nearly $200 \mu\text{mol kg}^{-1}$ difference in TC at the in-shore end-member was much greater than that in TA (less than $100 \mu\text{mol kg}^{-1}$).

Supplementary nutrient data in April, June, and October were shown in Fig. 4.4. NO_x ($\text{NO}_2 + \text{NO}_3$) concentration was below $1 \mu\text{mol kg}^{-1}$ in April and June at surface water across the shelf of the SAB, while its concentration reached $5 \mu\text{mol kg}^{-1}$ at the in-shore end-member in October. Phosphate concentrations at the in-shore end-member also increased from below $0.6 \mu\text{mol kg}^{-1}$ in April to over $1 \mu\text{mol kg}^{-1}$ in October. At the off-shore end-member, surface phosphate concentrations were low ($< 0.2 \mu\text{mol kg}^{-1}$) and varied little between cruises. Non-conservative mixing behavior was clear during all cruises for phosphate (Fig. 4.4). In addition to biological activity, particle absorption/desorption also likely attributed to the non-conservative behavior of phosphate during mixing (Froelich, 1988). Large removal/addition of phosphate usually occurred at the inner-shelf (Fig. 4.4), which was consistent with high turbidity of near-shore water. Property-salinity plots also indicated that silicate mixed non-conservatively. From April to June, silicate concentration at the in-shore end-member almost doubled (30 to $54 \mu\text{mol}$

kg⁻¹), while it decreased from June to October. The surface water was almost free of silicate at the off-shore end-member for all surveys. In October, the possible third end-member mixing may also influence the mixing curves of nutrients.

Along-shore Gradient. Before the research vessel turned toward Wassaw Sound, sea surface $p\text{CO}_2$ varied within 8% of its value during the along-shore survey in May, 2002 (Fig. 4.5). Along-shore variation of TC and TA was even smaller (< 1%). Underway DO, fluorescence, salinity and temperature also showed little along-shore variations (Fig. 4.5). Unlike the large cross-shelf gradients mostly occurring within the CFZ (Fig. 4.2), the along-shore survey suggested that the along-shore gradients were small and surface water was uniform. This is consistent with along-shore water advection in the SAB (Menzel, 1993). Large cross-shelf variability and weak along-shore variability are actually common features for many shelf regions mostly due to a strong cross-shelf density gradient generated by coastal freshwater inputs and buoyancy-driven along-shore flow (Münchow and Garvine, 1993; Chen et al., 1999). As for the CO_2 system, such a pattern is also evident in the U.S. Middle Atlantic Bight (DeGrandpre et al., 2002) and the East China Sea (Tsunogai et al., 1999). All of these results provide us confidence to integrate cross-shelf CO_2 and TC fluxes to the entire SAB in the later discussion.

Air-sea CO_2 Fluxes. To estimate the annual air-sea CO_2 fluxes in the SAB, the daily fluxes were first calculated using cruise mean $\Delta p\text{CO}_2$ (Table 4.1) daily interpolated over an annual cycle and the daily wind record obtained from NOAA Buoy 41008 (Gray Reef; Fig. 4.1). Since the flux calculation requires 10-m wind speed (u_{10}) (Wanninkhof 1992; Liss and Merlivat, 1986), the daily wind speed from Buoy was adjusted to 10-m

from its original 5-m measurements (u_5) ($u_{10} = 1.06 \times u_5$; Wanninkhof pers. comm.). The daily fluxes were then integrated to annual fluxes for each region of the SAB and the entire SAB (Table 4.2). Although many coastal CO₂ studies (e.g. DeGrandpre et al., 2002; Frankignoulle and Borges, 2001; Boehme et al., 1998) have used 360 μatm as the atmospheric CO₂ level, we believe that 370 μatm is more realistic for two reasons. First, it is consistent with our on-board measurements. LiCOR-measured atmospheric CO₂ during all cruises averaged at $370 \pm 10 \mu\text{atm}$ with larger values occurred mostly near shore and lower values off shore. Second, the study area is close to coastal marsh systems where higher atmospheric CO₂ concentrations (380 – 390 μatm) were often observed during our cruises.

All three regions of the SAB were annual net sources of CO₂ to the atmosphere (Table 4.2). The annual areal flux for the inner-shelf was 3 – 4 times the mid- or outer-shelf value. This is consistent with the finding that coastal marshes discharge large amounts of inorganic carbon to the near shore water that supports surface water CO₂ degassing (Cai et al., 1999; Cai et al., 2000; Chapter 5). Annual CO₂ fluxes at the mid- and outer-shelves, however, only differed slightly (Table 4.2). The flux calculation revealed that the SAB was a strong net atmospheric CO₂ source of $29.8/17.3 \text{ gC m}^{-2} \text{ yr}^{-1}$ or $2.7/1.6 \times 10^{12} \text{ gC yr}^{-1}$ (W/LM) (Table 4.1). This conclusion would be strengthened by using an atmospheric $p\text{CO}_2$ of less than 370 μatm for the flux calculation. The annual CO₂ flux in the SAB is similar in magnitude to those estimated in the East China Sea and European Atlantic shelf ($\sim -35 \text{ gC m}^{-2} \text{ yr}^{-1}$ from W method), while they differed in direction.

Carefully choosing wind record is a major step to reduce uncertainty in flux calculation since the gas transfer velocity (k) is calculated from wind speed. The wind record from mid-shelf Tower R2 adjacent to the surveyed transect (Fig. 4.1) was compared with the Buoy 41008 record used for the flux calculation. R2 wind speed was measured at 50-m (u_{50}). If using the R2 wind speed, after adjusting the 50-m data to 10-m ($u_{10} = 0.88 \times u_{50}$; Wanninkhof pers. comm.), the flux calculation only has a 2% difference from the results listed in Table 4.2. We chose Buoy 41008 data because they were more complete. Efforts were also taken to use instantaneous ship-board wind speed during each cruise to estimate CO_2 flux for comparison. In this practice, daily mean CO_2 flux instead of mean $\Delta p\text{CO}_2$ was first calculated for each cruise and was interpolated over an annual cycle. The annual flux by this treatment was 60% lower than the result in Table 4.1. Such a large difference is primarily a combined result of low wind speed during the cruises, limited temporal coverage of wind, and the non-linear property between wind speed and flux. Therefore, one should avoid using ship-board wind speed to calculate annual CO_2 flux as it may significantly bias the result. Finally, current and previous (DeGrandpre et al., 2002) studies both found that averaging wind speed (hourly, daily, and monthly) would lead to little uncertainty in the CO_2 flux calculation.

In our case, the CO_2 fluxes estimated from Wanninkhof's and Liss and Merlivat's parameterizations of gas transfer velocity (k) differ by 43% on average (Table 4.2). Such a significant difference has been recognized by numerous past CO_2 studies, and has been identified as a major source of uncertainty of calculating CO_2 flux (e.g. Wanninkhof, 1992; DeGrandpre et al., 2002). On the other hand, the uncertainty induced by averaging $p\text{CO}_2$ within each region of the SAB was similar to that by choosing different k

parameterizations (Table 4.2). Such an uncertainty mainly reflects the cross-shelf variation of sea surface $p\text{CO}_2$. In the along-shore direction, $p\text{CO}_2$ variation would lead to significantly smaller uncertainty as discussed earlier (Fig. 4.5). Overall, the uncertainty associated with the flux calculation in this study is likely 40 – 50% for either variability of $p\text{CO}_2$ or different parameterizations.

Discussion

Inorganic Carbon Export to the Open Ocean. Subsurface transport of TC to the open ocean via isopycnal mixing was proposed to be the key process of maintaining the “continental shelf pump” or the uptake of CO_2 from atmosphere at sea surface on the shelf (Tsunogai et al., 1999). In order to examine the “shelf pump” and to build carbon balance in the SAB, TC export from the SAB into the open ocean was estimated based on field measured TC concentrations and the procedure that has been used in the East China Sea (Tsunogai et al., 1997). The method is basically a one-box model approach which assumes the system is at the steady-state and water mixing only involves two end-members. According to the TA data (Fig. 4.3), two end-member mixing likely occurs most time of the year in the SAB. The in-shore end-member in the SAB is the water influenced by river discharge and marsh exchange and shows large seasonal variability; however, the off-shore end-member is relatively stable (Fig. 4.3). The procedure only needs the definition of the off-shore end-member, and thus avoids possibly large uncertainty in choosing the in-shore end-member.

The method uses normalized TC (NTC) and excess NTC (ENTC) concepts combining system residence time to evaluate TC export rate. To calculate NTC, salinity

and TC at the off-shore end members were first determined based on the sampling results of TC and TA (Fig. 4.3). In cases where several data points were clustered around end-members, an average was taken with a standard deviation less than 0.15 % of TA and TC values. The results are listed as follows (TC and TA are in the unit of $\mu\text{mol/kg}$):

Off-shore end-member:

Dec. 2000	S = 36.465; TC = 2077.3; TA = 2398.9
Apr. 2002	S = 36.387; TC = 2065.3; TA = 2388.5
Jun. 2002	S = 36.272; TC = 2043.9; TA = 2402.5
Oct. 2002	S = 36.260; TC = 2027.8; TA = 2416.8

Although the surveys did not reach the shelf-break in December and April, the difference in off-shore end-members between these two cruises and the June cruise was rather small. We herein assume that no appreciable seasonal change occurs at the open ocean end-members, and mid-shelf water is undifferentiable from the Gulf Stream water in terms of TC and salinity. Both assumptions likely hold in the SAB according to our data (Fig. 4.3) and previous studies (Menzel, 1993). S15 – S17 were then assumed to have the same TC concentrations and salinity as the farthest off-shore station (S13 or S14) for the December and April cruises. The field measured TC was first normalized to the off-shore end-member salinity (S_n) ($\text{NTC} = \text{TC}/S \times S_n$) to eliminate mixing effect. ENTC was the difference between NTC at each station and NTC at the off-shore end-member; therefore, ENTC at the off-shore end member is zero by definition. In other words, ENTC is the amount of TC that exceeds the open-ocean value after correction for mixing. The calculated ENTC for all cruises was presented in Fig. 4.6, and depth and distance weighted mean ENTC for each cruise was listed in Table 4.3. Under a steady state where

terrestrial TC input to the SAB equals to its export to the open ocean, the time to replace the total ENTC inventory will be the residence time of the SAB. Such a concept reflects the definition of the residence time for a system at steady-state. The export rate of TC (R_{TC}) from the SAB to the open ocean is then estimated using weighted mean ENTC ($ENTC_{wmean}$), mean residence time (τ), and total volume (V) of the SAB.

$$R_{TC} = ENTC_{wmean} \times V / \tau \quad (\text{Equation 4.2})$$

where $\tau = 3$ months and $V = 2470 \text{ km}^3$ (Menzel, 1993). The estimated R_{TC} for each cruise and the annual mean was listed in Table 4.3. Using the same procedure, TA export from the SAB to the open ocean was also evaluated (Table 4.3).

The uncertainty associated with this method comes from several sources in addition to possible non-steady state of the SAB. First, the residence time likely varies with seasons in the SAB. If we choose τ to be 60 days in winter and spring (possible faster turnover in winter and spring), 120 days for summer, and 90 days for fall, the calculated export rate would be 17% more than if using the mean residence time of 3 months (Table 4.3). Second, the assumption that the off-shore end-members in December and April are the same as the mid-shelf water (S13 or S14) would induce uncertainty. However, if using the small salinity changes between S14 and S17 in June and October to linearly extrapolate the off-shore end-members in December and April, the relative difference is <5%, suggesting such an assumption should lead to small uncertainty. Third, only surface water TC and TA measurements were used in this calculation because limited water samples were collected at depth. Unlike temperature and salinity, eight profiles in April and June did not show a noticeable gradient, and the ratios of TC and TA at depths to TC and TA at surface water were between 1.000 and 1.004. For the October

cruise, the ratios were larger (1.018 – 1.055). In winter (December), the water column is considered to be well-mixed, thus no vertical TC gradient was expected (Menzel, 1993). Therefore, the uncertainty associated with vertical gradients should also be small. Last, limited temporal and spatial (along-shore) coverage of the data set may generate uncertainty. As discussed earlier, the along-shore gradient of the CO₂ system should be negligible suggesting the associated uncertainty is small. With respect to limited temporal coverage of the data, our results may be an underestimate because the salt marsh maintains a high rate of TC export to the SAB in summer and fall, and even in November (Chapter 5), while our data only give the snap-shots in June and October. Based on these uncertainty analyses, the annual export rates of TC and TA (Table 4.3) may represent their lower limits.

Annual Respiration in the SAB. The annual water-column respiration rate was evaluated in the SAB from our on-board TC-based incubation (measuring TC changes during respiration incubation). The incubation results (Table 4.4) showed that respiratory rates were virtually identical in April and June for both inner-shelf and mid- to outer-shelf stations but significantly lowered in October and December. The mean respiratory rate for the inner-shelf (S04) in April and June was $212.1 \pm 31.2 \text{ mg C m}^{-3} \text{ d}^{-1}$, or $0.74 \pm 0.11 \text{ } \mu\text{M O}_2 \text{ h}^{-1}$ if using a respiratory quotient of 1 (Jahnke et al., 2000; Hopkinson, 1985). This was similar to the mean summer value of previous O₂-based measurements (measuring O₂ changes during respiration incubation) (Griffith and Pomeroy, 1995; Table 4.5). The mid- to outer-shelf in April and June (W27 and WL01) had a mean respiratory rate ($60.8 \pm 16.6 \text{ mg C m}^{-3} \text{ d}^{-1}$, or $0.21 \pm 0.06 \text{ } \mu\text{M O}_2 \text{ h}^{-1}$) of only 1/6 of O₂-based rates ($1.3 \pm 0.28 \text{ } \mu\text{M O}_2 \text{ h}^{-1}$) (Table 4.5). Our October and December rates for inner-shelf were

significantly lower than mean O₂-based rates in winter, while their mid- to outer-shelf values fell in the lower range of previous measurements on the outer-shelf and in Georgia estuaries in winter (Table 4.4 and Table 4.5). The annual mean respiratory rates for the inner- and mid- to outer-shelf were 139.2 ± 30.8 and 40.8 ± 17.7 mg C m⁻³ d⁻¹, respectively (Table 4.4). Integrating the seasonal rates annually using the water volume of the SAB (Menzel, 1993) and assuming equal number of days for each season, the annual respiratory rate in the water column was $4.72 \pm 1.73 \times 10^{13}$ gC (Table 4.4).

We are not aware of significant systematic bias and artifacts in this TC-based incubation method. All of our measurements have showed good reproducibility (variance of the measurements were small, Table 4.4) at all incubation sites. The small changes of TC during the October and December incubations at mid- to outer-shelf were close to the detection limit of the TC sample analysis (0.1 to 0.15%). However, the difference of measured respiratory rates in October and December between this TC-based and the O₂-based methods (Table 4.4 and Table 4.5) was much larger than analytical errors. O₂ changes had also been measured during our incubations using DO electrode (YSI or WTW) for comparison (data not shown due to possible large uncertainty from the instruments). These concurrently measured O₂-based rates were generally even smaller than the TC-based rates.

The previous O₂-based rates reflect the multiple-year average and do cover a large range, while our measurements fall in its lower range (Griffith and Pomeroy 1995; Pomeroy et al., 2000). The O₂-based method has been widely used for measuring respiratory rates for decades. Although this method has its potential problems, such as non-linear property of O₂ decrease and H₂O₂ production/decomposition, the associated

errors are generally small under careful operation (Griffith and Pomeroy, 1995; Pomeroy et al., 1994; Pomeroy et al., 1995; Pamatmat, 1997). A fixed C-to-O₂ ratio, usually a measured respiratory quotient, has to be used to convert O₂-based respiratory rates to C-based values. This ratio is believed to be variable in terms of time, space, and respiratory pathways (Hargrave and Phillips, 1981; Howes et al., 1984; Hopkinson, 1985; Williams and Robertson, 1991), which may induce some errors. However, none of these causes seem to be significant enough to explain the large difference between previous O₂-based and our TC-based rates. Further study is needed to examine the difference between the two methods. On the other hand, the TC-based incubation is a direct and synoptic method to measure inorganic carbon changes during respiration without worrying C-to-O₂ converting ratio. Therefore, respiratory incubation based on TC measurements should have advantages over O₂ measurements while using carbon as a metabolic currency to evaluate energy and material flow through a system.

Carbon Balance and Heterotrophy in the SAB. Previous biogeochemical and oceanographic studies have tried to build an organic carbon balance in the SAB by measuring and integrating shelf-wide primary production and respiration. However, the results indicate that there is a large imbalance between the amount of organic carbon broken down (respiration) and the amount of organic carbon produced (primary production) and imported (river, benthic, and atmosphere inputs) in the SAB (Menzel, 1993; Jahnke et al., 2000; Pomeroy et al., 2000). The total primary production on the SAB continental shelf was reported to be 44×10^{12} gC yr⁻¹, in which 35×10^{12} gC yr⁻¹ comes from water-column production (Menzel, 1993), and the sea floor contributes 9×10^{12} gC yr⁻¹ (Jahnke et al., 2000). If using recently reported O₂-based respiratory rates

(Pomeroy et al., 2000; Table 4.5) and a respiratory quotient of 1 (Hopkinson, 1985; Jahnke et al., 2000), water-column respiration is ca. 230×10^{12} gC yr⁻¹. This is over 5 times the shelf-wide primary production. Apparently, the SAB respire more organic carbon than it produces, implying that the system is net heterotrophic annually and that allochthonous sources of organic carbon must contribute the imbalance between respiration and primary production.

Combining our TC-based respiratory rates, estimated TC export, CO₂ air-sea exchange, and previous reported carbon budget in the SAB, a new carbon inventory is presented in Table 4.6. The new estimate of annual water-column respiration lowered the O₂-based value by ca. 70%, and the new shelf-wide total (water-column + benthic) is 61.0×10^{12} gC yr⁻¹. This value is still about 30% more than the shelf-wide primary production (water-column + benthic) and leaves the imbalance or net heterotrophy of 17×10^{12} gC yr⁻¹ in the SAB (Table 4.6). The new inventory also indicates that total inorganic carbon export from the SAB to the open ocean and to the atmosphere through water transport and CO₂ air-sea exchange was 5.3×10^{12} gC yr⁻¹. This inorganic carbon loss rate is over 10% of the shelf-wide primary production (Table 4.6).

Now we want to see if there are enough allochthonous sources of organic carbon to fuel the newly estimated net heterotrophy in the SAB. Based on previous findings, atmospheric inputs of organic carbon are small (Menzel, 1993). If using average concentrations of riverine dissolved organic carbon (DOC) (8.6 mg l⁻¹; Alberts and Takács, 1999) and the mean total river discharge into the SAB (84 km³ yr⁻¹; Atkinson et al., 1985), the DOC input by rivers was estimated to be 0.72×10^{12} gC yr⁻¹ (Table 4.6). By the similar calculation, input of particulate organic carbon (POC) from rivers is $0.20 \times$

10^{12} gC yr⁻¹ (Atkinson et al., 1985; Otero et al., 2000; Table 4.6). Then the total riverine input of organic carbon into the SAB is only 0.9×10^{12} gC yr⁻¹. Another organic carbon source is the export from the salt marsh along the coast of the SAB (Hopkinson, 1985; Chalmers et al., 1985). If extrapolating the areal marsh export of DOC and POC of 260 gC m⁻² yr⁻¹ (Chalmers et al., 1985) to the entire salt marsh of the SAB (457050 ha; Reimold, 1977), the total marsh export of organic carbon is ca. 1.2×10^{12} gC yr⁻¹. Apparently, the sum of riverine and marsh inputs of organic carbon can not balance the huge net heterotrophy in the SAB (Table 4.6). The organic carbon imbalance is then listed as 15×10^{12} gC yr⁻¹ in Table 4.6 as calculated from shelf-wide respiration, primary production, and terrestrial inputs of organic carbon. Note that if using previous reported O₂-based respiration in the SAB, such an imbalance is significantly larger.

Several possibilities may explain this imbalance. First, the shelf-wide respiration may still be overestimated, although our estimate has narrowed the carbon imbalance in the SAB to ca. 30%. The limited temporal and spatial coverage of our respiration incubations left uncertainty in un-sampled seasons, and integration of surface water results to the whole water column. Although previous studies argued that seasonality of respiration in the SAB is weak (Menzel, 1993; Pomeroy et al., 2000), Griffith and Pomeroy (1995) showed pelagic microbial community respiratory rates experienced strong seasonal changes. Hopkinson (1985) also found that both pelagic and benthic respiration had a seasonal pattern off the Sapelo Island within the inner-shelf of the SAB. Second, the primary production may be underestimated. This is possible because the SAB often experiences sub-surface water intrusion or upwelling from the Gulf Stream that usually triggers short-term phytoplankton blooms (Menzel, 1993; Atkinson et al., 1984;

Atkinson et al., 1996; Pomeroy et al., 2000). Subsurface blooms may also occur at the locations where nitrate-rich ground-water emerges (Moore, 1999). The short-term and patchy phytoplankton blooms make it difficult to estimate shelf-wide primary production. Last, there may be other important organic carbon sources in the SAB, which have not been recognized or estimated. Shelf water in the SAB has been reported to have higher concentrations of DOC than its adjacent open ocean (Moran et al., 1991; Moran et al., 1999). Therefore, the open ocean is unlikely to be an organic carbon source for the SAB. Ground-water intrusion may be another source (Moore, 1999), but its significance to the SAB carbon budget is not clear. In summary, it is highly possible that the above discussed causes have a combined effect.

One critical point emerging from the above imbalance discussion is that shelf-wide respiration and primary production are both one order of magnitude higher than any estimated organic and inorganic fluxes in the SAB (Table 4.6). Given a 20-30% of uncertainty of either respiration or primary production in the SAB, the imbalance would be changed. It is highly possible that the respiration and primary production in the SAB only differ by a small margin; however, the uncertainty of using their difference to build the carbon budget makes it difficult to achieve a satisfactory result as all input/output carbon fluxes are rather “insignificant” compared to shelf-wide respiration and primary production in the SAB (Table 4.6). Later, in Chapter 6 of this dissertation, we will propose an alternate method which uses inorganic carbon fluxes to constrain the carbon budget in the SAB.

In spite of large imbalance of organic carbon, greater total respiration than total primary production indicates that the SAB is a net heterotrophic system annually. The

measurement of benthic and pelagic metabolism in nearshore waters off Sapelo Sound was consistent with this conclusion (Hopkinson, 1985). On an annual basis, the SAB releases CO₂ to the atmosphere and exports inorganic carbon to the open ocean, also suggesting that the system is net heterotrophic (Smith and Hollibaugh, 1993). In the meantime, seasonality of sea surface pCO₂ and export of inorganic carbon (Fig. 4.2; Table 4.3) indicates that such a net heterotrophy has a seasonal pattern with a maximum in summer or fall and a minimum in winter. Primary production previously measured along virtually the same cross-shelf transect outside Wassaw Sound showed a distinct seasonal pattern with a summer production rate about 2 to 4 times of the winter value (Verity et al., 1993; Jahnke et al., 2000). If the trophic status of the SAB indeed changes seasonally, respiration should also show a seasonal pattern, which is contradictory to the finding by Menzel (1993) and Pomeroy et al. (2000). However, the limited temporal and spatial coverage of the current inorganic carbon data set is not sufficient to resolve such a contradiction.

Seasonality of the CO₂ Source and Sink. Seasonal changes in sea surface pCO₂ in the SAB were as much as 200 – 300 μatm between winter and the other seasons (Table 4.1), which was much larger than that in other studied continental shelf regions. The SAB therefore showed significant seasonality in the CO₂ source/sink scenario. We hererin tried to examine the mechanisms that primarily govern the CO₂ source/sink in the SAB at different seasons.

It has been shown that temperature is a primary factor that controls variation of sea surface pCO₂ in many open-ocean studies (e.g. Tans et al., 1990; Bates et al., 2000). Consistent low temperature in the North Atlantic Ocean, where the dense deep water

forms, has long been recognized to be a major mechanism that causes the area to be a net sink of atmospheric CO₂ (Sarmiento and Gruber, 2002). More intensified shelf-cooling relative to the open ocean has also been proposed to be the key that sustain the CO₂ sink on the continental shelf (Tsunogai et al., 1999). Cooling will increase the solubility of CO₂ and hence decrease the partial pressure of CO₂ ($p\text{CO}_2$) at sea surface, which may induce CO₂ under-saturation in many cases and a CO₂ sink to the atmosphere. This is actually the key concept of the solubility pump (Sarmiento, 1993). A simple thermodynamic estimation of temperature effects on changes of sea surface $p\text{CO}_2$ will demonstrate whether winter cooling has significant influence on the CO₂ source/sink in the SAB. From October to December, the sea surface temperature drop in the SAB was 15, 10, and 9°C for the inner-, mid-, and outer-shelves, respectively. If using a temperature factor of 0.0423°C⁻¹ (Takahashi et al., 1993; also see later discussion) and assuming that other factors (TC, TA, and salinity) were unchanged, such a winter cooling alone would cause sea surface $p\text{CO}_2$ to correspondingly drop 346, 178, and 165 µatm from its October values, which well covered field-measured $p\text{CO}_2$ changes between these two months (Table 4.1). Therefore, temperature effects were substantial to change sea surface CO₂ from an atmospheric source during warm months to a winter sink in the SAB.

By further examining the underway data from the December cruise, we found a significant linear relation between the natural logarithms of sea surface $p\text{CO}_2$ and temperature from S10 to S13 (mid-shelf stations) (Fig. 4.7), where

$$\ln(p\text{CO}_2) = 0.0232 \times T + 5.2505 \quad (R^2 = 0.9553, n = 90) \quad (\text{Equation 4.3})$$

The slope of this linear equation (0.0232 °C⁻¹) is called temperature factor.

Takahashi et al. (1993) had experimentally and thermodynamically demonstrated that this

factor should be $0.0423 \text{ } ^\circ\text{C}^{-1}$ in the temperature range of 2° to 28°C by holding other parameters unchanged. By our simulation, the difference between the two temperature factors was primarily due to the small changes of TC, TA, and salinity occurred from S10 to S13. The tight correlation between temperature and sea surface $p\text{CO}_2$ once again suggested that temperature was a primary force controlling variation of sea surface $p\text{CO}_2$ at mid- to outer-shelf in winter in the SAB.

In the mean time, the observation in Fig. 4.7 may reflect a water-intrusion induced mixing, which also left fingerprints in the salinity plots of DO and relative fluorescence (Fig. 4.2). Although the exact cause of this mixing event was unknown due to limited physical data, it was possible that intrusion of the Gulf Stream may be the ultimate cause. This type of intrusion will bring nitrate-rich water on the outer-shelf and often trigger phytoplankton bloom in the sub-surface water (Pomeroy et al., 1983; Pomeroy et al., 2000). The intrusion water may reach the mid-shelf by surface advection under favorable wind (Menzel, 1993; Atkinson et al., 1996). Due to lowered respiration in winter (Table 4.4), the net heterotrophy in the SAB may be significantly decreased or even overturned (Griffith and Pomeroy, 1995). If this is the case, water-intrusion induced phytoplankton bloom will be more “visible” in lowering sea surface $p\text{CO}_2$ and favoring a winter CO_2 sink in the SAB. Meanwhile, significantly decreased export of inorganic carbon from the SAB salt marsh (Cai et al., 1999; Cai et al., 2000; Chapter 5) will also help to maintain a CO_2 sink on the shelf.

On the contrary, the physical and biological settings in spring, summer and fall are mostly opposite to the winter conditions in the SAB. First, high water temperature (over 22°C in April and over 27°C in June and October) or heating greatly benefits CO_2

degassing from sea surface. Second, the SAB does not have annual spring blooms followed by a period of assimilation in summer and fall (Verity et al., 1993; Menzel, 1993; Jahnke et al., 2000; Pomeroy et al., 2000). Although phytoplankton blooms may occur during water intrusion from the Gulf Stream, they are mostly small-scale (Pomeroy et al., 1983; Atkinson et al., 1984; Menzel, 1993; Atkinson et al., 1996; Moore, 1999; Pomeroy et al., 2000). Third, intensified respiration (Table 4.4) exceeds primary production (Verity et al., 1993; Jahnke et al., 2000), which results in net heterotrophy in the SAB and directly supports the CO₂ source at sea surface. Four, increased marsh export of inorganic carbon in summer and fall (Cai et al., 1999; Cai et al., 2000; Chapter 5) also contributes directly to over-saturation of sea surface *p*CO₂. As a combined result, a strong CO₂ source to the atmosphere is developed and sustained during the warm months in the SAB.

“Continental Shelf Pump” in the SAB. The key concept behind the “continental shelf pump” hypothesis (East China Sea, Tsunogai et al., 1999) is that the world’s continental shelf is a significant CO₂ sink to the atmosphere. The hypothesis was basically proposed to explain how this CO₂ sink can be sustained on the continental shelf. Distinct from the solubility pump and biological pump of the open ocean (Sarmiento 1993), the “continental shelf pump” is a collective activity that has a combination of air-sea exchange, biological uptake, and physical transport processes. Briefly, in a typical continental shelf, the shallow seafloor restricts the convection of cooling water, and thus cooling is greater for shelf waters than for nearby open ocean waters. This leads to the production of relatively cold and dense water, which in combination with the solubility and biological pumps, results in a greater uptake of atmospheric CO₂ on the continental

shelf. The influx carbon may be transported in this denser water into the sub-surface layer of the open ocean via isopycnal mixing processes. Cooling, carbon transport, and primary production over respiration are therefore the key processes that sustain the shelf pump. Similar annual CO₂ flux into the European Atlantic shelf (Frankignoulle and Borges, 2001) provides a direct support to this concept.

Contrarily, the estimate of the air-sea CO₂ flux demonstrated that the SAB is a strong net source of atmospheric CO₂ annually (Table 4.1), suggesting that not all continental shelf regions act as net CO₂ sinks. Therefore, simple extrapolation of the ECS result globally may significantly exaggerate the world's continental shelf as a net atmospheric CO₂ sink. This conclusion is also supported by the CO₂ studies in the U.S. Middle Atlantic Bight (MAB), north of the SAB (Boehme et al., 1998; DeGrandpre et al., 2002). DeGrandpre et al. (2002) reported the annual net influx of atmospheric CO₂ to be ca. $1 \pm 0.6 \times 10^{12}$ gC yr⁻¹ (ca. -12 gC m⁻² yr⁻¹), which is much smaller compared to that in the ECS and European Atlantic shelf (~ -35 gC m⁻² yr⁻¹).

Over-saturation of sea surface *p*CO₂ in the SAB was significant and it lasted a long period of time over an annual cycle (spring, summer, and fall) (Table 4.1), the direct result of which was an annual CO₂ source to the atmosphere. As discussed earlier, the CO₂ source in the SAB during the warm months is likely a combined result of intensive heating, lack of regular phytoplankton blooms, high respiration, and elevated input of inorganic carbon from coastal salt marshes. Contrarily, winter is probably the season when the physical setting in the SAB is close to that in the ECS where cooling for the shelf water is substantial and is greater than for the nearby open ocean (Fig. 4.2). Consequently, the strong solubility pump results in CO₂ under-saturation at sea surface,

and an atmospheric CO₂ sink is developed. Therefore, if the continental shelf pump exists, it may function in the SAB on a seasonal basis.

Behind this CO₂ source/sink issue is that the SAB may function differently from other shelf regions. Both the ECS and the European Atlantic shelf during the warm months (spring – fall) are net CO₂ sinks with respect to atmosphere, primarily due to action of the biological pump (Tsunogai et al., 1997; Tsunogai et al., 1999; Wang et al., 2000; Frankignoulle and Borges, 2001). The phytoplankton blooms and high primary production take up large amount of inorganic carbon and lower the sea surface *p*CO₂ significantly; the systems are likely net autotrophic. Contrarily, primary production based on recycled nutrients is probably dominant in the SAB during the warm months (Hanson and Robertson, 1988; Hanson et al., 1990). Except for the near-shore water (Verity et al., 1993) and the intrusions from sub-surface of the Gulf Stream (Lee et al., 1991; Menzel, 1993; Paffenhofer et al., 1994) where diatom production occurs, the SAB tends toward a microbial food web, with inefficient carbon transfer (Pomeroy et al., 2000). Therefore, small-scale (near shore) and sporadic (water intrusion) events are likely overwhelmed by a much larger scale biological regime, where net heterotrophy is prominent. Note that the SAB also exports inorganic carbon to the open ocean (Table 4.3), which is similar to the ECS (Tsunogai et al., 1999). Such an export was proposed to be the main mechanism that sustains the CO₂ sink in the ECS, where atmospheric CO₂ is absorbed by the shelf water and is subsequently exported (Tsunogai et al., 1999). However, the scenario is different in the SAB where the system can maintain both a CO₂ source and an export of inorganic carbon on an annual basis. Compared to the Middle Atlantic Bight (MAB), the two systems are similar in that sea surface *p*CO₂ is over-saturated and biological uptake is

weak during the warm months (DeGrandpre et al., 2002). The small net CO₂ sink (ca -12 gC m⁻² yr⁻¹) on an annual basis in the MAB is due to a larger CO₂ influx in winter than CO₂ outflux in summer, probably as a result of stronger wind in winter than in summer (DeGrandpre et al., 2002). However, much higher degree of over-saturation of sea surface pCO₂ in the SAB results in an opposite scenario.

In summary, for a continental shelf to be a net CO₂ sink, the processes that result in CO₂ ingasing (organic carbon fixation, inorganic carbon export, and cooling) would dominate the processes that result in CO₂ degassing (organic remineralization, inorganic carbon import, and heating) (DeGrandpre et al., 2002). In other words, the combined effects of trophic status (net heterotrophy vs. autotrophy), net input/output, and hydrological setting would determine whether a system is net CO₂ source or sink to atmosphere. The continental shelf is a system where the carbon system experiences a series of modifications and transformations under complex and intensive biogeochemical processes. How the CO₂ system functions for a shelf system is determined by its unique climatological regime, hydrology, biology and ecosystem function, all of which do not likely fall in an average or universal scenario.

Figures

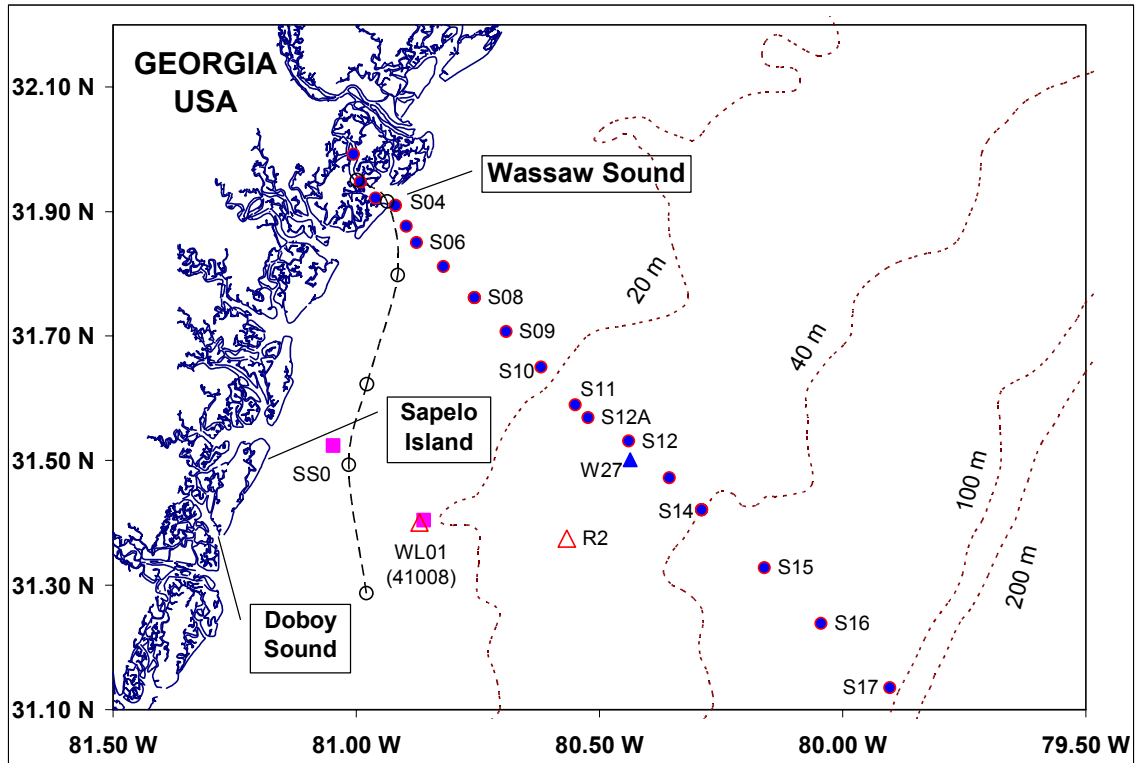


Fig 4.1. Study area showing the cross-shelf transect and its sampling stations in the South Atlantic Bight of the southeastern United States. Broken line with circles represents the along-shore underway survey and sampling stations conducted on May 1, 2002. Unfilled triangles mark the locations of NOAA Tower R2 and Buoy Station 41008.

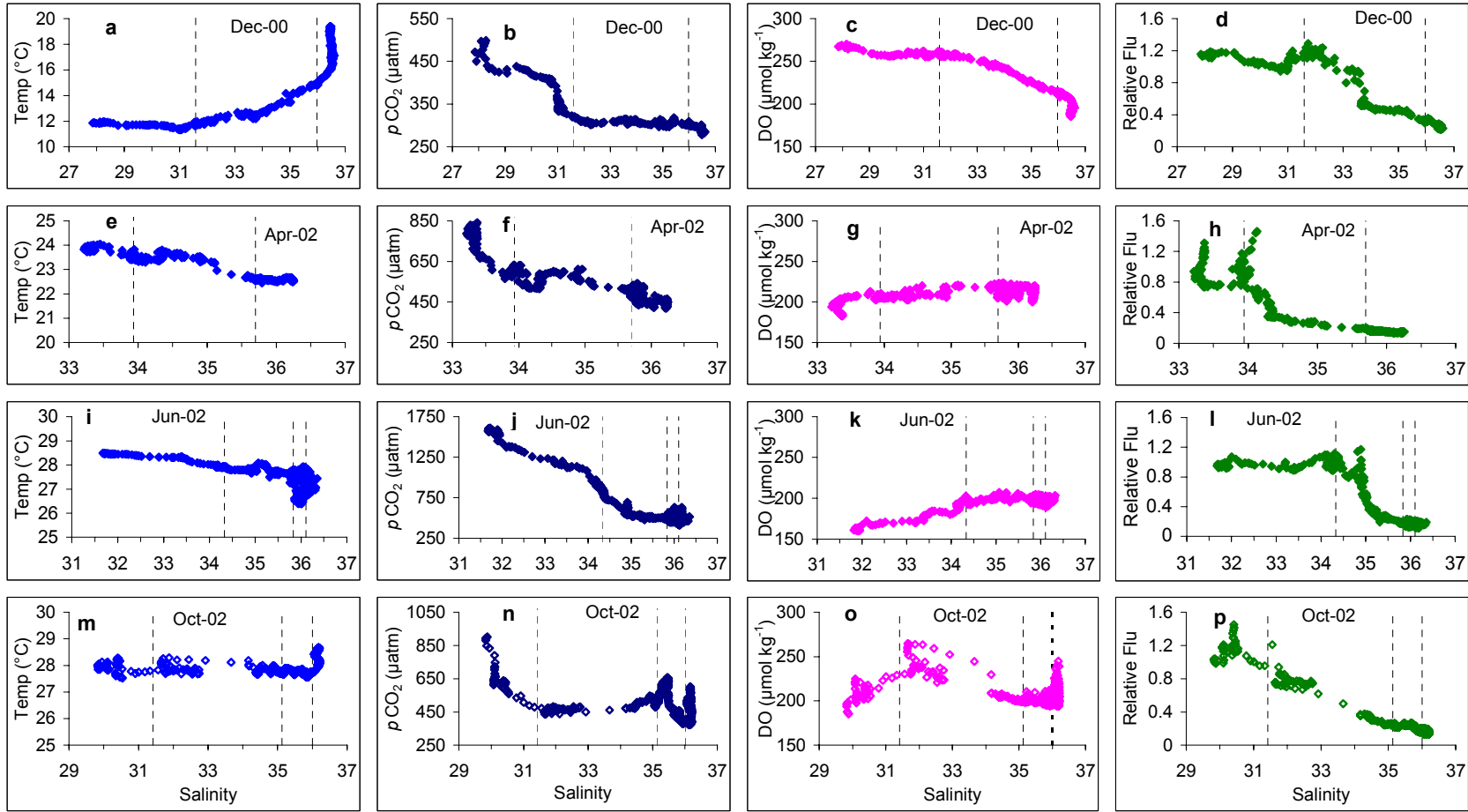


Fig. 4.2. Property-salinity plots of sea surface temperature, $p\text{CO}_2$, DO, and relative fluorescence for the underway measurements along the cross-shelf transect. The first vertical dashed line from left on the x-axis in each plot shows the salinity of S04, which is located near the mouth of Wassaw Sound; the second dashed line marks the salinity of S08, the boundary between inner- and mid-shelf; the third dashed line in the June and October plots shows the salinity of S14, which is the in-shore boundary of the outer-shelf.

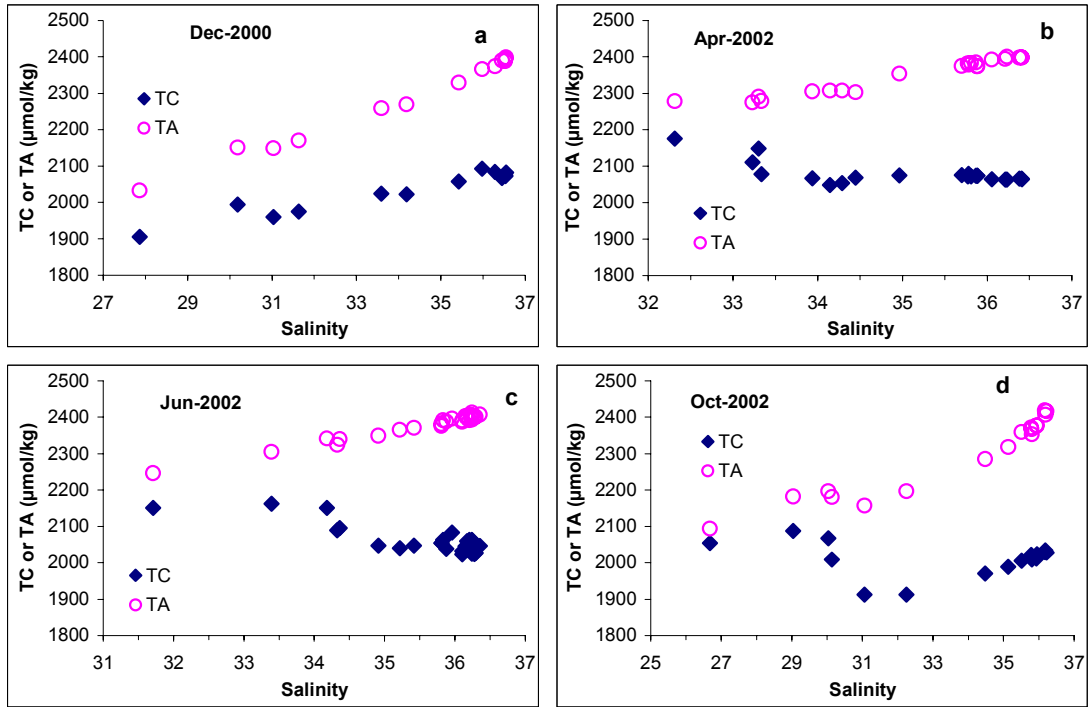


Fig. 4.3. TC- and TA-salinity plots along the cross-shelf transect in the SAB. a. December, 2000; b. April, 2002; c. June, 2002; d. October, 2002.

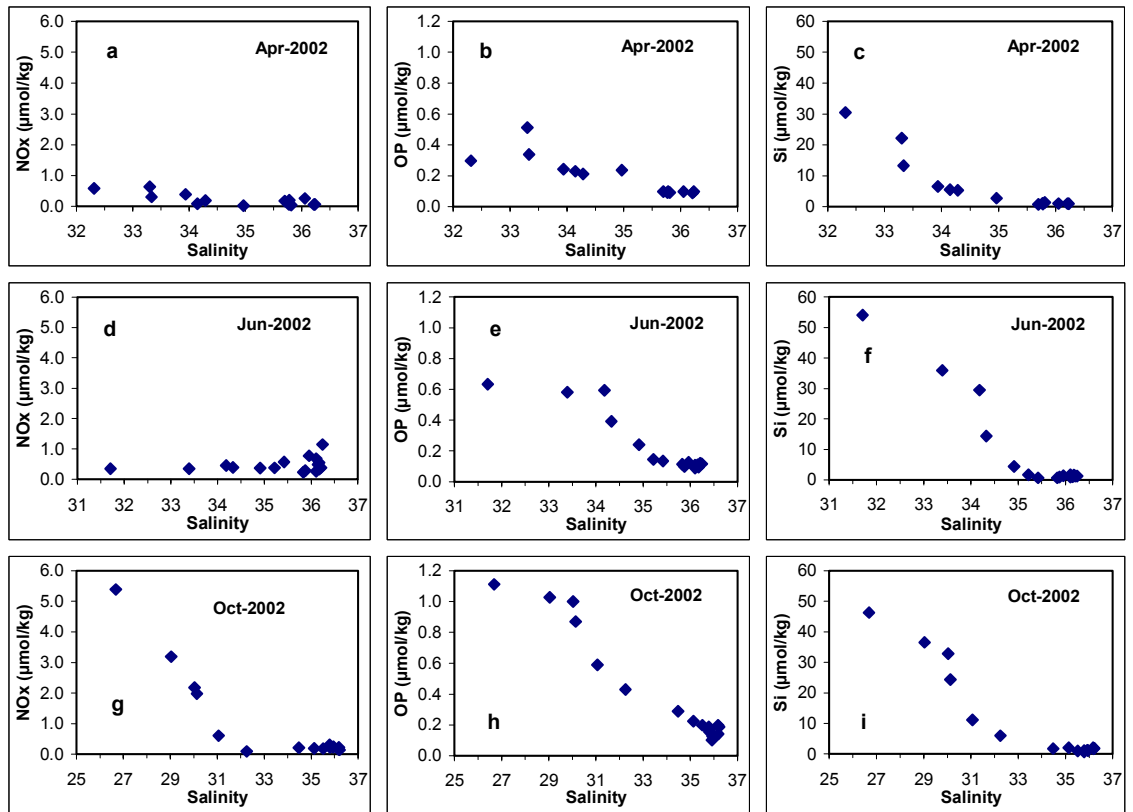


Fig. 4.4. Property-salinity plots for NO_x (NO₂ + NO₃), phosphate (OP) and silicate (Si) along the cross-shelf transect in the SAB. a – c. December, 2000; d – f. April, 2002; g – i. June, 2002. Ammonium data, which was patchy, was not shown.

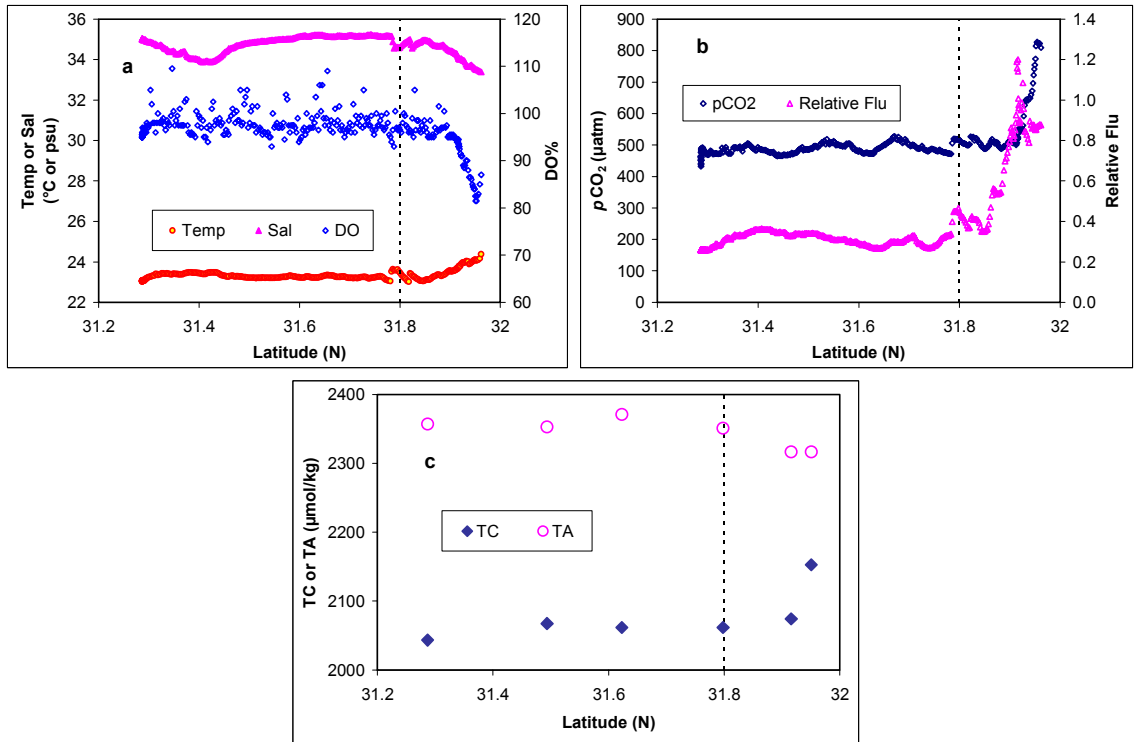


Fig. 4.5. Spatial distributions of underway measurements during the along-shore survey on May 1, 2002. a. temperature, salinity and DO%; b. $p\text{CO}_2$ and relative fluorescence; c. TC and TA. The dotted lines indicate the location where the research vessel turned toward Wassaw Sound.

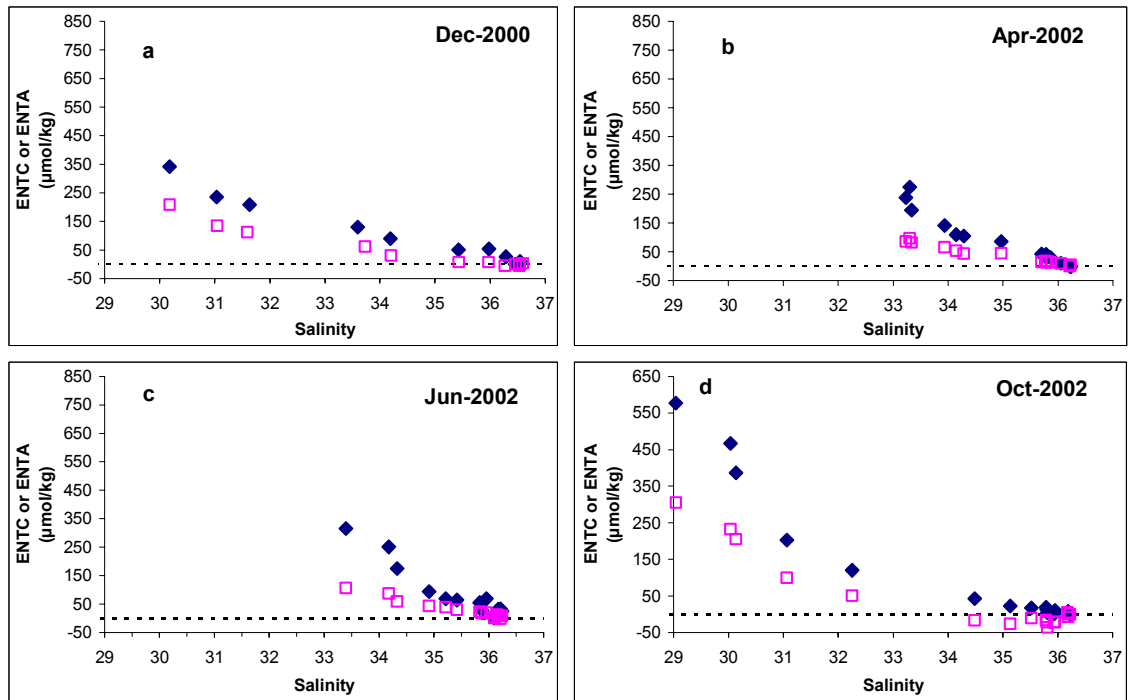


Fig. 4.6. Salinity distributions of excess normalized TC (ENTC) (filled diamonds) and excess normalized TA (ENTA) (squares) along the cross-shelf transect in the SAB. a. December, 2000; b. April, 2002; c. June, 2002; d. October, 2002. Dashed lines in the plots mark the zero of ENTC and ENTA.

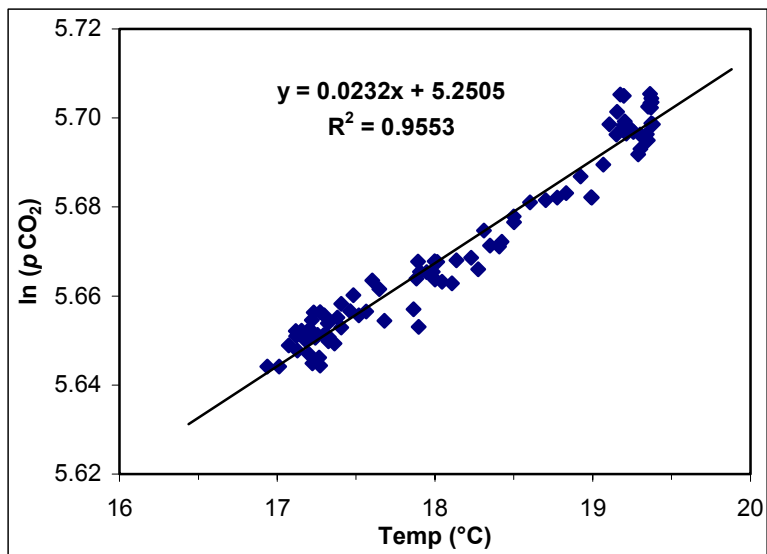


Fig. 4.7. The relationship between sea surface $p\text{CO}_2$ (natural logarithm scale) and temperature for the underway monitoring from S10 to S13 during the December cruise of 2000. The solid line is the linear best-fit of the data points

Tables

Table 4.1. Cruise mean air-sea CO₂ gradients ($\Delta p\text{CO}_2 = p\text{CO}_{2w} - p\text{CO}_{2a}$) for three regions of the SAB. The cruise mean gradients were calculated by averaging underway sea surface $p\text{CO}_2$ of each region (Fig. 4.2). The data inside Wassaw Sound (S02 – S04) were area-weighted while calculating inner-shelf mean gradients. The atmospheric $p\text{CO}_2$ level was measured to be $370 \pm 10 \mu\text{atm}$. Because the research vessel did not reach the outer-shelf during the December and April cruises, the corresponding $p\text{CO}_2$ gradients were estimated from the data with water depth greater than 35 m (near S13 and S14, the in-shore boundary of the outer-shelf). The areas of inner- (28900 km²), mid- (45300 km²), and outer- (16400 km²) shelves (Menzel, 1993) were used to calculate the area-weighted mean $\Delta p\text{CO}_2$. Unit is in μatm . (File: dailyco2flux.xls)

	Inner-shelf	Mid-shelf	Outer-shelf	Area-weighted Mean
12/6/2000	-52.5	-79.0	-70.8	-69.1
4/29/2002	223.5	102.3	79.3	136.8
6/17/2002	289.6	125.9	140.7	180.8
10/3/2002	166.3	30.8	62.0	79.6

Table 4.2. Regional and the entire SAB annual mean air-sea CO₂ fluxes. The annual mean flux for each region was calculated using cruise mean $\Delta p\text{CO}_2$ (Table 4.1) daily interpolated over an annual cycle and the daily mean wind speed measured at Buoy 41008 (Fig. 4.1). Uncertainty reflects the standard deviation propagated from calculating cruise mean $\Delta p\text{CO}_2$ (Table 4.1). The CO₂ fluxes calculated from both Wanninkhof (1992) (W) and Liss and Merlivat (1986) (LM) methods are listed. Positive flux indicates that sea surface is a CO₂ source to the atmosphere. (File: dailyco2flux.xls)

	Unit	W	LM	Uncertainty
Inner-shelf	gC m ⁻² yr ⁻¹	60.8	35.3	±35%
Mid-shelf	gC m ⁻² yr ⁻¹	14.5	8.4	±60%
Outer-shelf	gC m ⁻² yr ⁻¹	17.5	10.2	±64%
SAB Areal	gC m ⁻² yr ⁻¹	29.8	17.3	±44%
SAB Total	gC yr ⁻¹	2.70×10^{12}	1.57×10^{12}	±44%

Table 4.3. Exports of total inorganic carbon (TC) and total alkalinity (TA) from the SAB to the open ocean. The Daily TC and TA exports were calculated from depth and distance weighted mean ENTC and ENTA, mean residence time (3 months), and total volume of the SAB (290, 1360, and 820 km³ for inner-, mid-, and outer-shelves, respectively; Menzel, 1993). For the December and April cruises, outer-shelf stations (S15 – S17) were not sampled. S15 – S17 were assumed to have same TC and TA concentrations and salinity as the most off-shore station (S13 or S14) in order to calculate weighted mean ENTC and ENTA for the entire SAB. Assuming linear variation between cruises, daily TC and TA exports from the SAB were integrated to the annual values. (File: wtrans-spl.xls)

	Dec	Apr	Jun	Oct
Weighted Mean Excess NTC ($\mu\text{mol kg}^{-1}$)	15.9	18.6	30.9	22.0
Daily TC Output ($\times 10^9 \text{ gC d}^{-1}$)	5.38	6.27	10.4	7.42
Annual TC output (gC yr^{-1})	2.62×10^{12}			
Weighted Mean Excess NTA ($\mu\text{mol kg}^{-1}$)	5.4	8.8	12.3	-3.7
Daily TA Output ($\times 10^9 \text{ gC d}^{-1}$)	1.81	2.97	4.14	-1.23
Annual TA output (gC yr^{-1})	0.69×10^{12}			

Table 4.4. Respiratory rates from on-board TC-based incubations in the SAB. Oxygen unit is converted from carbon unit using a respiratory quotient of 1 (Hopkinson, 1985; Jahnke et al., 2000). (File: wtrans-spl.xls)

	Inner-shelf (S04 or SS0)				Mid- to Outer-shelf (W27, WL01, S14, or S10)			
	$\text{mg C m}^{-3} \text{ d}^{-1}$	S.D.	$\mu\text{M O}_2 \text{ h}^{-1}$	S.D.	$\text{mg C m}^{-3} \text{ d}^{-1}$	S.D.	$\mu\text{M O}_2 \text{ h}^{-1}$	S.D.
Apr-2002	201.8	36.7	0.70	0.13	63.0	16.1	0.22	0.06
Jun-2002	222.3	25.7	0.77	0.09	58.6	17.0	0.20	0.06
Oct-2002	81.5	40.1	0.28	0.14	25.0	15.6	0.09	0.05
Dec-2002	51.0	20.6	0.18	0.07	16.8	21.9	0.06	0.08
Mean	139.2	30.8	0.48	0.11	40.8	17.7	0.14	0.06
Annual SAB Total (gC yr^{-1})					$4.72 (\pm 1.73) \times 10^{13}$			

Table 4.5. Respiratory rates from O₂-based incubations in the SAB and Georgia estuaries (Pomeroy et al., 2000). Unit is in $\mu\text{M O}_2 \text{ h}^{-1}$

	Inner-shelf	Mid-shelf	Outer-shelf	Georgia Estuaries
Winter	1.1 (± 0.14)	0.7 (± 0.11)	0.3 (± 0.1)	0.08 ~ 0.23
Summer	0.95 (± 0.08)	1.3 (± 0.28)	1.0 (± 0.3)	0.66 ~ 1.15

Table 4.6. Carbon inventory in the SAB. Only the CO₂ flux calculation from Wanninkhof's (1992) parameterization was listed. The organic carbon imbalance in the SAB was the difference between the total shelf-wide respiration (water-column + benthic) and the total primary production (water-column + benthic) plus organic carbon (DOC and POC) input from rivers and salt marshes. (File: wtrans-spl.xls)

Process	Reference	Carbon Inventory ($\times 10^{12}$ gC yr⁻¹)
<i>Water-Column Respiration</i>	This study	47.2
<i>Benthic Respiration</i>	Jahnke et al., 2000	13.8
<i>Water-Column Primary Production</i>	Menzel, 1993	35.0
<i>Benthic Primary Production</i>	Jahnke et al., 2000	9.00
<i>CO₂ Air-Sea Exchange (sea to air)</i>	This study	2.70
<i>TC Export to Ocean</i>	This study	2.62
<i>TC Input from Rivers</i>	Cai and Wang, 1998	0.63
<i>DOC Input from Rivers</i>	Atkinson et al, 1985; Alberts and Takacs, 1999	0.72
<i>POC Input from Rivers</i>	Atkinson et al., 1985; Otero et al., 2000	0.20
<i>DOC and POC Input from SAB Salt Marshes</i>	Chalmers et al., 1985; Reimold, 1977	1.19
<i>Organic Carbon Imbalance</i>	This study	14.9

CHAPTER 5

SEASONAL CHANGES OF THE CO₂ SYSTEM IN MARSH-INFLUENCED COASTAL WATER SYSTEMS OF THE SOUTHEASTERN UNITED STATES

Introduction

The marsh-influenced estuaries, tidal creeks, and coastal waters adjacent to Sapelo Island, Georgia have been the subject of pioneer ecological studies on marsh-water interaction since the 1950s (e.g. Ragotzkie and Pomeroy, 1957; Teal, 1962; Odum, 1968). The original “outwelling” hypothesis (Odum, 1968), which states that intertidal marshes serve as a net source of organic matter and nutrients that fertilize adjacent estuarine and coastal water, was proposed based on studies conducted in this area. For decades, this hypothesis, though controversial, has fascinated the scientific community in the field and triggered a series of intensive scientific debate (e.g. Nixon, 1980; Wiegert et al., 1981; Hopkinson, 1985; Chalmers et al., 1985; Dame et al., 1986; Dame, 1994; Childers et al., 1993; Odum, 2000; Childers et al., 2000). The current paradigm is that marsh-water column or marsh-estuarine interaction of a particular system is inherently complicated and depends on many climatological, biogeochemical, and hydrological factors such as geological age, developmental status, and tidal range (Dame, 1994; Childers, 1994). Consequently, the “outwelling” hypothesis should be viewed as “a conceptual stimulus of ideas and not as a strict statistical hypothesis that must be proven or disproven” (Childers et al., 2000).

Until recently, inorganic carbon had not been a major topic in the discussion of the “outwelling” hypothesis. However, the concentrations, temporal changes, and spatial variations of total dissolved inorganic carbon (TC), total alkalinity (TA), and surface water $p\text{CO}_2$ provide critical data to reveal how these systems function at the biogeochemical level (Smith and Hollibaugh, 1993; Gattuso et al., 1998; Cai et al., 2000). Not only does inorganic carbon data provide a key to assess metabolism of a coastal

system (Smith and Hollibaugh, 1993), it also has direct implications for global carbon cycling (e.g. Van Green et al., 2000; Tsunogai et al., 1999; Cai and Wang, 1998; Frankignoulle and Borges, 2001; DeGrandpre et al., 2002). Recent data sets of inorganic carbon and surface water $p\text{CO}_2$ in coastal systems revealed that estuaries and in-shore systems are net heterotrophic and are potential significant sources of atmospheric CO_2 (Frankignoulle et al., 1996; Gattuso et al., 1998; Cai and Wang, 1998; Raymond et al., 1997), while continental shelf regions absorb a significant amount of atmospheric CO_2 annually (net CO_2 sinks) (Tsunogai et al., 1999; Wang et al., 2000; Frankignoulle and Borges, 2001). In the former case, marsh-influenced estuaries have been identified as important sources of inorganic carbon to estuarine and coastal waters (Winter et al., 1996; Cai and Wang, 1998; Cai et al., 2000; Raymond et al., 2000). The latter led to the “continental shelf pump” hypothesis (Tsunogai et al., 1999), which proposes how and why continental shelf area is a net sink of CO_2 with respect to atmosphere. However, extrapolating this “pump” to world’s continental shelf may have exaggerated this CO_2 sink (Chapter 4).

The metabolic state of a system reflects trophic balance between gross primary production (GPP) and total respiration (R) or net ecosystem production (NEP) (Smith and Hollibaugh, 1993; Kemp et al. 1997; Smith and Hollibaugh, 1997; Gattuso et al., 1998). In a general sense, for a net autotrophic system where $\text{GPP} > \text{R}$, the excess organic carbon ($\text{GPP} - \text{R}$) synthesized by photosynthesis is exported or buried, and the concentrations of nutrients and inorganic carbon generally remain low; in a net heterotrophic system, $\text{R} > \text{GPP}$, which results from breaking down allochthonous organic matter and releasing inorganic nutrients and CO_2 . The central concept of NEP therefore

reflects the balance between organic carbon production and decomposition or the balance between organic carbon export and import for a particular system.

With respect to inorganic carbon, if a water system is heterotrophic, excess inorganic carbon resulting from respiration would be exported through water exchange and/or lost as CO₂ to the atmosphere by air-water exchange. In addition to river input, a marsh-influenced riverine estuary may also receive substantial amounts of inorganic carbon from the adjacent marsh, while exporting inorganic carbon to coastal water and degassing CO₂ to the atmosphere (Raymond et al., 1997; Cai and Wang, 1998; Cai et al., 1999; Cai et al., 2000; Raymond et al., 2000). For marsh-influenced non-riverine estuaries, tidal creeks, and embayments, the scenario is simpler due to limited fresh water input; marsh effects with respect to inorganic carbon is often overwhelming (Winter et al., 1996; Cai et al., 2000). Many Georgia coastal systems, such as Sapelo Sound and the Duplin River, fall into this category. This type of coastal systems are termed as “marsh-dominated water systems” (MDWS) in the context of this study. A marsh-dominated water system is defined as the main-channel water area, but it does not include the intertidal marshes.

Furthermore, we herein use “apparent net heterotrophy” (ANH) to define the sum of the two inorganic carbon sinks, inorganic carbon export and CO₂ degassing, in marsh-dominated water systems (Fig. 5.1). The ANH simply represents the total inorganic carbon loss from such a system (Fig. 5.1) and is used as an indicator of marsh export of inorganic carbon in the later discussion. Raymond et al. (2000) argued that the sum of these two inorganic carbon sinks must be balanced by net heterotrophy in the York River estuary, which does not cover adjacent marsh area. This argument should be modified

given that the estuary also receives its inorganic carbon from the surrounding marsh and that excess estuarine respiration over primary production only partially supports the two inorganic carbon sinks.

Along the Georgia Atlantic coast, marsh-influenced water systems, including both riverine and non-riverine (marsh-dominated) systems, are probably net heterotrophic in nature. This is due to the fact that most of the primary production is by marsh grasses and sedges that take up most of their CO₂ from the atmosphere, while produced organic carbon is exported, buried and decomposed (and subsequently exported as inorganic carbon) (Pomeroy and Wiegert, 1981; Wiegert et al., 1983; Chalmers et al., 1985; Hopkinson 1985; Hopkinson, 1988; Pomeroy et al., 2000; Cai et al., 2000). Therefore, there may be a major input of carbon, both organic and inorganic, into the marsh-influenced water systems.

The accumulation of inorganic carbon data from the on-going Georgia Coastal Ecosystem (GCE) Long Term Ecological Research (LTER) project allows us to study seasonal variations of the CO₂ system in the marsh-influenced estuaries. Meanwhile, it sets up a new stage to re-visit the “outwelling” hypothesis (Odum, 1968) from the inorganic carbon point of view. In this study, we present inorganic carbon data obtained seasonally from the GCE-LTER surveys for three marsh-influenced water systems (Altamaha Sound, Doboy Sound, and Sapelo Sound) near Sapelo Island, Georgia. Inorganic carbon data collected monthly from the Duplin River, a marsh-dominated blind tidal river in Sapelo Island, is used to quantify TC exports and CO₂ degassing from the system in order to investigate seasonal changes of the total loss of inorganic carbon or the ANH, which is apparently associated with seasonal variations of marsh “outwelling” of

inorganic carbon. A testing hypothesis behind this study is whether the Georgia intertidal marsh is a significant source of inorganic carbon to its adjacent shelf water. To examine this hypothesis, an areal marsh export of inorganic carbon in the Duplin River is evaluated and is subsequently extrapolated to the entire salt marsh of the South Atlantic Bight (SAB) for comparison.

Study Site and Methods

Study Site. The study was conducted in the GCE-LTER study area which comprises the Altamaha River Estuary (Altamaha Sound), Doboy Sound, Sapelo Sound, and their adjacent marsh complexes surrounding Sapelo Island, Georgia (Fig. 5.2). Briefly, the largest local freshwater input is from the Altamaha River with annual average flow of $380 \text{ m}^3 \text{ sec}^{-1}$. The high flow season is typically in winter and spring, and low flow season in summer and fall. The watershed of the Altamaha River and its estuary are among the least developed regions in the eastern seaboard of the United States and are devoted mostly to agriculture. The Altamaha River is the largest river in Georgia and classified as a fast-flow, piedmont river. Its estuary, Altamaha Sound, is strongly riverine influenced, but it also receives material input from riparian marshes. Doboy Sound is a lagoonal estuary, receiving a small fraction of Altamaha River water via the Darien River at its head. Freshwater from the Altamaha River can also reach lower Doboy Sound through the connecting Intercoastal Waterway and marsh channels. Other limited freshwater input includes rainfall and emergence of groundwater. Sapelo Sound lies to the north of Sapelo Island and receives no freshwater impact from the Altamaha River. Sapelo Sound is also a lagoonal estuary with freshwater input as precipitation,

groundwater and surface inflow. The three estuaries, from south to north, form a natural gradient in terms of riverine influence and salinity excursion.

The Duplin River is a tidal slough with its entrance into Doboy Sound (Fig. 5.2). The use of the term “river” for sections of braided estuaries is unique to coastal South Carolina and Georgia. The Duplin River is therefore not a real “river” in the normal meaning of the word. Detailed site description can be found in Wiegert et al. (1981). In general, it is a marsh-dominated water system, and its upper stream is in fact marsh water (Imberger et al., 1983). The only freshwater sources at the headwaters are rainfall on the surrounding marshes and island groundwater runoff. Salinity at its mouth is largely determined by salinity variation in Doboy Sound.

Sample Collection, Analysis and Underway Monitoring. Table 5.1 summarizes the research surveys in Altamaha, Doboy, and Sapelo Sounds during the first one and a half years of the on-going GCE-LTER project. Surface water samples for TC and TA taken at designated stations in the study area (Fig. 5.2 and Table 5.1) followed the same sampling protocols described in Chapter 4. Besides designated stations, non-fixed stations were sampled to provide adequate coverage of salinity for all investigated areas. pH was also measured at a constant temperature (25°C), using a flow cell and a Ross glass pH electrode (Orion Research Inc., MA). The calibration was conducted using standard buffer solutions (pH = 4, 7, 10) with NBS scale. The relative accuracy of pH measurement was ± 0.01 pH unit. Surface water was also continuously monitored for $p\text{CO}_2$, salinity, and temperature using on-board underway systems (see Chapter 4 for technical details) during each sampling survey. To investigate effects of tidal exchange on the water-column CO_2 system over tidal cycles, continuous monitoring and surface

water sampling were performed at an anchor station inside the Duplin River (Fig. 5.2) for each survey. Each anchoring lasted 5 to 36 hrs depending on the survey schedule, and water sampling was conducted at one or three-hour intervals. Community respiration rates were also measured by inorganic carbon-based incubation (measuring the change of TC over incubation time in dark bottles) at the mouth of the Duplin River during each survey (see technical details in Chapter 4).

The Duplin River data, including TC, TA, pH, temperature and salinity, were collected monthly (September, 2000 – April, 2002) from six fixed stations (Marsh Landing, Little Sapelo Island, Barn Creek, Lumber Landing, Hunt Camp, and Flume Dock) (Fig. 5.2). There was no sampling in October, 2000. During the sampling day of each month, surface water at the six stations was collected twice for consecutive high and low tides, and water samples were stored for later TC, TA and pH analyses. The storage and analysis procedures were described in Chapter 4. Surface water $p\text{CO}_2$ was calculated from temperature, salinity, TC and pH data along with carbonate equilibrium constants (K_0 – Weiss, 1974; K_1 and K_2 – Cai and Wang, 1998).

Results

Spatial and Temporal Changes of TC and TA. The lowest TC and TA among available data in Altamaha Sound occurred in March at the headwater (Fig. 5.3). This is most likely a result of dilution of a weathering signal in the drainage basin by high river discharge (Cai, 2003). TC and TA at the river end-member and the rest of the estuary continued to rise in June, September, and October (Fig. 5.3). During all surveys, salinity diagrams in Altamaha Sound showed a low-to-high-concentration mixing of both TC and

TA between river and coastal water (Fig. 5.3). This suggested that riverine influence is one of the major factors determining the spatial distributions of TC and TA in this estuary, since water in the Altamaha River is characterized as low TC and TA content in comparison with sea water. One consistent feature of mixing in Altamaha Sound was that TC and TA were almost indiscernible when salinity was less than 20, but they began to separate thereafter with higher TA values. This differentiation is the result of water mixing between a bicarbonate-dominated system (river water, ca 99% of TC is HCO_3^-) and a less bicarbonate-dominated system (sea water, ca. 90% of TC is HCO_3^-). Since HCO_3^- has only one proton binding capacity, $\text{TA} \approx \text{TC}$ in typical river water with low pH. As pH increases during mixing, an equilibrium shift of the carbonate buffer system would increase carbonate ion (CO_3^{2-}) concentration and separate TA and TC from each other due to a 2-to-1 ratio in such an increase. Another noticeable feature was the non-conservative behaviors of TA and TC mixing in September and October in Altamaha Sound (Fig. 5.3) where both TA and TC mixing curves showed convex structure at intermediate salinity range. This indicates existence of internal sources and/or inputs of TC and TA (Cai et al., 2000).

In Doboy and Sapelo Sounds, TC and TA mixing behavior showed a pronounced seasonal progression along the salinity gradient (Fig. 5.3). Both TC and TA at the low salinity end were lower than those at the sea end-member in March, and a low-to-high concentration mixing curve was clear. In June, TA and TC values at the low salinity end climbed up to be comparable to or slightly higher than those in coastal water. From September to October, low-salinity sound water had higher TC and TA contents compared to high-salinity coastal water; a high-to-low concentration mixing structure

was fully developed. At the end of November, this structure was still clear, but the concentration gradients of TC and TA were smaller than September and October. TC and TA values also increased in the coastal water from March to November, but magnitude of change was much smaller than that of sound water. In both Doboy and Sapelo Sounds, the large high-to-low concentration gradients of TC between sound and coastal waters in later summer and fall (Fig. 5.3) indicated that these estuaries are dominated by marsh processes and likely export inorganic carbon to the adjacent continental shelf.

In Doboy Sound, the riverine influence from the Altamaha River was believed to be high in March due to high-flow season as illustrated by larger difference in the salinity range of Doboy Sound (20 – 28 psu) in comparison with Sapelo Sound (30 – 33 psu) (Fig. 5.3). Low-salinity water (20 – 28 psu) was also found in Doboy Sound in June. The major cause may still be the riverine influence from the Altamaha River as indicated by the fact that low-salinity water (< 5 psu) occupied the entire estuary during the June survey (Fig. 5.3). The rain fall was not likely responsible for lowering salinity in Doboy Sound in June since Sapelo Sound did not show low-salinity water during the same survey. Because of limited freshwater input and negligible riverine influence from the Altamaha River, temporal and spatial variations of TC and TA in Sapelo Sound primarily reflected a combined result of marsh processing and tidal mixing. Fig. 5.3 therefore shows a picture of gradient from Altamaha Sound to Sapelo Sound, in which riverine influence on spatial and temporal distributions of TC and TA dampens while relative importance of marsh effect on the CO₂ system increases.

Spatial and Temporal Changes of pCO₂. Spatial and temporal distributions of surface water pCO₂ in three estuaries also reflected seasonal changes and the riverine-

influence gradient (Fig. 5.4). In March, Doboy and Sapelo Sounds had the lowest surface water $p\text{CO}_2$ (500 – 1000 μatm) among all surveys. Surface water $p\text{CO}_2$ was over 3200 μatm at the river end-member of Altamaha Sound in March but quickly dropped to 500 μatm at salinity of 15 psu. These low $p\text{CO}_2$ values were likely a combined result of low temperature and low respiratory rates in both marsh and estuarine water (Pomeroy et al., 2000; Pomeroy et al., 1972; Griffith and Pomeroy, 1995). Super-saturation of $p\text{CO}_2$ at the freshwater end-member in Altamaha Sound reflected the carbonate chemistry of river water where low pH (≈ 6.6) condition prevailed (Cai and Wang, 1998). From June to September, as TC and water temperature increased, surface water $p\text{CO}_2$ climbed to reach the maximum for all three estuaries (Fig. 5.4). $p\text{CO}_2$ decreased from September to October (Fig. 5.4) despite the fact that TC concentrations in all three estuaries were still at their annual high (Fig. 5.3). Such a decrease was accompanied by decrease of water temperature and increase of pH (data not shown). Surface water $p\text{CO}_2$ continued to decrease at the end of November and was close to the March value for all three estuaries (Fig. 5.4). Concurrently, water temperature, TA, and pH all dropped from their respective October values. Over-saturation of surface water $p\text{CO}_2$ with respect to atmospheric $p\text{CO}_2$ (380 μatm on average measured during the LTER surveys) during all surveys (Fig. 5.4) suggested that these estuaries degas CO_2 to the atmosphere year-round. The intrusion of freshwater from Altamaha River into Doboy Sound was noticeable during the March cruise as shown by low-salinity water compared to Sapelo Sound (Fig. 5.4). In June, a high rate of flushing pushed low-salinity (~ 5 psu) water out of the mouth of Altamaha Sound even during high water survey (Fig. 5.4). Consistently, surface water during the

high-water survey in June in Doboy Sound exhibited higher $p\text{CO}_2$ values but much lower salinity than in Sapelo Sound (Fig. 5.4).

Anchor Monitoring in the Duplin River. Anchor monitoring in the Duplin River (Fig. 5.2) also indicated that inorganic carbon parameters experience seasonal variations (Fig. 5.5). In March, low-tide water contained less inorganic carbon and had lower TA values compared to high-tide water (Fig. 5.5a). Meanwhile, surface water $p\text{CO}_2$ was as low as ca. 500 μatm at high tide and 1600 μatm at low tide (Fig. 5.5a). The maximum $p\text{CO}_2$ at the low water in June increased to about 2500 μatm , while the high-water minimum only reached 700 μatm (Fig. 5.5b). Variation of TA and TC during one tidal cycle was small in this early summer month with a difference of only 100 $\mu\text{mol kg}^{-1}$ between low- and high-tide water (Fig. 5.5b). TC and TA gradients with respect to salinity in the Duplin River was virtually identical to the situation of Doboy Sound in June (Fig. 5.3) indicating that the marsh is experiencing a transition from spring to summer condition. $p\text{CO}_2$ value and magnitude of variation with respect to tide were similar in September compared to June (Fig. 5.5c). TA and TC contents at low tide were higher than at high tide with a difference of over 200 $\mu\text{mol kg}^{-1}$ (Fig. 5.5c). Such a pattern continued in October and November (Fig. 5.5d and e) during which surface water $p\text{CO}_2$ lowered dramatically. In late November, surface water $p\text{CO}_2$ dropped back to the March level (Fig. 5.5e).

Anchor monitoring in March, October, and November (Fig. 5.5a, d, and e) occurred over the daily light and dark conditions. However, the variability of inorganic carbon parameters was mostly related to tidal period. Diurnal changes, if any, should account for an insignificant portion of the total changes as indicated by small difference

of $p\text{CO}_2$, TA, and TC between the light and dark conditions at a similar tidal phase (Fig. 5.5d and e). Tidal exchange with marshes, therefore, probably plays a crucial role in modifying the water-column CO_2 system. On the other hand, such modification has pronounced seasonality, indicating that a marsh system functions differently at different seasons.

Monthly Data in the Duplin River. The monthly data in the Duplin River was representative of the CO_2 system's annual variation in the water column of a marsh-dominated tidal river (Fig. 5.6). Generally, TC and TA at a fixed station in the Duplin River co-varied with salinity with annual minimum values occurring in March and maximum in December during the sampling period (Fig. 5.6). This indicates that seasonal changes of TC and TA were dominated by salinity effect. On the other hand, annual variations of TC and TA showed a phase-mismatch to annual variation of temperature with its fall and rise occurring about two to three months earlier. Spatially, TC generally increased upstream from Marsh Landing to Flume Dock except for April 2001, suggesting marsh indeed is a source of inorganic carbon during most time of the year. This spatial pattern was also observed for TA, but with more exceptions (February, 2001; April, 2001; January – April, 2002).

Annual variation of calculated $p\text{CO}_2$ was negatively correlated to pH for all stations in the Duplin River (Fig. 5.6). In addition to pH, temporal distribution of temperature was also parallel to annual variation of $p\text{CO}_2$ (Fig. 5.6) indicating that cooling and heating may play a major role in shaping the temporal distribution pattern of $p\text{CO}_2$. A large difference of $p\text{CO}_2$ between high- and low-tide at a fixed station, especially downstream stations (Marsh Landing, Little Sapelo Island, Barn Creek), was

clear from June to December (Fig. 5.6). The high- and low-water difference was also prominent from October to December for TC and TA (Fig. 5.6). Although our sampling in the Duplin River did not necessarily capture the same water mass at a fixed station during two consecutive tidal stages for each sampling event, such a difference likely indicated export of inorganic carbon primarily produced by marsh respiration in summer and fall.

Estimates of TC Export, CO₂ Degassing and Apparent Net Heterotrophy. The longitudinal gradients of TC in the Duplin River as illustrated by higher concentrations of TC at more upstream stations relative to Marsh Landing during most times of the year (Fig. 5.6) confirmed that TC export did occur. Meanwhile, over-saturation of surface water $p\text{CO}_2$ indicated that the Duplin River is also an annual net CO₂ source to the atmosphere. With basic information on geomorphology, hydrology, and meteorology of the Duplin River, air-water CO₂ fluxes and TC exports can be quantified on a monthly basis. In a marsh-dominated system like the Duplin River with limited freshwater input, its ANH is primarily supported by input of inorganic carbon from adjacent marshes via tidal exchange (see later discussion). This quantification would therefore provide a detailed picture of seasonal variations of TC export and air-water CO₂ exchange in the Duplin River and allow us to assess annual variability of the marsh as an inorganic carbon source.

Air-water CO₂ fluxes were calculated based on the same mathematical consideration as in Chapter 4 (Equation 4.1). Two sets of equations were used to calculate gas transfer velocity (k) for comparison. One was taken from Wanninkhof (1992) (hereinafter referred to as W); another was from Raymond et al. (2000)

(hereinafter referred to as R). Both methods used a k vs. wind speed relationship. However, the W method has been mostly applied to open-ocean conditions, while the R method was derived from estuarine tracer experiments (Clark et al., 1994; Carini et al., 1996). It was believed that morphology and physical conditions in estuaries are different from the open ocean (Raymond et al., 2000; Clark et al., 1994; Carini et al., 1996; Cai and Wang, 1998; Frankignoulle et al., 1998), so that the traditional relationship between wind-speed and gas transfer velocity applied in oceanic studies may not be suitable for calculation of CO₂ fluxes in estuarine waters. We therefore used both relationships in this study to examine their potential difference.

The Duplin River was divided into five segments (1 – 5) in order to determine spatial variations of CO₂ flux and to obtain an area-weighted mean CO₂ flux for the entire river. The limits of each segment were set by two consecutive sampling stations from Marsh Landing to Flume Dock (Fig. 5.2). The segment mean $p\text{CO}_2$, which was calculated by averaging high- and low-water $p\text{CO}_2$ at a station, followed by taking the average between two consecutive stations, were used to estimate CO₂ flux of each segment. The segment CO₂ fluxes for each sampling event were area-weighted to obtain a mean CO₂ flux for the entire river (Table 5.2). CO₂ fluxes calculated from the W method were lower than those from the R method except for one case when the averaged wind speed was over 4 m s⁻¹ (Table 5.2). The difference between the two methods was 52% on average for river mean CO₂ fluxes at wind speed less than 3.5 m s⁻¹, while the difference was only 11% for wind speed between 3.5 and 4.0 m s⁻¹. Higher CO₂ fluxes from the R method might be expected because of inherently greater turbulence in estuarine environments (Elsinger and Moore, 1983; Cai and Wang, 1998; Cai et al., 1999; Frankignoulle et al.,

1998; Raymond et al. 2000). However, more independent studies are necessary to constrain CO₂ flux calculation in estuarine waters.

The net export flux of TC from Marsh Landing in the Duplin River can be evaluated based on a diffusion-type equation due to the finding that exchange between the upper and lower water masses takes place by eddy diffusion (Imberger et al., 1983):

$$Q = \varepsilon \langle A \rangle \frac{C_i - C_{ML}}{L} \quad (\text{Equation 5.1})$$

where Q represents the flux; ε is the effective longitudinal diffusion coefficient; $\langle A \rangle$ is the cross-sectional area of the river at Marsh Landing; $\frac{C_i - C_{ML}}{L}$ is the concentration gradient; C_i and C_{ML} are the tidal average of the mean TC at station i and Marsh Landing, respectively; L is the distance along the river from Marsh Landing to station i. The same equation has also been used in the estimation of organic carbon (DOC and POC) exports from the Duplin River (Wiegert et al., 1981; Chalmers et al., 1985). Imberger et al., (1983) derived an average ε of 38 m² s⁻¹ based on mass-balance calculation of the longitudinal salt flux along the Duplin River. Possible variation of this diffusion coefficient (e.g. due to storm event and spring-neap tide cycle) was ignored in the flux calculation. $\langle A \rangle$ was estimated to be 654 m² from river width (130 m) and average water depth (5.0 m) at Marsh Landing. The distance L was obtained from Imberger et al. (1983). C_{ML} and C_i were calculated by averaging high- and low-water TC concentrations at individual stations for each sampling event. Daily export flux of TC (mmol d⁻¹) from the Duplin River was calculated using the mean TC gradient by averaging the individual gradients between Marsh Landing and five upstream stations (Table 5.3). The resulting daily TC export fluxes (mmol d⁻¹) were divided by the total surface area from Marsh Landing to

Flume Dock to convert the values to areal export fluxes ($\text{mmol m}^{-2} \text{d}^{-1}$) (Table 5.3).

Finally, apparent net heterotrophy (ANH) in the Duplin River was calculated by summing TC export and CO_2 degassing (Fig. 5.7A).

The upper two sections between Lumber Landing and Flume Dock in the Duplin River (Fig. 5.2) are mostly occupied by marsh water (Imberger et al., 1983; Chalmers et al., 1985). For comparison, the entire procedure presented above was also used to estimate TC export and CO_2 degassing from these two sections (Fig. 5.7B).

Discussion

Seasonal Variation of Apparent Net Heterotrophy. The ANH estimated for the entire Duplin River (Fig. 5.7A) and the upper two sections (Fig. 5.7B) both showed a distinct and similar seasonal pattern with the maximum rate found in later summer and fall and the minimum in spring. No negative values of the ANH occurred over a one-year sampling period for this marsh-dominated tidal river (Figs. 5.7A and B). Except for late winter and spring when surface water $p\text{CO}_2$ was below or near $1000 \mu\text{atm}$ (Fig. 5.6), CO_2 degassing accounted for the major portion of the ANH (Figs. 5.7A and B) and followed the seasonal pattern of the ANH more closely. However, both TC export and CO_2 degassing in general were of equal importance in determining the ANH of the system. A sudden jump of the ANH in March, 2001 (Figs. 5.7A and B) corresponded to the large dips of TC for all sampling stations (Fig. 5.6). As noted earlier (Fig. 5.3, Fig. 5.4 and Fig. 5.5), freshwater intrusion from the Altamaha River into Doboy Sound may be responsible for this sudden increase of TC export. The fresher water with low TC concentration from the Altamaha River (Fig. 5.3) may enter the Duplin River via advection in this event.

Therefore, the estimate of TC export in this case may have large uncertainty because we based our calculation on the diffusion-type equation (Equation 5.1), and assumed the advection is negligible (Imberger et al., 1983). Precipitation was not likely associated with this event because meteorological data (http://gce-lter.marsci.uga.edu/lter/data/gce_data.htm) indicate that there was no rainfall during the five-day period before the sampling date in March, 2001. No sudden jump of TC export occurred in spring, 2002, and its variation was more gradual (Figs. 5.7A and B).

Integrating monthly results from Table 5.2, the annual CO₂ degassing in the Duplin River (January, 2001 – December, 2001) was 306 gC m⁻² yr⁻¹ (R method) or 256 gC m⁻² yr⁻¹ (W method). In the meantime, the Duplin River discharge TC of 109 gC m⁻² yr⁻¹ to Doboy Sound (Table 5.3). The annual ANH was then 416/356 (R/W) gC m⁻² yr⁻¹, of which CO₂ degassing accounted for ca. 70%. Such a total loss of inorganic carbon (ANH) from the Duplin River was about 4 times of the value estimated for the York River estuary, Chesapeake Bay (Raymond et al., 2000), but both followed a similar seasonal pattern. The annual export of TC in the Duplin River is, on the other hand, only one-tenth of the estimate in the Swartkops estuary, South Africa (1083 g C m⁻² yr⁻¹) (Winter et al., 1996). Similar to the Duplin River, Swartkops estuary is also a marsh-dominated non-riverine tidal river, while the York River estuary receives influence from both river and marsh.

If the ANH in the Duplin River is primarily associated with inorganic carbon export from marsh, and local inorganic carbon release (i.e. estuarine respiration) is in secondary importance, annual variation of ANH in the Duplin River (Figs. 5.7A and B)

generally reflects the annual variation of inorganic carbon release from marsh. We now discuss the marsh's role in maintaining the ANH of the system.

Controls on Apparent Net Heterotrophy. Cai et al. (1999) have shown that respiration rates in estuarine water of the five major Georgia river estuaries (Savannah, Ogeechee, Altamaha, Satilla, and St. Marys) alone are not sufficiently large to support O₂ consumption and CO₂ degassing; the difference must be balanced by more respiration in the water over intertidal marsh and in the marsh sediment. Cai et al. (2000) further demonstrated that Georgia intertidal marsh is a source of inorganic carbon based on the estimates of TC flux and CO₂ degassing in the Satilla River estuary. Recent studies in Swartkops estuary (Winter et al., 1996), York River estuary (Raymond et al., 2000), and Hudson River (Raymond et al., 1997) all conclude that intertidal marshes adjacent to estuaries are sources of inorganic carbon. In this study, the quantification of CO₂ degassing and TC export in the Duplin River implies that marsh export of inorganic carbon supports the ANH of its adjacent water system (Figs. 5.7A and B).

Further discussion is needed to conclude that much of the ANH in the Duplin River is indeed a result of marsh processes. There are 3 tidal excursions in the length of the Duplin River (Imberger et al., 1983; Ragotzkie and Bryson, 1955). A water mass from the upper Duplin River probably never reaches Doboy Sound advectively. However, salt and other materials can be transported along the river by continuous eddy diffusion. At the headwaters of the Duplin River, Imberger et al. (1983) defined a Lagrangian control volume which was bounded by their stations D165 and D175, approximately corresponding to the positions of Hunt Camp and Flume Dock, respectively (Fig. 5.2). The water in this control volume was highly marsh-influenced water since it is contained

within the marsh during a typical high tide. In other words, changes in inorganic carbon signal in this volume reflect the net results of marsh processing. Meanwhile, the areal ratio of the marsh to the open water in the Duplin River is approximately 5 : 1 (Ragotzkie and Bryson, 1955), and there are side creeks all the way down the river nearly to Doboy Sound. Therefore, we may argue there is marsh influence on most of the water in the Duplin River with the least influence near the mouth. Based on the calculation of CO₂ degassing (Table 5.2), the river section between Hunt Camp and Flume Dock (section 5) indeed had the highest rates of CO₂ degassing all the times. Furthermore, the lowest rate of CO₂ degassing exclusively occurred in the section 1 (adjacent to Doboy Sound) (Table 5.2) except in February, 2001, and the degassing rate increased upstream. Such a gradient was largest in late summer and fall and lowest in spring (Table 5.2). In the meantime, the water at Flume Dock and Hunt Camp had higher TC concentrations than the rest of the downstream stations during most of the year (Fig. 5.6). Also, TC export from the upper two sections was larger than that from the Duplin River (Marsh Landing) year-round (Figs. 5.7A and B). The scenario can be explained as the following: as the river water moves away from Doboy Sound water, surface area becomes smaller, while marsh area increases; thus, marsh effect grows stronger. At Flume Dock, the most upstream station, the water is the actual marsh water (Imberger et al., 1983), and the marsh effect is overwhelming. Therefore, the ANH in the Duplin River must be primarily supported by marsh processes as a result of interaction between river water and the marsh.

Previous and current measurements of respiratory rates in marsh and estuarine water also provide evidence that inorganic carbon released from estuarine respiration alone can not sufficiently support observed TC export and CO₂ degassing in the Duplin

River (Table 5.4). The estuarine respiratory rates measured in spring, summer and fall at the mouth of the Duplin River varied from 20 to 89 mmol C m⁻² d⁻¹, which were all less than the estimated ANH (99 ~ 158 mmol C m⁻² d⁻¹) during the same period (Table 5.4). In contrast, the total respiratory rates in the marsh (marsh sediment + overlaying water) was 82 – 183 mmol C m⁻² d⁻¹ which covered the range of ANH in the Duplin River (Table 5.4; Pomeroy et al., 1972; Cai et al., 1999). Although the current inorganic carbon data set did not allow us to separate the contribution of ANH from intertidal marsh and from estuarine respiration, available evidence presented leads us to conclude that a major portion of the ANH was attributed to marsh processes. On one hand, temporal variation of the ANH in the Duplin River (Figs. 5.7A and B) reflects the seasonal pattern of water-marsh interaction with a high rate of inorganic carbon release from the marsh in later summer and fall, and a low rate in winter and spring; on the other hand, marsh respiration is likely a primary control on the ANH in river water.

A significant positive relationship existed between the average temperature and the ANH in the Duplin River (Fig. 5.8) suggesting that temperature was probably a major factor mediating respiratory release of inorganic carbon from the marshes. Temperature dependency of respiratory rates was significant in the marshes (Dame, 1989) and in the five Georgia riverine estuaries (Pomeroy et al., 2000). The ANH in April, 2001, which was clearly away from the linear regression in Fig. 5.8, corresponded to the only negative TC flux from the Marsh Landing (Fig. 5.7A).

In order to examine the TA signal in the context of inorganic carbon export from the Duplin River and the marshes, areal export of TA was also estimated by using the same mathematical calculation as used for TC export (Figs. 5.7A and B). TA export

generally matched seasonal variation of TC export most of the year except for some months in summer and fall when TA and TC exports had certain degree of mismatch (Fig. 5.7A and B). Aerobic respiration and its reverse reaction – photosynthesis – have significantly less influence on TA change compared to O₂ and TC changes (Millero, 1995; Cai and Wang, 1998; Boehme et al., 1998) because the stoichiometry of these two reactions are 106C : 17H⁺ : -138O₂. However, most anaerobic pathways of respiration such as sulfate reduction and denitrification would significantly change TA by consuming large amount of H⁺ and producing bicarbonate ions (Liss, 1992). Calcium carbonate dissolution/precipitation would also change TA and TC in a ratio of 2 : 1. Many studies (Bernier et al., 1970; Kempe, 1982; Hoppema, 1993; Smith and Hollibaugh, 1997; Raymond et al., 2000) have proposed or showed that sulfate reduction in sediment can be the dominant anaerobic pathway that creates a source of TA. For Georgia estuary-marsh complex, it has also been argued that addition of TA in estuarine water mainly results from sulfate reduction in ambient marsh sediment (Cai and Wang, 1998; Cai et al., 1998). So far as we are aware, there have been no studies that show carbonate dissolution/precipitation as a major process responsible for change of TA in marsh-dominated water systems. Consequently, anaerobic respiration in marshes may be the primary cause for the concurrent TC and TA exports from the Duplin River (Fig. 5.7A). More paralleled TC and TA exports from the upper two sections (Fig. 5.7B), where marsh effects were overwhelming, further support this conclusion. We can then interpret the TA export as a semi-quantitative indicator of accumulative effects of various anaerobic processes in the marshes of the Duplin River, which also likely experienced seasonal changes.

TC and TA exports in the Duplin River showed a weak co-variation in summer and fall (Figs. 5.7A and B). This may reflect the fact that large amount of labile organic carbon was first degraded in the water column and surface sediment of the marsh via aerobic pathway, which released TC but had little effect on TA; thereafter, anaerobic respiration increased and broke down more refractive organic carbon; TA export thus reached a peak in later summer and fall (Figs. 5.7A and B). Meanwhile, this weak co-variation may also be attributed to high rates of CO₂ degassing in summer and fall (Table 5.2) that significantly modified TC concentration but left TA unchanged.

Significance of Marsh Export of Inorganic Carbon. Cai and Wang (1998) estimated TC export from the Altamaha and Satilla River to be 6.7 and 0.2×10^9 mol yr⁻¹, respectively. By extrapolating these results to the entire South Atlantic Bight (SAB), the total river TC export was estimated to be 0.6×10^{12} gC yr⁻¹ (Cai and Wang, 1998). However, TC export from marsh to coastal water via non-riverine marsh-dominated estuaries had not been documented prior to this study. Detailed analysis and quantification of TC and CO₂ fluxes in the Duplin River provide direct evidence that Georgia marshes discharge inorganic carbon into adjacent oceanic sounds and coastal water via tidal exchange. In the mean time, this inorganic carbon source from marsh shows a seasonal pattern (Fig. 5.7). The positive TC concentration gradient from low to high salinity in summer and fall in Doboy and Sapelo Sounds (Fig. 5.3 and Fig. 5.4) confirmed that TC export to coastal water via tidal mixing must occur. Assuming the same eddy diffusion coefficient in Sapelo Sound as in the Duplin River (Equation 5.1), its annual TC export is estimated to be 268 gC m⁻² yr⁻¹, over twice the value from the Duplin River (Table 5.3). This may be an underestimate since the actual longitudinal diffusion

coefficient in Sapelo Sound is likely higher than that in the Duplin River due to higher tidal flow rates; in addition, possible off-sound advection may enhance transport of inorganic carbon released from the marshes. Such a coarse estimate suggests that inorganic carbon leaving the marshes is likely transported to the coast efficiently. To investigate whether marsh TC export has significant influence on the CO₂ system in the SAB, we estimated the areal marsh TC export and extrapolated it to the entire salt marshes of the SAB. The estimation is also meaningful later when we evaluate the net ecosystem heterotrophy of the SAB based on inorganic carbon fluxes (Chapter 6).

Chalmers et al. (1985) used Equation 5.1 to calculate the areal marsh export of DOC and POC in the Duplin River based on the data collected in the upper boxes of the river which approximately match the segment between Lumber Landing and Flume Dock (Fig. 5.2). Because the river water in this segment is the actual marsh water that covers the upper marshes in the Duplin River (Wiegert et al., 1981; Imberger et al., 1983; Chalmers et al., 1985), the material export from this segment reflects the export from the marshes. We therefore calculated the annual total TC export from this segment using the same procedure as presented earlier. The total TC export ($1.02 \times 10^8 \text{ gC yr}^{-1}$) was then divided by the upper marsh area of 65 ha. (Chalmers et al., 1985) to convert it to areal marsh export for extrapolation (Table 5.5). Note that the extrapolation only included the SAB salt marshes (North Carolina, South Carolina, Georgia, and Florida), and excluded the mangroves in Florida. Also note that the extrapolation was based on the work in the upper Duplin River where transport parameter is known.

The extrapolated total TC export from the SAB salt marshes ($0.7 \times 10^{12} \text{ gC yr}^{-1}$) alone represents ca. 30% of either annual air-sea CO₂ flux or TC export to the open ocean

in the SAB (Table 5.5). Combining the riverine TC export (0.6×10^{12} gC yr⁻¹; Cai and Wang, 1998), the total terrestrial input of TC (1.3×10^{12} gC yr⁻¹) accounts for about half the annual CO₂ degassing in the SAB or its annual TC export (Table 5.5). Although the TC export from the salt marshes only represents 8% of the marsh net primary production (Table 5.5), the conclusion is that such an export has significant influence on the CO₂ dynamics in the SAB. The total loss of inorganic carbon via marsh CO₂ degassing and TC export, approximately representing the total respiration by heterotrophs in the marsh, accounts for 20 – 30% of net primary production in the marshes (Table 5.5). This is consistent with the previous finding that about 36% of the net primary production in the marsh is respired (Hopkinson, 1988).

In the context of testing Odum “outwelling” hypothesis, Chalmers et al. (1985) estimated areal marsh exports of DOC and POC in the Duplin River to be 129gC m⁻² yr⁻¹ and 131 gC m⁻² yr⁻¹, respectively. These fluxes were similar to our estimate of annual marsh TC export (Table 5.5). They also found that the export showed a seasonal pattern with summer maximum and winter minimum. Furthermore, Hopkinson (1985) concluded that outwelling of organic carbon from intertidal marsh must occur by measuring primary production and metabolism in the nearshore water and sediment off Sapelo Island. Combining these previous findings with our current conclusion, we argue that Georgia salt marshes “outwell” both organic and inorganic carbon to coastal waters. In the summary of net export in marsh-estuarine systems on the Atlantic coast of North America, Dame (1994) also indicated net export of both organic and inorganic materials in 6 out of 10 systems. Winter et al. (1996) studied exports/imports of both organic and inorganic carbon in a salt marsh-dominated estuary in South Africa. They concluded that

salt marshes were net exporters of both organic and inorganic carbon, but TC flux was about 10 times the values of either POC or DOC export. Therefore, it seems to be a common phenomenon for many coastal wetlands, if not most, that intertidal marshes export carbon products from both primary production and respiration. This implies that marsh-dominated water systems may serve as a “passer” that delivers organic and inorganic carbon exported from salt marshes to the coastal waters. Therefore, these systems are likely to be both apparently and actually net heterotrophic in nature. However, caution must be taken while examining the import/export scenario for a particular marsh-estuarine system because the inherent nature of the issue is complicated, and the net fluxes are likely a function of many biogeochemical factors such as geological age, tidal range, system morphology, and exogenous environmental forcing (Dame, 1994; Childers, 1994; Childers et al., 2000). Mechanisms governing one particular system may not be applied for other systems or even different parts of one system.

Summary. We have shown in this study that Georgia salt marsh exports inorganic carbon as respiratory product to its adjacent estuaries and to the coastal ocean. This export has distinct seasonal pattern with spring minimum and late-summer and fall maximum. Although such an export may represent only a small portion of primary production of the marsh, it is significant to CO₂ biogeochemistry of adjacent estuaries and continental shelf. The direct impact of marsh inorganic carbon export is reflected by high over-saturation state of surface water $p\text{CO}_2$ in these systems. The seasonality of this inorganic carbon source also plays a crucial role in modifying temporal and spatial distribution of inorganic carbon along Georgia coast. Therefore, future studies on carbon cycling of this region must put this source under consideration. From another aspect, both

marsh-adjacent estuaries and continental shelf are net CO₂ sources to the atmosphere annually. However, if the large CO₂ fixation by marsh primary producer is added into the picture, the net result may still be a CO₂ sink. Such a mechanism is actually a carbon sequestration process via an integrated marsh-estuary-shelf system. At one end of this system, large amount of atmospheric CO₂ is fixed through marsh biological pump; at the other end, inorganic carbon is exported to the open ocean via water transport and is lost to the atmosphere from water surface. This may have important implication to the global carbon cycling and CO₂ budget if a large fraction of the global coastal wetland and their adjacent water systems behave similarly to the systems investigated in this study.

Figures

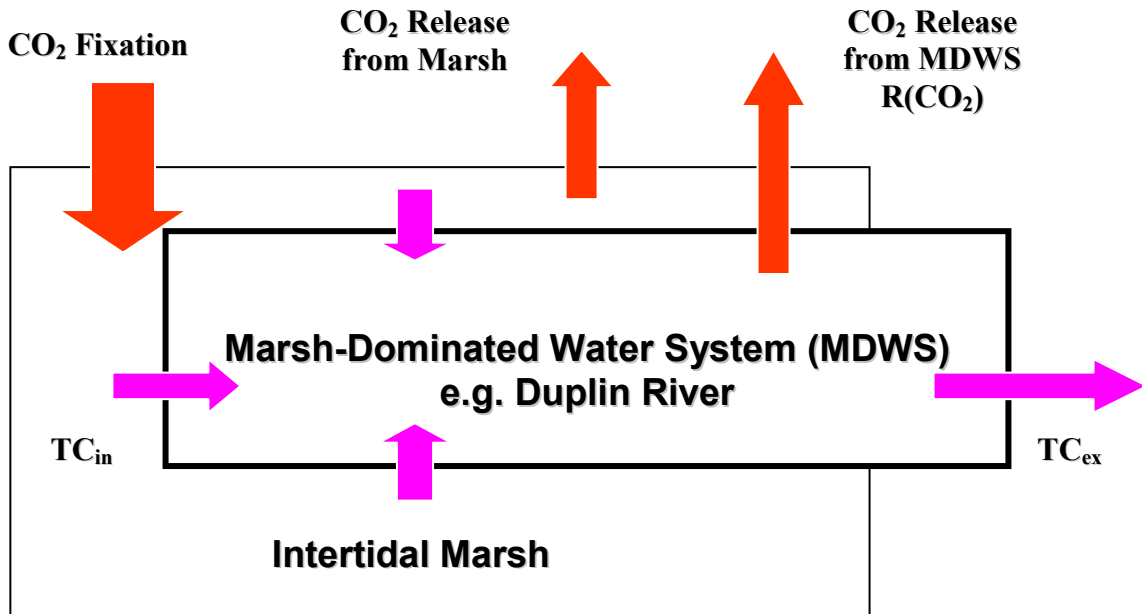


Fig. 5.1. A conceptual presentation of apparent net heterotrophy (ANH) and inorganic fluxes for marsh-dominated water systems (MDWS). $R(\text{CO}_2)$, CO_2 release from MDWS; TC_{ex} , export of total dissolved inorganic carbon from MDWS; $\text{ANH} = \text{TC}_{\text{ex}} + R(\text{CO}_2)$.

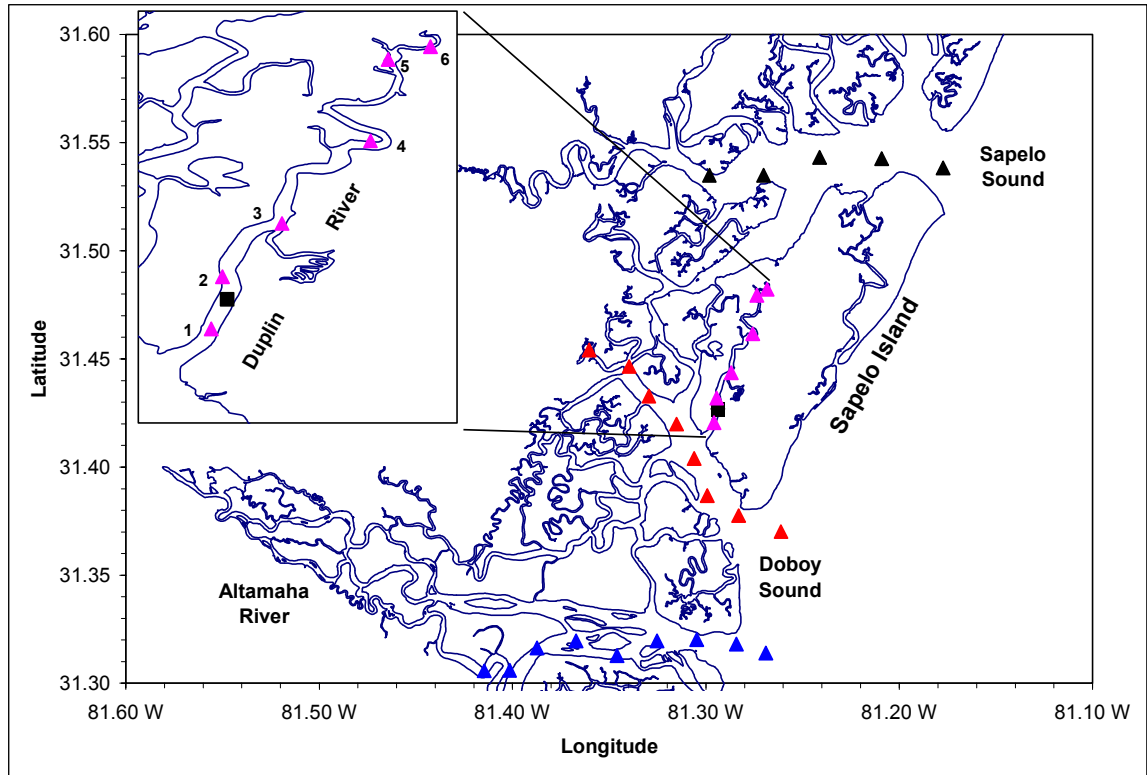


Fig. 5.2. Study area and sampling stations. Designated sampling stations are in filled triangles, and filled square represents the Anchor Stations in the Duplin River. Six stations along the Duplin River (inset), from the river mouth upstream, were Marsh Landing (1), Little Sapelo Island (2), Barn Creek (3), Lumber Landing (4), Hunt Camp (5), and Flume Dock (6).

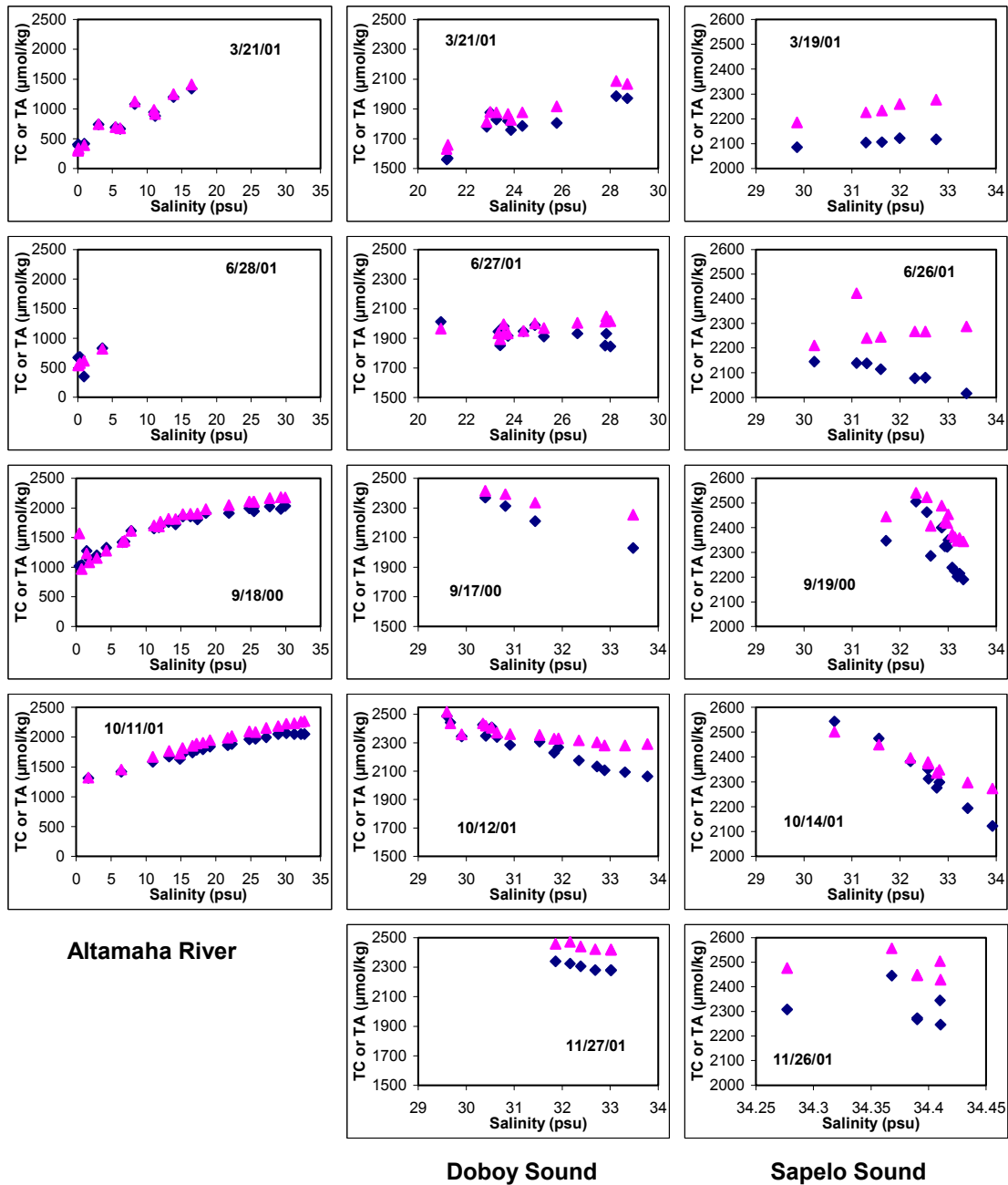
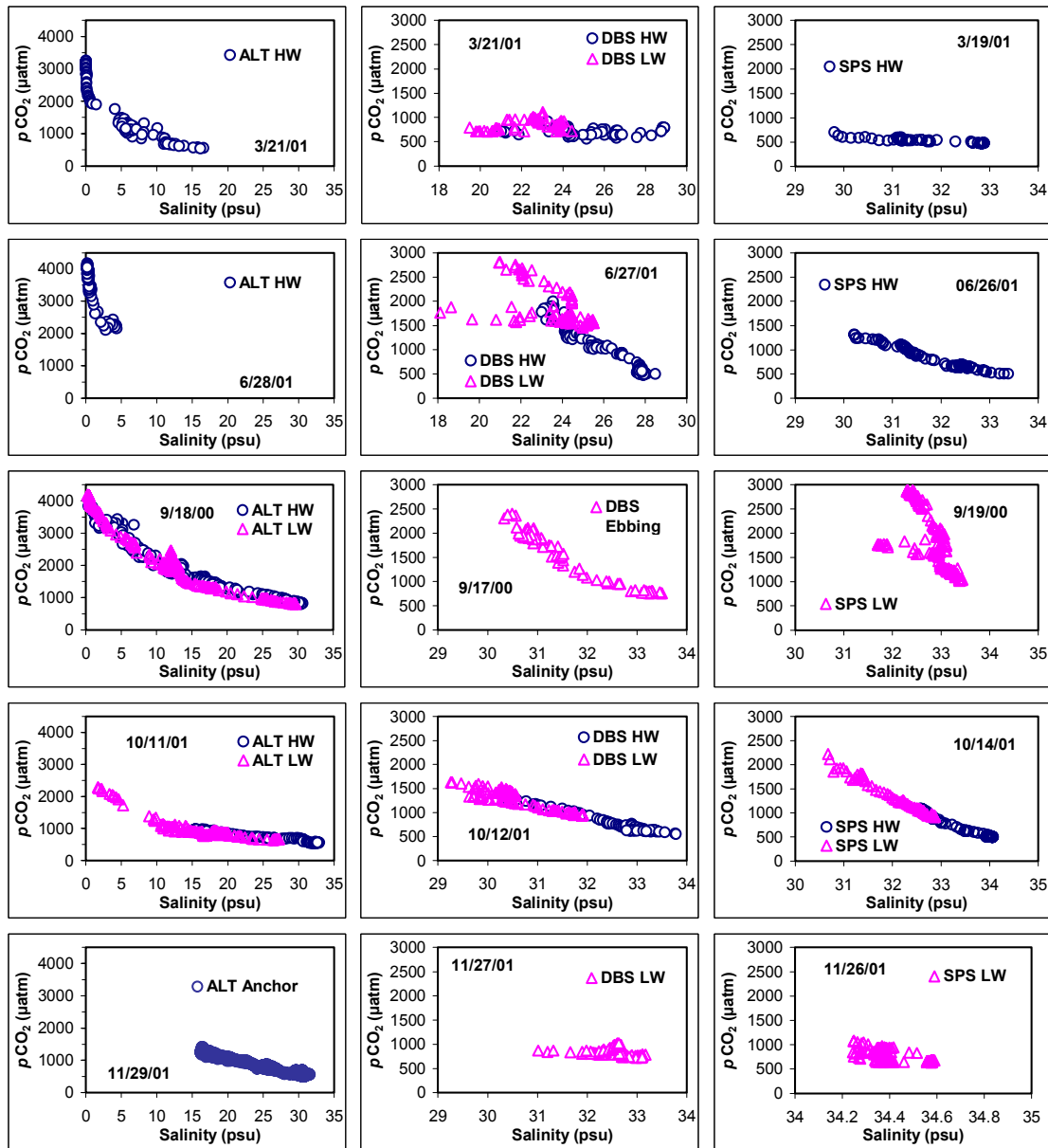


Fig. 5.3. Salinity distributions of TC and TA in Altamaha Sound, Doboy Sound, and Sapelo Sound during five surveys from Sept. 2000 to Nov. 2001. TC is as filled diamond, and TA as filled triangle.



**Altamaha River
(ALT)**

**Doboy Sound
(DBS)**

**Sapelo Sound
(SPS)**

Fig. 5.4. Salinity distributions of surface water $p\text{CO}_2$ in Altamaha Sound, Doboy Sound, and Sapelo Sound during five surveys from Sept. 2000 to Nov. 2001. HW and LW represent high water and low water sampling, respectively.

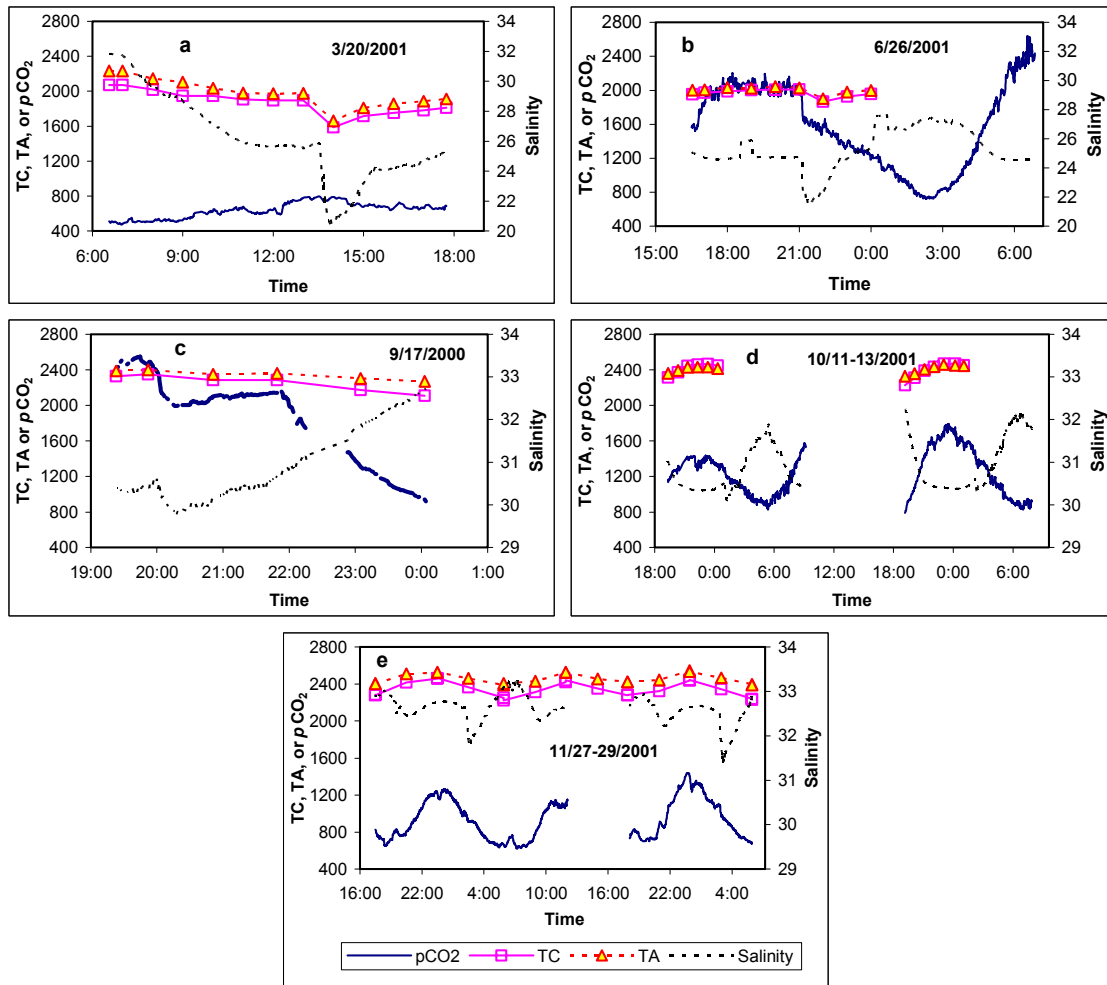


Fig. 5.5. Time series plots of surface water $p\text{CO}_2$, TC, TA, and Salinity at the Anchor Station in the Duplin River during the five GCE-LTER surveys. a. March 20, 2001; b. June 26, 2001; c. September 17, 2001; d. October 11 – 13, 2001; e. November 27 – 29, 2001. TC and TA are in units of $\mu\text{mol kg}^{-1}$, and $p\text{CO}_2$ is in μatm .

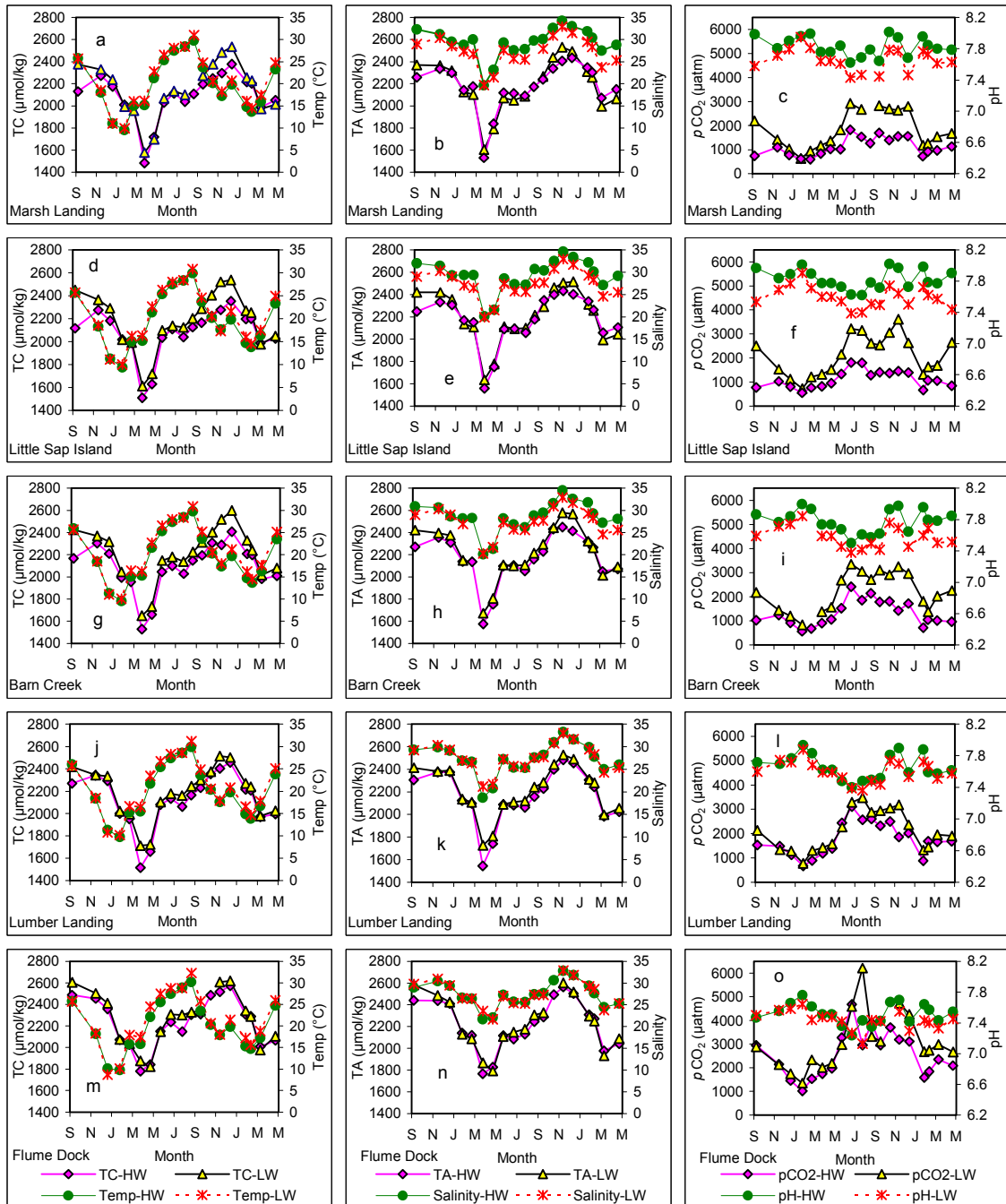


Fig. 5.6. Annual variations of surface water TC, TA, temperature, salinity, pH, and $p\text{CO}_2$ (calculated from TC and pH data) at Marsh Landing (a – c), Little Sapelo Island (d – f), Barn Creek (g – i), Lumber Landing (j – l), and Flume Dock (m – o) in the Duplin River. The data from Hunt Camp, which is close to Flume Dock, is not shown to accommodate space. HW and LW in the plots refer high water and low water sampling, respectively.

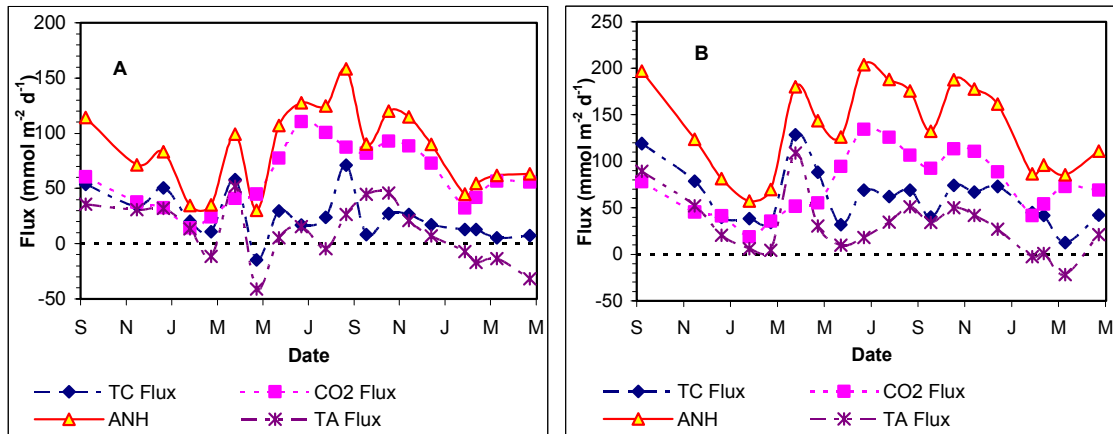


Fig. 5.7. Areal fluxes of TC export, air-water CO₂ exchange, TA export, and the apparent net heterotrophy in the Duplin River. A. Relative to Marsh Landing; B. Relative to Lumber Landing. Only CO₂ fluxes calculated from Raymond et al.'s (2000) method were displayed.

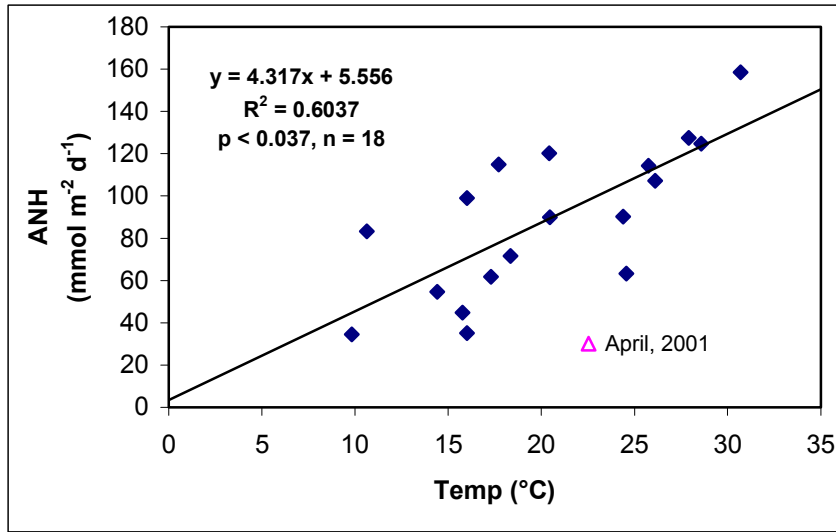


Fig. 5.8. Temperature dependence of the apparent net heterotrophy (ANH) in the Duplin River. Only the ANH presented in Fig. 5.7A was used. The solid line represents the linear best-fit of the data points with $R^2 = 0.6037$, $p < 0.037$, $n = 18$. The data from April, 2001 was not included in the regression.

Tables

Table 5.1. Summary of research surveys during the first one and a half years of the GCE-LTER project where the CO₂ system of surface water was sampled.

Date	Survey Regime	Designated Stations		
		Altamaha Sound	Doboy Sound	Sapelo Sound
Sept 17-19, 2000	Altamaha Sound (HW ¹ and LW ²); Doboy Sound (ebbing); Sapelo Sound (LW); The Duplin River Anchor	ALT+00 ³ , ALT+02, ALT+04, ALT+06, ALT+08, ALT+10, ALT+12, ALT+14	DBS+00, DBS+03, DBS+06, DBS+09	SPS+00, SPS+02, SPS+04, SPS+06, SPS+08, SPS+10, SPS+12
Mar 19-21, 2001	Altamaha Sound (HW); Doboy Sound (HW and LW); Sapelo Sound (HW); The Duplin River Anchor	ALT+00, ALT+04, ALT+08, ALT+12	DBS+00, DBS+03, DBS+06, DBS+09, DBS+12	SPS+04, SPS+06, SPS+08, SPS+10, SPS+12
Jun 26 -28, 2001	Altamaha Sound (HW); Doboy Sound (HW and LW); Sapelo Sound (HW); The Duplin River Anchor	ALT+00, ALT+04, ALT+08, ALT+12	DBS+00, DBS+03, DBS+06, DBS+09, DBS+12	SPS+00, SPS+02, SPS+04, SPS+06, SPS+08, SPS+10, SPS+12
Oct 11-14, 2001	Altamaha Sound (HW and LW); Doboy Sound (HW and LW); Sapelo Sound (HW and LW); The Duplin River Anchor	ALT-02, ALT+00, ALT+02, ALT+04, ALT+06, ALT+08, ALT+10, ALT+12, ALT+14	DBS-02, DBS+00, DBS+02, DBS+04, DBS+06, DBS+08, DBS+10, DBS+12	SPS+00, SPS+03, SPS+06, SPS+09, SPS+12
Nov 26-29, 2001	Doboy Sound (LW); Sapelo Sound (LW); The Duplin River Anchor	No sampling stations	DBS-02, DBS+00, DBS+02, DBS+04, DBS+06, DBS+08, DBS+10	SPS+00, SPS+03, SPS+06, SPS+09, SPS+12

Notes: 1 HW - high water survey.

2 LW - low water survey.

3 ALT+00 - the first three letters represent the name of the estuary; "+" and "-" indicates upstream or down-stream from the estuarine mouth, respectively; the last two digits indicate the longitudinal distance (km) from the estuarine mouth.

Table 5.2. Estimates of CO₂ fluxes in the Duplin River. Numbers are in mmol m⁻² d⁻¹ unless otherwise indicated. The results calculated from both Wanninkhof (1992) (W) and Raymond et al. (2000) (R) parameterizations were listed. The annual flux was calculated by integrating daily flux from January, 2001 to December, 2001. Positive values indicate fluxes are from water to the atmosphere. Segment 1, Marsh Landing to Little Sap Island; Segment 2, Little Sap Island to Barn Creek; Segment 3, Barn Creek to Lumber Landing; Segment 4, Lumber Landing to Hunt Camp; Segment 5, Hunt Camp to Flume Dock. Area-weighted average CO₂ fluxes were calculated by multiplying each segment's flux by its surface area, summing the five segment fluxes, and dividing by the total surface area of five segments. Surface areas (all in 10⁵ m²) are 0.9, 1.3, 4.9, 3.0, 0.5 for segments 1-5, respectively, which were estimated based on the distance between two consecutive stations (Imberger et al., 1983) and the river width measured from a 1 : 80,000 scale map.

Date	Average Daily Wind Speed (m/s)	Segment 1		Segment 2		Segment 3		Segment 4		Segment 5		Area-Weighted Average	
		W-Flux	R-Flux	W-Flux	R-Flux	W-Flux	R-Flux	W-Flux	R-Flux	W-Flux	R-Flux	W-Flux	R-Flux
Sep-00	3.95	45.4	46.7	48.0	49.4	51.9	53.5	72.5	74.6	93.5	96.2	58.9	60.6
Nov-00	2.79	17.6	30.9	18.3	32.2	19.6	34.4	24.8	43.5	32.0	56.2	21.4	37.5
Dec-00	3.55	18.3	22.2	20.8	25.3	24.7	30.1	32.9	40.0	39.6	48.2	26.8	32.6
Jan-01	3.04	6.1	9.4	7.0	10.8	8.1	12.5	11.4	17.5	17.1	26.5	9.2	14.2
Feb-01	3.11	12.5	18.6	11.4	16.9	12.8	19.0	22.4	33.3	33.0	49.1	16.4	24.3
Mar-01	4.26	32.1	29.4	35.3	32.4	41.0	37.6	54.2	49.8	67.9	62.3	44.7	41.0
Apr-01	3.75	30.5	34.1	32.6	36.4	37.0	41.4	47.8	53.4	58.7	65.6	40.1	44.8
May-01	3.95	46.9	48.3	60.2	62.0	72.4	74.5	89.5	92.1	104.7	107.7	75.3	77.5
Jun-01	3.61	67.8	80.3	76.2	90.2	87.7	103.8	110.0	130.3	133.8	158.4	93.4	110.6
Jul-01	3.62	62.9	74.3	68.9	81.4	78.1	92.2	102.6	121.2	128.6	151.9	85.3	100.8
Aug-01	3.50	37.7	46.9	55.9	69.5	68.4	85.1	83.8	104.2	97.3	121.0	70.2	87.3
Sep-01	3.38	49.5	64.9	52.1	68.4	61.6	80.8	69.6	91.3	75.6	99.1	62.5	81.9
Oct-01	3.86	65.1	69.6	70.9	75.7	81.3	86.9	103.5	110.6	121.1	129.4	87.1	93.0
Nov-01	3.47	58.0	73.1	61.6	77.7	61.6	77.6	84.5	106.5	106.2	133.9	70.1	88.4
Dec-01	2.94	36.8	59.8	38.6	62.7	40.6	66.0	52.1	84.7	68.2	110.9	44.7	72.7
Jan-02	2.86	12.4	21.0	15.6	26.4	16.9	28.6	22.9	38.8	33.8	57.2	18.9	32.1
Feb-02	3.01	19.7	30.8	21.2	33.1	23.8	37.2	33.3	52.1	41.8	65.4	26.8	41.9
Mar-02	3.60	31.5	37.4	35.8	42.6	43.4	51.6	59.1	70.3	73.7	87.6	47.5	56.5
Apr-02	3.40	34.6	44.9	37.7	49.0	38.6	50.1	51.8	67.3	60.4	78.5	43.0	55.9
										gC m⁻² yr⁻¹		256.2	306.4
Annual										mmol m⁻² d⁻¹		58.5	70.0

Table 5.3. Estimates of TC export fluxes from the Duplin River. Mean TC gradient for each sampling event was obtained by averaging TC gradients between Marsh Landing and the other five sampling stations (TC Gradient 1 – 5). Daily export flux (mmol d^{-1}) was calculated based on Equation 5.1 using mean TC gradients, a longitudinal diffusion coefficient of $38 \text{ m}^2 \text{ s}^{-1}$ (Imberger et al., 1983), and a cross-sectional area of the river at Marsh Landing (654 m^2). Daily areal TC export flux for each sampling event was calculated by dividing TC export fluxes by the total surface area ($1.1 \times 10^6 \text{ m}^2$) from Marsh Landing to Flume Dock. Positive numbers indicate the flux direction is from the Duplin River to Doboy Sound. The annual export was calculated by integrating TC areal fluxes from January, 2001 to December, 2001. ML, Marsh Landing; LSI, Little Sap Island; BC, Barn Creek; LL, Lumber Landing; HC, Hunt Camp; FD, Flume Dock.

Sampling Date	TC Gradient 1 (LSI - ML) mmol m^{-4}	TC Gradient 2 (BC - ML) mmol m^{-4}	TC Gradient 3 (LL - ML) mmol m^{-4}	TC Gradient 4 (HC - ML) mmol m^{-4}	TC Gradient 5 (FD - ML) mmol m^{-4}	Mean Gradient mmol m^{-4}	Daily Export Flux mmol d^{-1}	Daily Areal Export Flux $\text{mmol m}^{-2} \text{ d}^{-1}$
Sep-00	0.0425	0.0243	0.0145	0.0251	0.0265	0.0266	5.7E+07	53.7
Nov-00	0.0267	0.0203	0.0067	0.0146	0.0161	0.0169	3.6E+07	34.1
Dec-00	0.0442	0.0319	0.0173	0.0159	0.0160	0.0251	5.4E+07	50.6
Jan-01	0.0246	0.0108	0.0017	0.0066	0.0066	0.0101	2.2E+07	20.3
Feb-01	0.0264	-0.0100	0.0001	0.0048	0.0053	0.0053	1.1E+07	10.8
Mar-01	0.0430	0.0340	0.0135	0.0263	0.0268	0.0287	6.2E+07	58.0
Apr-01	-0.0497	-0.0062	-0.0028	0.0112	0.0111	-0.0073	-1.6E+07	-14.7
May-01	0.0232	0.0266	0.0066	0.0083	0.0087	0.0147	3.2E+07	29.7
Jun-01	0.0005	0.0101	0.0053	0.0129	0.0133	0.0084	1.8E+07	17.0
Jul-01	0.0178	0.0087	0.0069	0.0121	0.0140	0.0119	2.6E+07	24.1
Aug-01	0.0795	0.0434	0.0153	0.0192	0.0187	0.0352	7.6E+07	71.1
Sep-01	-0.0125	0.0108	0.0050	0.0092	0.0082	0.0041	8.9E+06	8.4
Oct-01	0.0027	0.0247	0.0084	0.0157	0.0157	0.0134	2.9E+07	27.1
Nov-01	0.0132	0.0085	0.0113	0.0169	0.0156	0.0131	2.8E+07	26.5
Dec-01	-0.0144	0.0276	0.0038	0.0129	0.0127	0.0085	1.8E+07	17.2
Jan-02	-0.0033	0.0186	0.0014	0.0068	0.0079	0.0063	1.4E+07	12.7
Feb-02	0.0149	0.0017	0.0013	0.0071	0.0066	0.0063	1.4E+07	12.8
Mar-02	0.0011	0.0108	-0.0011	0.0012	0.0011	0.0026	5.6E+06	5.3
Apr-02	0.0077	0.0065	-0.0038	0.0032	0.0047	0.0036	7.8E+06	7.4
Annual Areal Flux							$\text{gC m}^{-2} \text{ yr}^{-1}$	109
							$\text{mmol m}^{-2} \text{ d}^{-1}$	24.9

Table 5.4. Comparison of estuarine and marsh respiratory rates and the apparent net heterotrophy (ANH) in the Duplin River. The respiratory rates of estuarine water were measured at the mouth of the Duplin River during the LTER surveys using inorganic carbon based incubations; all results were converted from the unit of $\text{mmol C m}^{-3} \text{ d}^{-1}$ to $\text{mmol C m}^{-2} \text{ d}^{-1}$ by multiplying the water depth of 5 m at the station. Marsh respiratory rates were listed as the sum of benthic (Cai et al., 1999) and overlying water rates (Pomeroy et al., 1972) in the marsh measured in summer and fall near the Duplin River.

Unit	Estuarine Respiration (Mar. – Nov., 2001)	Marsh Respiration	ANH in the Duplin River (Mar. – Nov., 2001)
$\text{mmol C m}^{-2} \text{ d}^{-1}$	20 ~ 89	82 ~ 183	99 ~ 158

Table 5.5. Summary of inorganic carbon fluxes in the SAB and its coastal salt marsh. For comparison, organic carbon fluxes in the marsh are also listed. The total salt marsh area of the SAB, which includes the marshes in North Carolina, South Carolina, Georgia, and Florida, is 457050 ha (Reimold, 1977), and is used to convert the annual areal values to the annual total. Annual areal CO₂ degassing rate from marsh water was estimated by adjusting the CO₂ degassing rate in the segment 5 of the Duplin River (Table 5.2) by a factor of ¼ (daily marsh inundation time, 6 hr) and a factor of ½ (sluggish wind for the marsh water, Cai and Wang, 1998).

Processes	Annual Areal (gC m ⁻² yr ⁻¹)	Annual Total (× 10 ¹² gC yr ⁻¹)	Reference
Net Primary Production in Marsh	2025	9.74	Hopkinson, 1988
TC Export from Marsh	156	0.71	This Study
CO ₂ Degassing from Marsh Water	56	0.27	This Study
CO ₂ Degassing from Marsh Sediment	223 - 328	1.07 – 1.58	Morris and Whiting, 1986
DOC and POC Export from Marsh	260	1.25 – 1.6	Chalmers et al., 1985; Dame et al., 1986
TC Export from the SAB to the Open Ocean	28.9	2.62	Chapter 4
CO ₂ Air-Sea Exchange (sea to air) in the SAB	29.8	2.70	Chapter 4

CHAPTER 6

SUMMARY

A Carbon Transport and Mass Balance Model. In addition to indications of CO₂ source/sink and export/import, the inorganic carbon fluxes estimated in Chapters 4 and 5 are meaningful on the ecosystem level. As a summary of the findings, a carbon transport and mass balance model (Fig. 6.1) is presented in order to estimate the net ecosystem heterotrophy (NEH) of the South Atlantic Bight (SAB). The model can be generalized and applied to other ecosystems. The net ecosystem heterotrophy or production (NEH/NEP) is defined as the balance between the total ecosystem respiration (R) and the gross primary production (P). Traditionally, respiration and primary production are measured for individual components of a system and the results are integrated to constrain the balance. In Chapter 4, we have used P and R to estimate the NEH of the SAB. However, the outcome is not promising since we simply cannot identify enough allochthonous sources to fill the large imbalance of organic matter derived from this method. The major point is that both R and P values are usually large compared to import/export fluxes, and the difference between the two rates is rather small. Therefore, the uncertainty is often magnified by taking the difference of R and P to evaluate the NEH/NEP of an ecosystem. For example, if assuming only 10-20% uncertainty for both P and R of the SAB, the inheriting error in their difference is still a large number with respect to both organic and inorganic fluxes (Table 4.5). Estimating the NEH/NEP from organic carbon balance may also be problematic due to the complex nature of living and

non-living organic carbon. Inorganic carbon fluxes on the other hand are most likely on the same order of magnitude as organic carbon fluxes for an ecosystem (e.g. Table 5.5). Their mass balance can be evaluated fairly accurately for the shelf system. Therefore, it is relatively easy and simple to constrain the NEH/NEP within a more reasonable range even with magnified uncertainty that migrates down the calculation.

Based on the model concept (Fig. 6.1), the net export of inorganic carbon ($TC_{ex} + CO_{2a-s} - TC_{in} + TC_b$) represents the NEH of the system. For the SAB, the total export of inorganic carbon ($TC_{ex} + CO_{2a-s}$) is 5.3×10^{12} gC yr⁻¹ (Chapter 4), and the total input from rivers and marshes is 1.3×10^{12} gC yr⁻¹ (TC_{in}) (Chapter 5). The only unknown inorganic carbon flux is the benthic flux (TC_b), which should be small due to near balance between primary production and respiration in the SAB sediment (Jahnke et al., 2000). We therefore choose to ignore this term. Then the NEH in the SAB is estimated to be 4.0×10^{12} gC yr⁻¹, which is one order of magnitude lower than the estimated NEH from P and R (Chapter 4). It is also on the same order of magnitude of the current estimate of total organic carbon input of 2.1×10^{12} gC yr⁻¹ from SAB rivers and marshes (Fig 6.1; Chapters 4). Although organic carbon are still not balanced in the SAB, the current study has constrained the NEH of the SAB within a range that is more reasonable with respect to organic carbon fluxes and therefore significantly reduced the large imbalance of organic carbon as discussed in Chapter 4. Based on the measurements of DOC in the SAB (Moran et al., 1999), the DOC also shows the positive concentration gradient in the off-shore direction in the SAB, and thus export of organic carbon likely occurs. If using the same procedure as presented in Chapter 4 while calculating the TC export from the SAB, the DOC export from the SAB should be on the order of 10^{12} gC

yr⁻¹. This is consistent with our estimation of the NEH in the SAB, since the NHE can also be evaluated by the net organic carbon fluxes ($OC_{in} - OC_{ex}$, Fig. 6.1) which are likely on the same order of 10^{12} gC yr⁻¹.

Extended Continental Shelf Pump. As discussed in Chapter 4, the “continental shelf pump” (Tsunogai et al., 1999) may only function seasonally (e.g. in winter) in the SAB. On an annual basis, the SAB is a net source of CO₂ with respect to the atmosphere and exports inorganic carbon to the open ocean. The over-saturated sea surface pCO_2 during most of the year can only be maintained if there exist excess TC sources which may constitute excess respiration over primary production and external TC input. Since the SAB is heterotrophic (Chapter 4 and Fig. 6.1), excess respiration is confirmed. Chapter 5, on the other hand, suggests that external TC input consists of TC exports from rivers and marshes, which are significant to the CO₂ system in the SAB.

Georgia marsh systems are highly productive (Hopkinson, 1988; Dame, 1994; Dai and Wiegert, 1996; Odum, 2000) with net annual primary production one order of magnitude higher than any single export flux of either organic or inorganic carbon estimated in previous and current studies (Table 5.5). Such high annual primary production is able to support high respiration, carbon exportation, and accumulation of carbon inside the marsh (Wiegert et al., 1981; Chalmers et al., 1985). Export of inorganic carbon from the marsh has significant influence on the CO₂ system of its adjacent continental shelf (Chapter 5). If the SAB is extended to include its adjacent in-shore and marsh systems, it would generate a new view on the CO₂ biogeochemistry in this land-to-ocean continuum. We herein present an “extended continental shelf pump” hypothesis

(Fig. 6.2) in order to summarize the interaction and seasonal variation of inorganic carbon signals within this integrated system.

This extended pump consists of two individual pumps: a “marsh pump” which represents interaction between marshes and surrounding water systems, and a “continental shelf pump” which retains the original meaning of the concept proposed by Tsunogai et al. (1999) (Fig. 6.2). The seasonality of these two pumps generates a series of scenarios (Table 6.1). In spring and early summer when marsh primary producers are at their annual maximum growth rate (Dame, 1989), the marsh “biological pump” draws large amount of inorganic carbon from the atmosphere and assimilates it into organic carbon through photosynthesis; marsh export of inorganic carbon is at its annual minimum (Chapter 5) which corresponds to the weakest “marsh pump” stage. Consequently, the apparent net heterotrophy (ANH) of nearby water systems is at their annual minimum (Chapter 5). However, the shelf surface water is still over-saturated with respect to atmospheric $p\text{CO}_2$ (Chapter 4) in spite of the weak “marsh pump”. This is probably due to combined effect of heating, lack of spring phytoplankton blooms, and previously accumulated inorganic and organic carbon that support over-saturation of sea surface $p\text{CO}_2$ directly and/or through respiration. This is viewed as a weak “continental shelf pump” situation. As the season goes on, marsh primary production decreases while respiration increases, or the “marsh pump” grows stronger as export of inorganic carbon from the marsh increases. The ANH in marsh-dominated water systems is enhanced. In the meantime, the “continental shelf pump” is further weakened due to further elevated water temperature. In late summer and fall, the “marsh pump” operates at the annual maximum rate (maximum export of inorganic carbon from the marsh) while the

“continental shelf pump” is at the annual weakest stage due to high water temperature. This results in an apparent net heterotrophic peak in marsh-dominated systems and probably the annual highest degree of CO₂ over-saturation in the SAB. During the winter, primary production and respiration in the marsh are all at the annual low, and export from the marsh is also less intensive. The degree of the ANH in marsh-dominated water systems declines. It is during this time of the year when the “continental shelf pump” may primarily function as proposed in the SAB: cooling and transport of inorganic carbon to the open ocean produces a net sink for atmospheric CO₂. This corresponds to a strong “continental shelf pump” situation. The new concept demonstrates that the marsh processes play critical roles in maintaining the seasonal pace of carbon cycling in Georgia coastal and continental shelf systems.

This new hypothesis is, however, an over-simplified conceptual model; climatological and biogeochemical processes as well as their complex and interweaved feedbacks may change this seasonal progression in a less predictable way. Also, due to different temporal and spatial scales of biogeochemical processes that this hypothesis may involve, causes and responses may mismatch in terms of time and space. However, this new hypothesis does provide a generalized view on CO₂ biogeochemistry in the “land-to-ocean continuum” along the Georgia shoreline of the Atlantic Ocean. The implication from the hypothesis is that export of inorganic carbon from the marsh is one of the major mechanisms that cause this “land-to-ocean continuum” to be annual net sources of atmospheric CO₂.

Figures

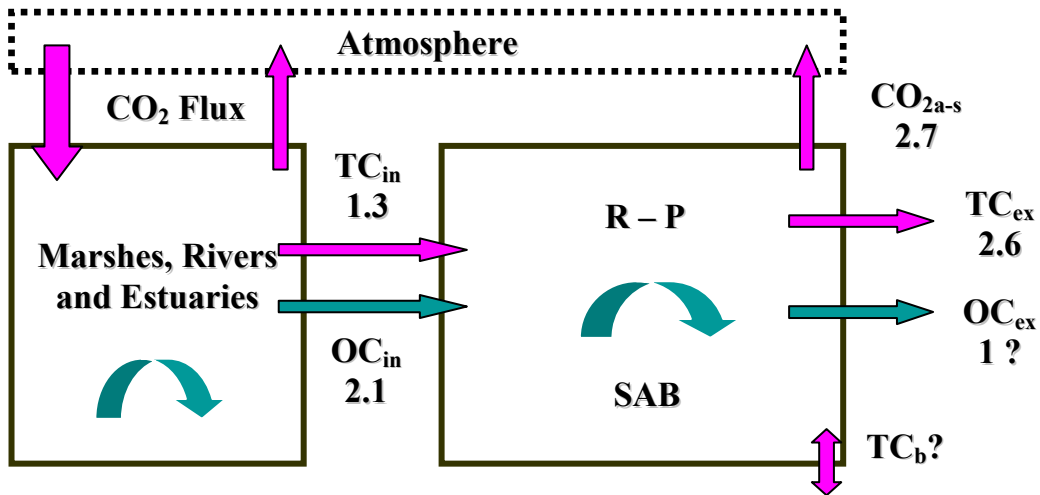


Fig. 6.1. A conceptual carbon transport and mass balance model for the South Atlantic Bight (SAB). For a given ecosystem, $\text{NEH} = \text{R} - \text{P} = \text{TC}_{\text{ex}} + \text{CO}_{2\text{a-s}} - \text{TC}_{\text{in}} + \text{TC}_b = \text{OC}_{\text{in}} - \text{OC}_{\text{ex}}$, where the NEH denotes the net ecosystem heterotrophy; R is the total ecosystem respiration; P is the gross primary production; TC_{ex} is inorganic carbon export; TC_{in} is inorganic carbon input; $\text{CO}_{2\text{a-s}}$ is air-sea CO_2 exchange; TC_b is the benthic inorganic carbon flux; OC_{in} is organic carbon input; OC_{ex} is organic carbon exchange with the open ocean. Fluxes are in $10^{12} \text{ gC yr}^{-1}$.

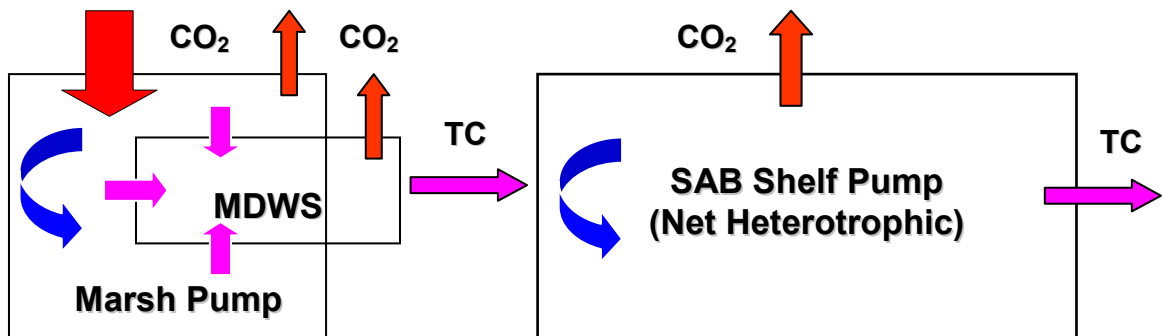


Fig. 6.2. A presentation of "extended continental shelf pump" hypothesis. MDWS denotes marsh-dominated water systems.

Tables

Table 6.1. Summary of the seasonality of the “extended continental shelf pump”.

Season	Marsh Pump	ANH in MDWS	Shelf Pump	SAB CO₂ Over-Saturation
Spring	Weakest	Lowest	Weakened	Small
Summer	Strengthened	Increase	Further weakened	Increase
Late Summer – Fall	Strongest	Highest	Begin to strengthen	Reach maximum and begin to decrease
Winter	Weakened	Decrease	Strong	Under-saturation

REFERENCES

- Alber, M. and Sheldon, J. E. 1999. Use of a date-specific method to examine variability in the flushing times of Georgia estuaries. *Estuar. Coast. Shelf Sci.* 49: 469-482.
- Albert, J. J. and Takács, M. 1999. Importance of humic substances for carbon and nitrogen transport into the southeastern United States streams. *Organic Geochem.*, 30: 385-395.
- Alhadeff, S. J., Landers, M. N., and McCallum, B. E. 1999. Surface-water data, Georgia, water year 1999. Water-Data Report GA-99-1. Atlanta, Georgia: United States Geological Survey.
- Anderson, J. M. 1974. Nitrogen and phosphorus budgets and the role of sediments in six shallow Danish lakes. *Arch. Hydrobiol.* 74: 528-550.
- Atkinson, L. P. and Targett, T. E. 1983. Upwelling along the 60m isobath from Cape Canaveral to Cape Hatteras and its relationship to fish distribution. *Deep-Sea Res.*, 30: 221-226.
- Atkinson, L. P., Lee, T. N., Blanton, J. O., and Paffenhofer, G.-A. 1987. Summer upwelling on the southeastern continental shelf of the USA during 1981: hydrographic observations. *Prog. in Oceanogr.*, 19: 231-266.
- Atkinson, L. P., Miller, J. L., Lee, T. N., and Dunstan, W. M. 1996. Nutrients and chlorophyll at the shelf break off the southeastern United States during the Genesis of Atlantic Lows Experiments: winter 1986. *J. Geophys. Res.*, 101, 20,565-20,578.
- Atkinson, L. P., O'Malley, P. G., Yoder, J. A., and Paffenhofer, G. -A. 1984. The effect of summertime shelf break upwelling on nutrient flux in southeastern United States continental shelf waters. *J. Mar. Res.*, 42: 969-993.
- Baehr, M. M., DeGrandpre, M. D., 2002. Under-ice CO₂ and O₂ variability in a freshwater lake. *Biogeochemistry* (in press).
- Balls, P. W. 1992. Nutrient behaviour in two contrasting Scottish estuaries, the Forth and Tay. *Oceanol. Acta* 15: 261-277.
- Balls, P. W. 1994. Nutrient inputs to estuaries from Nine Scottish east coast rivers: influence of estuarine processes on inputs to the North Sea. *Estuar. Coast. and Shelf Sci.* 39: 329-352.

- Balls, P. W., Brockie, N., Dobson, J., and Johnston, W. 1996. Dissolved oxygen and nitrification in the upper forth estuary during summer (1982-92): patterns and trends. *Estuar. Coast. and Shelf Sci.* 42: 117-134.
- Bates, N. R., Merlivat, L., Beaumont, L., and Pequignet, A. C. 2000. Intercomparison of shipboard and moored CARIOCA buoy seawater $f\text{CO}_2$ measurements in the Sargasso Sea. *Mar. Chem.*, 72: 239-255.
- Bates, N. R., Takahashi, T., Chipman, D. W., and Knap, A. H., 1998. Variability of $p\text{CO}_2$ on diel to seasonal timescales in the Sargasso Sea. *J. Geophys. Res.*, 103, 15,567-15,585.
- Beck, K. C., Reuter, J. H., and Perdue, E. M. 1974. Organic and inorganic geochemistry of some coastal plain rivers of the southeastern United State. *Geochim. Cosmochim. Acta* 38: 341-364.
- Berner, R. A., Scott, M. R., and Thomlinson, C. 1970. Carbonate alkalinity in the pore waters of anoxic marine sediments. *Limnol. Oceanogr.*, 15: 544-549.
- Blanton, J. O. and Pietrafesa, L. J. 1978. Flushing of the continental shelf south of Cape Hatteras by the Gulf Stream. *Geophys. Res. Lett.*, 5: 495-498.
- Blanton, J. O., Alexander, C., Alber, M., and Kineke, G. 1999. The mobilization and deposition of mud deposits in a coastal plain estuary. *Limnologia*, 29: 293-300.
- Blanton, J. O., Oey, L.-Y., Amft, J. and Lee, T. N. 1989. Advection of momentum and buoyancy n a coastal frontal zone. *Journal of Physical Oceanography* 19, 98-115.
- Boehme, S. E., Sabine, C. L., and Reimers, C. E. 1998. CO_2 fluxes from a coastal transect: a time-series approach. *Mar. Chem.*, 63: 49-67.
- Borges, A. V. and Frankignoulle, M. 1999. Daily and seasonal variations of the partial pressure of CO_2 in surface seawater along the Belgian and southern Dutch coastal areas. *J. Mar. Syst.*, 19: 251-266.
- Boyle, E., Collier, R., Dengler, A. T., Edmond, J. M., Ng, A. C., and Stallard, R. R.. 1974. On the chemical mass-balance in estuaries. *Geochim. Cosmochim. Acta* 38: 1719-1728.
- Brewer, P. G. and Goldman, J. C. 1976. Alkalinity changes generated by phytoplankton growth. *Limnol. Oceanogr.* 21, 108-117.
- Broecker, W. S. and Peng, T. H. 1982. Tracers in the sea. Eldigio, Palisades, NY, 690pp.
- Byrne, R. H. and Breland, J. A. 1989. High precision multiwavelength pH determinations in seawater using cresol red. *Deep-sea Res.*, 36: 803-810.

- Byrne, R. H., Liu, X. W., Kaltenbacher, E., and Sell, K. 2002. Spectrophotometric measurement of total inorganic carbon in aqueous solutions using a liquid core waveguide. *Anal. Chim. Acta*, 451: 221-229.
- Cai, W. J, Wang, Y., and Hodson, R. E. 1998. Acid-base properties of dissolved organic matter in the estuarine waters of Georgia. *Geochim. Cosmochim. Acta*. 62: 473-483.
- Cai, W. J. 2003. Riverine inorganic carbon flux and rate of biological uptake in the Mississippi River plume. *Geophys. Res. Lett.* (in press)
- Cai, W. J. and Wang, Y. 1998. The chemistry, fluxes and sources of carbon dioxide in the estuarine waters of the Satilla and Altamaha River, Georgia. *Limnol. Oceanogr.*, 43: 657-668.
- Cai, W. J., Pomeroy, L. R., Moran, M. A., and Wang, Y. 1999. Oxygen and carbon dioxide mass balance for the estuarine-intertidal marsh complex of five rivers in the southeastern U.S. *Limnol. Oceanogr.* 44: 639-649.
- Cai, W. J., Wiebe, W. J., Wang, Y., and Sheldon, J. E. 2000. Intertidal marsh as a source of dissolved inorganic carbon and a sink of NO₃⁻ in the Satilla River-estuarine complex in the southeastern U.S. *Limnol. Oceanogr.* 45: 1743-1752.
- Carini, S., and others. 1996. Gas exchange in the Parker Estuary, MA. *Bio. Bull.* 191: 333-334.
- Chalmers, A. G., Wiegert, R. G., and Wolf, P. L. 1985. Carbon balance in a salt marsh: Interactions of diffusion export, tidal deposition, and rainfall-caused erosion. *Estuarine Coastal Shelf Sci.* 21: 757-771.
- Chen, C. T. A., Liu, K. K., and MacDonald, R. 2001. Continental margin exchanges. In Fasham, M. J. R. [ed], *Ocean biogeochemistry*. Springer, revised.
- Chen, C., Zheng, L., and Blanton, J. O. 1999. Physical processes controlling the formation, evolution, and perturbation of the low-salinity front in the inner shelf off the southeastern United States: A modeling study. *J. Geophys. Res. – Oceans* 104, 1259-1288.
- Chen, F., Gonzalez, J. M., Dustman, W. A., Moran, M. A., and Hudson, R. E. 1997. In situ reverse transcriptase: an approach to characterize genetic diversity and activity of prokaryotes. *Appl. Environ. Microbiol.*, 63: 4907-4913.
- Childers, D. L. 1994. Fifteen years of marsh flumes: A review of marsh-water column interactions in southeastern USA estuaries. In W. J. Mitsch [ed], *Global wetlands: Old world and new*. Elsevier. p277-293.
- Childers, D. L., Cofer-Shabica, S., and Nakashima, L. 1993. Spatial and temporal variability in marsh-water column interactions in a southeastern USA salt marsh estuary. *Mar. Ecol. Prog. Ser.* 95: 25-38.

- Childers, D. L., Day, J. W. Jr., and Mckellar, H. N. Jr. 2000. Twenty more years of marsh and estuarine flux studies: revisiting Nixon (1980). In Weinstein, M. P. and Kreeger, D. A. [eds], Concepts and controversies in tidal marsh ecology. Kluwer Academic. p391-423.
- Christian, R. R., Boyer, J. N. and Stanley, D. W. 1991. Multi-year distribution patterns of nutrients within the Neuse River Estuary, North Carolina. Mar. Ecol. Prog. Series 71: 259-274.
- Church, T. M. 1986. Biogeochemical factors influencing the residence time of microconstituents in a large tidal estuary, Delaware Bay. Mar. Chem. 18: 393-406.
- Clark, J. F., Wanninkhof, R., Schlosser, P., and Simpson, H. J. 1994. Gas exchange rates in the tidal Hudson river using a dual tracer technique. Tellus 46b: 274-285.
- Clayton, T. D. and Byrne, R. H. 1993. Spectrophotometric seawater pH measurements: total hydrogen ion concentration scale calibration of m-cresol purple and at-sea results. Deep-sea Res., 40: 2315-2329.
- Dai, T. and Wiegert, R. G. 1996. Ramet population dynamics and net aerial primary productivity of *Spartina alterniflora*. Ecology, 77: 276-288.
- Dame, R. F. 1994. The net flux of materials between marsh-estuarine systems and the sea: the Atlantic coast of the United States. In W. J. Mitsch [ed], Global wetlands: Old world and new. Elsevier. p295-305.
- Dame, R. F., Chrzanowski, TH., Bildstein, K., Kjerfve, B., Mckellar, H., Nelson, D., Spurrier, J., Stancyk, S., Stevenson, H., Vernberg, J., and Zingmark, R. 1986. The outwelling hypothesis and North Inlet, South Carolina. Mar. Ecol. Prog. Ser. 33: 217-229.
- Dame, R. R. 1989. The importance of *Spartina alterniflora* to Atlantic coast estuaries. Crit. Rev. Aquat. Sci., 1: 639-660.
- Dame, R. R., Childers, D., and Koepfler, E. T. 1992. A geohydrologic continuum theory for the spatial and temporal evolution of marsh-estuarine ecosystems. Neth. J. Sea Res., 30: 63-72.
- DeGrandpre, M. D. 1993. Measurement of seawater $p\text{CO}_2$ using a renewable-reagent fiber optic sensor with colorimetric detection. Anal. Chem., 65: 331-337.
- DeGrandpre, M. D., Baehr, M. M., and Hammar, T. R. 1999. Calibration-free optical chemical sensors. Anal. Chem., 71: 1152-1159.
- DeGrandpre, M. D., Hammar, T. R., and Wirrick, C. D. 1998. Short-term $p\text{CO}_2$ and O_2 dynamics in California coastal waters. Deep-sea Res., 45, 1557-1575.

- DeGrandpre, M. D., Hammar, T. R., Smith, S. P., and Sayles, F. L. 1995. In situ measurements of seawater $p\text{CO}_2$. *Limnol. Oceanogr.*, 40: 969-975.
- DeGrandpre, M. D., Hammar, T. R., Wallace, D. W. R., and Wirick, C. D. 1997. Simultaneous mooring-based measurements of seawater CO_2 and O_2 off Cape Hatteras, North Carolina. *Limnol. Oceanogr.* 42: 21-28.
- DeGrandpre, M. D., Jenkins, W. J., and Wirick, C. D. 1996. Air-sea exchange of CO_2 , O_2 and noble gases in coastal waters. *Coastal Ocean Processes (CoOP) Newsletter* 3, 7.
- DeGrandpre, M.D., Olbu G.D., Beatty, C.M. and Hammar, T. R. 2002. Air-sea CO_2 fluxes on the U.S. Middle Atlantic Bight. *Deep-Sea Res. II*, 49: 4355-4367.
- Dettmann, E. H. 2001. Effect of water residence time on annual export and denitrification of nitrogen in estuaries: a model analysis. *Estuaries* 24: 481-490.
- Dickson, A. G. 1993. The measurement of sea water pH. *Mar. Chem.*, 44: 131-142.
- Dickson, A.G. and Millero, F.J. 1987. A comparison of the equilibrium constants for the dissociation of carbonic acid in seawater media. *Deep-Sea Res.* 36: 1733-1743.
- Edmond, J. M. and Gieskes, J. M. 1970. On the calculation of degree of saturation of seawater with respect to calcium carbonate under in situ conditions. *Geochim. Cosmochim. Acta*, 34: 1261-1291.
- Elsinger, R.J. and Moore, W. S. 1983. Gas exchange in the Pee Dee River based on ^{222}Rn evasion. *Geophys. Res. Lett.* 10:443-446.
- Eyre, B. and Twigg, C. 1997. Nutrient behavior during post-flood recovery of the Richmond River Estuary, Northern NSW, Australia. *Estuar. Coast. and Shelf Sci.* 44: 311-326.
- Falkowski, P.G., Flagg C.N., Rowe G.T., Smith S.L., Whitedge T.E., and Wirick C.D. 1988. The fate of a spring phytoplankton bloom: export or oxidation? *Continental Shelf Res.*, 8:457-484.
- Feely, R. A, Wanninkhof, R., Milburn, H. B., Cosca, C. E., Stapp, M., and Murphy, P. P. 1998. A new automated underway system for making high precision $p\text{CO}_2$ measurements onboard research ships. *Anal. Chim. Acta*, 377: 185-191.
- Frankignoulle M., Bourge I., and Wollast R. 1996a. Atmospheric CO_2 fluxes in a highly polluted estuary (the Scheldt). *Limnol. Oceanogr.*, 41(2):365-369.
- Frankignoulle, M. and Borges A.V. 2001. European continental shelf as a significant sink for atmospheric carbon dioxide. *Global Biogeochem. Cycles*. 15:569-576.

- Frankignoulle, M., Abril, G., Borges, A., Bourge, I., Canon, C., Delille, B., Libert, E., and Theate, J-M. 1998. Carbon dioxide emission from European estuaries. *Science*, 282: 434-436
- Frankignoulle, M., Bourge I., Canon C., and Dauby P. 1996b. Distribution of surface partial CO₂ pressure in the English Channel and in the Southern Bight of the North Sea. *Continental Shelf Res.* 16:381-395.
- Froelich, P. N. 1988. Kinetic control of dissolved phosphate in natural rivers and estuaries: a primer on the phosphate buffer mechanism. *Limnol. Oceanogr.*, 33: 649-668.
- Gallagher, J., Reimold, R., Linthurst, R. A., and Pfeiffer, W. J. 1980. Aerial production, mortality and mineral accumulation-export dynamics in *Spartina alterniflora* and *Juncus roemerianus* plant stands in a Georgia salt marsh. *Ecology*, 61: 303.
- Gao, H. and Zepp, R. G. 1998. Factors influencing photoreactions of dissolved organic matter in a coastal river of the southeastern United States. *Environ. Sci. Technol.*, 32: 2940-2946.
- Gattuso, J.-P., Frankignoulle M., and Wollast R. 1998. Carbon and carbonate metabolism in coastal aquatic ecosystems. *Ann. Rev. Ecol. Syst.*, 29: 405-434.
- Giurgevich, J. R. and Dunn, E. L. 1981. A comparative analysis of the CO₂ and water vapor responses of two *Spartina* species from Georgia coastal marshes. *Estuarine, Coastal and Shelf Science*, 12: 561-568.
- Giurgevich, J. R. and Dunn, E. L. 1982. Seasonal patterns of daily net photosynthesis, transpiration and net primary productivity of *Juncus roemerianus* and *Spartina alterniflora* in a Georgia salt marsh. *Oecologia*, 52: 404-410.
- Gonzalez, J. M. and Moran, M. A. 1997. Numerical dominance of a group of marine bacteria in the α -subclass of the class Proteobacteria in coastal seawater. *Appl. Environ. Microbiol.*, 63: 4237-4242.
- Goyet, C., Beauverger, C., Brunet, C., and Poisson, A. 1991. Distribution of carbon dioxide partial pressure in surface waters of the Southwest Indian Ocean. *Tellus* 43B,: 1-11.
- Goyet, C., Walt, D. R. and Brewer, P. G. 1992. Development of a fiber optic sensor for measurement of $p\text{CO}_2$ in sea water: design criteria and sea trials. *Deep-Sea Res.*, 39: 1015-1026.
- Gran, G. 1952. Determination of the equivalence point in potentiometric titrations. Part II. *Analyst*, 77:661-671.

- Griffith, P. C. and Pomeroy, L. R. 1995. Seasonal and spatial variations in pelagic community respiration on the southeastern U.S. continental shelf. *Continental Shelf Res.* 15:815-825.
- Hanson, R. B. and Robertson, C. Y. 1988. Spring recycling rates of ammonium in turbid continental shelf waters off the southeastern United States. *Continental Shelf Res.*, 8: 49-68.
- Hanson, R. B., Robertson, C. Y., Yoder, J. A., Verity, P. G., and Bishop, S. S. 1990. Nitrogen recycling in coastal waters of southeastern U.S. during summer 1986. *J. Mar. Res.*, 48: 641-660.
- Hargrave, B. T. and Phillips, G. A. 1981. Annual in situ carbon dioxide and oxygen flux across a subtidal marine sediment. *Estuar. costl Shelf Sci.*, 12: 725-737.
- Harned, H. S. and Owen, B. B. 1958. *The physical chemistry of electrolyte solutions*, ACS Monogr. Ser. No. 137, p803. Reinhold.
- Harned, H. S., Owen, B. B., 1958. *The physical chemistry of electrolyte solutions*, ACS Monogr. Ser. No. 137, p803. Reinhold.
- Hollibaugh, J. T. and Pennings, S. C. 1999. 1999 Georgia Coastal Ecosystems LTER Proposal. http://gce-lter.marsci.uga.edu/lter/project/project_desc.htm.
- Hood, E. M., Merlivat, L., and Johannessen, T. 1999. Variations of $f\text{CO}_2$ and air-sea flux of CO_2 in the Greenland Sea gyre using high-frequency time series data from CARIOCA drift buoys. *J. Geophys. Res.*, 104: 20,571-20,583.
- Hooper, A. B. and Terry, K. R. 1974. Photoinactivation of NH_4^+ oxidation in *Nitrosomonas*. *J. Bacteriology* 119: 899-906.
- Hopkinson, C. S. 1985. Shallow-water and pelagic metabolism: Evidence of heterotrophy in the near-shore Georgia Bight. *Mar. Biol.* 87: 19-32.
- Hopkinson, C. S. 1988. Patterns of organic carbon exchange between coastal ecosystems the mass balance approach in salt marsh ecosystems. In B. -O. Jansson (Ed.), *Coastal-Offshore Ecosystem Interactions*. pp. 122-154. Springer-Verlag. Berlin, Heidelberg.
- Hopkinson, C. S., Sherr, B. R., and Wiebe, W. J. 1989. Size fractionated metabolism of coastal microbial plankton. *Mar. Ecol. Prog. Ser.* 51: 155-166.
- Hoppema J. M. J. 1993. Carbon dioxide and oxygen disequilibrium in a tidal basin (Dutch Wadden Sea). *Netherlands J. Sea Res.* 31:221-229.
- Horrigan, S. G. and Springer, A. L. 1990. Oceanic and estuarine NH_4^+ oxidation: Effects of light. *Limnol. Oceanogr.* 35: 479-482.
- Howes, B. L., Dacey, J., and King, G. 1984. Carbon flow through oxygen and SO_4 reduction pathways in salt marsh sediments. *Limnol. Oceanogr.*, 29: 1037-1051.

- Imberger, J., Berman, T., Christian, R.R., Sherr, E.B., Whitney, D.E., Pomeroy, L.R., Wiegert, R.G., and Wiebe, W.J. 1983. The influence of water motion on the distribution and transport of materials in a salt marsh estuary. *Limnol. Oceanogr.* 28:201-214.
- Inoue, H., Sugimura, Y. and Fushimi, K. 1987. $p\text{CO}_2$ and $\delta^{13}\text{C}$ in the air and surface sea water in the western North Pacific. *Tellus*, 39B: 228-242.
- Jahnke, R. A., Nelson, J. R., Marinelli, R. L., and Eckman, J. E. 2000. Benthic flux of biogenic elements on the Southeastern US continental shelf: influence of pore water advective transport and benthic microalgae. *Continental Shelf Research*, 20: 109-127.
- Jahnke, R.A. 1988. A simple, reliable, inexpensive pore water sampler. *Limnol. Oceanogr.*, 33:483-487.
- Jensen, M. A. and Rechnitz, G. A., 1979. Response time characteristics of the $p\text{CO}_2$ electrode. *Anal. Chem.*, 51: 1972-1977.
- Jones, M. N. 1984. NO_3^- reduction by shaking with cadmium: An alternative to cadmium columns. *Water Res.* 18: 643-646.
- Kaltenbacher, Steimle, E. T., E. Byrne, R. H., 2000. Proceedings of the 2000 International Symposium on Underwater Technology. May 23-26, 2000. Tokyo, Japan.
- Kaul, L. W. and Froelich, P. N. 1984. Modeling estuarine nutrient geochemistry in a simple system. *Geochim. Cosmochim. Acta* 48: 1417-1433.
- Kelly C. A., Rudd, J. M., Hesslein, R. H., Schindler, D. W., Dillon, P. J., Driscoll, C. T., Gherini, S. A., and Hecky, R. E. 1987. Prediction of biological acid neutralization in acid-sensitive lakes. *Biogeochem.* 3: 129-140.
- Kemp, W. M., Smith, E., Marvin-Dipasquale, M., and Boynton, W. R. 1997. Organic carbon balance and net ecosystem metabolism in Chesapeake Bay. *Mar. Ecol. Prog. Ser.*, 150: 229-248.
- Kempe S. 1982. Long term records of CO_2 pressure fluctuations in fresh waters. In *Transport of Carbon and Minerals in Major World Rivers, Pt.1.* (Ed. Degens, E.T) Mitt. Geol.-Palaont. Inst. Univ. Hamburg, SCOPE/UNEP Sonderbd. 52, pp 91-332.
- King, D. W. and Kester, D. R. 1989. Determination of seawater pH from 1.5 to 8.5 using colorimetric indicators. *Mar. Chem.*, 26: 5-20.
- Koroleff, F. 1983. Determination of ammonia, p. 150-157. In Grasshoff, K., M. Ehrhardt, and K. Kremling [eds], *Method of seawater analysis: second, revised and extended edition.* Verlag Chemie, Weinheim.

- Körtzinger, A., Mintrop, L., Wallace, D. W. R., Johnson, K. M., Neill, C., Tilbrook, B., Towler, P., Inoue, H. Y., Ishii, M., Shaffer, G., Saavedra, R. F. T., Ohtaki, E., Yamashita, E., Poisson, A. Brunet, C., Schauer, B., Goyet, C., and Eiseid, G. 2000. The international at-sea intercomparison of $f\text{CO}_2$ systems during the R/V Meteor cruise 36/1 in the North Atlantic Ocean. *Mar. Chem.*, 72, 171-192.
- Kourafalou, V. H., Oey, L.-Y., Wang, J. D., and Lee, T. N. 1996a. The fate of river discharge on the continental shelf. 1. Modeling the river plume and inner shelf coastal current. *J. Geophys. Res. – Oceans* 101, 3415-3434.
- Kourafalou, V. H., Lee, T. N., Oey, L.-Y., and Wang, J. D. 1996b. The fate of river discharge on the continental shelf. 2. Transport of coastal low-salinity waters under realistic wind and tidal forcing. *J. Geophys. Res. – Oceans* 101, 3435-3455.
- Krest, J. M., Moore, W. S., Gardner, L. R., and Morris, J. T. 2000. Marsh nutrient export supplied by groundwater discharge: Evidence from radium measurements. *Global Biogeochem. Cycles*. 14: 167-176.
- Lee, T. N. and Atkinson, L. P. 1983. Low frequency current and temperature variability from Gulf Stream frontal eddies and atmospheric forcing along the Southeast U.S. outer continental shelf. *J. Geophys. Res.*, 88:4541-4568.
- Lee, T. N., Ho, W.-J., Kourafalou, V., and Wang, J. D. 1984. Circulation on the continental shelf of the southeastern United States, Part I – subtidal response to wind and Gulf Stream forcing during winter. *J. Phys. Oceanogr.*, 14: 1001-1012.
- Lee, T. N., Kourafalou, V., Wang, J. D., and Evans, R. 1989. Response of South Carolina continental shelf waters to wind and Gulf Stream forcing during winter of 1986. *J. Geophys. Res.*, 94: 715-754.
- Lee, T. N., Yoder J. A., and Atkinson, L. P. 1991. Gulf Stream frontal eddy influence on productivity of the Southeast U.S. continental shelf. *J. Geophys. Res.*, 96(C):22191-22205.
- Lewis, E. and Wallace, D. W. R. 1998. Program developed for CO_2 system calculations. ORNL/CDIAC-105, Carbon Dioxide Information Analysis Center, Oak Ridge National Laboratory, U.S. Department of Energy, Oak Ridge, Tennessee.
- Li, C., Nelson, J., and Koziana, J. 2002. Initial observations of penetrating shelf front in the central Georgia Bight observed with Terra MODIS SST, submitted to *Geophysical Research Letter*.
- Li, Y. H. and Chan, L. H. 1979. Desorption of Ba and ^{226}Ra from river-borne sediments in the Hudson Estuary. *Earth Planet. Sci. Lett.* 43: 343-350.
- Lide, D. R. 1994. *CRC Handbook of Chemistry and Physics (75th Edition)*, pp 8-42. CRC press.

- Lipshultz, F. L., Wofsy, S. C., and Fox, L. E. 1985. Effects of light and nutrients on the rates of NH_4^+ transformation in a eutrophic river. *Mar. Chem.* 16: 329-341.
- Liss, P. S. 1976. Conservative and non-conservative behavior of dissolved constituents during estuarine mixing, p. 93-130. In J. D. Burton and P. S. Liss [eds], *Estuarine chemistry*. Academic.
- Liss, P. S. and Merlivat, L. 1986. Air-sea gas exchange rates: Introduction and synthesis. In Buat-Menard, P. (Ed.), *The role of air-sea exchange in geochemical cycling*. NATO Advanced Studies, Reidel Publishing, pp. 113-127.
- Liss, S. M. [ed.]. 1992. *An Introduction to Marine Biogeochemistry*. New York, Wiley.
- Longhurst, A., Sathyendranath, S., Platt, T., and Caverhill, C. 1995. Assessment of global primary production in the ocean from satellite radiometer data. *J. Plankton Res.*, 17:1245-1271.
- Mackenzie, F.T. 1991. What is the importance of ocean margin processes in global change? In *Ocean Margin Processes in Global Change* (ed., R.F.C. Mantoura, J.M. Martin, and R. Wollast). Pp 433-454. John Wiley, NY.
- Mackenzie, F.T., Ver L.M., and Lerman A. 2000. Coastal-zone biogeochemical dynamics under global warming. *Int. Geol. Rev.* 42:193-206.
- Mantoura, R.F.C., Martin, J-M., and Wollast, R. (eds). 1991. *Ocean margin processes in global change*. 469 pp. Chichester, UK: Wiley & Sons.
- Mehrbach, C., Culerson, C. H., Hawley, J. E., and Pytkowicz, R. M. 1973. Measurement of the apparent dissociation constants of carbonic acid in seawater at atmospheric pressure. *Limnol. Oceanogr.* 18, 897-907.
- Menzel, D. W. (ed.) 1993. *Ocean Processes: U.S. Southeast Continental Shelf*. U.S. Dept. of Energy, Report DOEIOSTI 11674.
- Merlivat, L. and Brault, P. 1995. CARIOCA buoy: carbon dioxide monitor. *Sea Technol.* 10, 23-30.
- Miller, W. L. and Moran, M. A. 1997. Interaction of photochemical and microbial processes in the degradation of refractory dissolved organic matter from a coastal marine environment. *Limnol. Oceanogr.*, 42: 1317-1324.
- Millero, F. J. 1995. Thermodynamics of the carbon dioxide system in the oceans. *Geochim. Cosmochim. Acta*, 59, 661-677.
- Mook, W. G. and Koene, B. K. S. 1975. Chemistry of dissolved inorganic carbon in estuarine and coastal brackish waters. *Estuar. Coastal Mar. Sci.* 3, 325-336.

- Moore, W. S. 1999. The subterranean estuary: a reaction zone of ground water and sea water. *Mar. Chem.*, 65: 111-125.
- Moran, M. A., Sheldon, W. M., and Sheldon, J. E. 1999. Biodegradation of riverine dissolved organic carbon in five estuaries of the southeastern United States. *Estuaries*, 22: 55-64.
- Moran, M.A., Pomeroy, L.R., Sheppard, E.S., Atkinson, L. P. and Hodson, R.E. 1991. Distribution of terrestrially derived dissolved organic matter on the Southeastern U.S. Continental Shelf. *Limnol. Oceanogr.* 36: 1134-1149.
- Morris, J. T. and Whiting, G. J. 1986. Emission of gaseous carbon dioxide from salt-marsh sediments and its relation to other carbon losses. *Estuaries*, 9: 9-19.
- Mulholland, P. J. and Olsen, C. R. 1992. Marine origin of Savannah river estuary sediments: Evidence from radioactive and stable isotope tracers. *Estuar. Coast. Shelf Sci.* 34: 95-107.
- Münchow, A. and Garvine, R. W. 1993. Dynamical properties of a buoyancy-driven coastal current. *J. Geophys. Res.*, 98: 20063-20077.
- Nelson, J. R., Eckman, J. E., Robertson, C. Y., Marinelli, R. L., and Jahnke, R. A. 1999. Variability in biomasses of benthic and planktonic microalgae on the continental shelf on the South Atlantic Bight. *Continental Shelf Research* 19, 477-505.
- Nixon, S. W. 1980. Between coastal marshes and coastal waters – a review of twenty years of speculation and research on the role of salt marshes in estuarine productivity and water chemistry. *In* Hamilton, P. and K. B. MacDonald [ed.], *Estuarine and Wetland Processes*. Plenum Press, New York, p. 437-525.
- Nixon, S. W., Ammerman, J. W., Atkinson, L. P., Berounsky, V. M., Billen, G., Boicourt, W. C., Boynton, W. R., Church, T. M., Ditoro, D. M., Elmgren, R., Garber, J. H., Giblin, A. E., Jahnke, R. A., Owens, N. J. P., Pilson, M. E. Q., and Seitzinger, S. P. 1996. The fate of nitrogen and phosphorus at the land-sea margin of the North Atlantic Ocean. *Biogeochem.* 35: 141-180.
- Odum, E. P. 1968. A research challenge: Evaluating the productivity of coastal and estuarine water, p. 63-64. *In* Proceedings Second Sea Grant Conference, Univ. Rhode Island.
- Odum, E. P. 1980. The status of three ecosystem-level hypotheses regarding salt-marsh estuaries: tidal subsidy, outwelling, and detritus-based food chains. *In* V. S. Kennedy [ed.], *Estuarine Perspectives*. Academic.
- Odum, E. P. 2000. Tidal marshes as outwelling/pulsing systems. *In* Weinstein, M. P. and Kreeger, D. A. (eds), *Concepts and Controversies in Tidal Marsh Ecology*. Kluwer Academic, 2000, pp3-7.

- Odum, W. E., Odum, E. P. and Odum, H. T. 1995. Nature's pulsing paradigm. *Estuaries*, 18: 547-555.
- Officer, C. B. 1979. Discussion of the behavior of the nonconservative dissolved constituents in estuaries. *Estuar. Coast. Mar. Sci.* 9: 911-914.
- Otero, E., Culp, R., Noakes, J. E., and Hodson, R. E. 2000. Allocation of particulate organic carbon from different sources in two contrasting estuaries of southeastern USA. *Limnol. Oceanogr.* 45: 1753-1763.
- Owens, N. P. J. 1986. Estuarine nitrification: a naturally occurring fluidized bed reaction. *Estuar., Coast. and Shelf Sci.* 22: 31-44.
- Paffenhofer, G.-A., Atkinson, L. P., Lee, T. N., Blanton, J. O., Sherman, B. K., and Stewart, T. B. 1994. Variability of particulate matter and abundant zooplankton off the southeastern United States during spring of 1984 and 1985. *Continental Shelf Res.*, 14: 629-654.
- Pakulski, J. D., Benner, R., Amon, R., Eadie, B., and Whitley, T. 1995. Community metabolism and nutrient cycling in the Mississippi river plume – evidence for intense nitrification at intermediate salinities. *Mar. Ecol. Prog. Ser.* 117: 207-218.
- Pakulski, J. D., Benner, R., Whitley, T., Amon, R., Eadie, B., Cifuentes, L., Ammerman, J., and Stockwell, D. 2000. Microbial metabolism and nutrient cycling in the Mississippi and Atchafalaya River Plumes.
- Pamatmat, M. M. 1997. Non-photosynthetic oxygen production and non-respiratory oxygen uptake in the dark: a theory of oxygen dynamics in plankton communities. *Mar. Bio.*, 129: 735-746.
- Perez, F. F., Rios, A. F., and Roson, G. 1999. Sea surface carbon dioxide off the Iberian Peninsula (North Eastern Atlantic Ocean). *J. Mar. Syst.*, 19: 27-46.
- Pernetta, J. C. and Milliman, J. D. (eds). 1995. Land-ocean interactions in the coastal zone. Implementation plan. IGBP Rep. 33:1-215.
- Plath, C. C., Johnson, K. S., and Pytkowicz, R. M. 1980. The solubility of calcite – probably containing magnesium – in seawater. *Mar. Chem.* 10, 9-29.
- Pomeroy L.R. and Wiegert R.G. [eds]. 1981. *The ecology of a salt marsh*. Springer-Verlag.
- Pomeroy, L. R., Atkinson, L. P., Blanton, J. O., Campbell, W. B., Jacobsen, T. R., Kerrick, K. H., and Wood, A. M. 1983. Microbial distribution and abundance in response to physical and biological processes on the continental shelf of southeastern U. S. A. *Continental Shelf Res.*, 2: 1-20.

- Pomeroy, L. R., Darley, W. M., Dunn, E. L., Gallagher, J. L., Haines, E. B., and Whitney, D. M. 1981. Primary production. In L. R. Pomeroy and R. G. Wiegert [eds], *The ecology of a salt marsh*. Springer-Verlag.
- Pomeroy, L. R., Sheldon, J. E., and Sheldon, W. M. Jr. 1994. Changes in bacterial numbers and leucine assimilation during estimations of microbial respiratory rates in seawater by the precision Winkler method. *Appl. Environ. Microbiol.*, 60: 328-332.
- Pomeroy, L. R., Sheldon, J. E., Sheldon, W. M., Blanton, J. O. Jr., Amft, J., and Peters, F. 2000. Seasonal changes in microbial processes in estuarine and continental shelf waters of the South-eastern U.S.A. *Estuarine, Coastal and Shelf Science*, 51, 415-428.
- Pomeroy, L. R., Sheldon, W. M. Jr., and Peters, F. 1995. Limits to growth and respiration of bacterioplankton in the Gulf of Mexico. *Mar. Ecol. Prog. Ser.*, 117: 259-268.
- Pomeroy, L. R., Shenton, L. R., Jones, R. D. H., and Reimold, R. J. 1972. Nutrient flux in estuaries. In *Nutrient and Eutrophication, Special Symposia, Vol. 1*, Amer. Soc. Limnol and Oceanogr.
- Ragotzkie, R. A. and Bryson, R. A. 1955. Hydrography of the Duplin River, Sapelo Island, Georgia. *Bulletin of Marine Science*, 5: 297-314.
- Ragotzkie, R. A. and Pomeroy, L. R. 1957. Life history of a dinoflagellate bloom. *Limnol. Oceanogr.* 2: 62-69.
- Raymond, P. A., Bauer J. E., and Cole, J. J. 2000. Atmospheric CO₂ evasion, dissolved inorganic carbon production, and net heterotrophy in the York River estuary. *Limnol. Oceanogr.*, 45: 1707-1717.
- Raymond, P. A., Caraco, N. F., and Cole, J. J. 1997. Carbon dioxide concentration and atmospheric flux in the Hudson River. *Estuaries*, 20: 381-390.
- Reimers, C.E., Jahnke, R.A., and McCorkle, D.C. 1992. Carbon fluxes and burial rates over the continental slope and rise off central California with implications for the global carbon cycle. *Global Biogeochem. Cycles*, 6:199-224.
- Reimold, R. J. 1977. Mangals and salt marshes of eastern United States. In Chapman, V. J. [ed], *Wet coastal ecosystems*. Elsevier. p157 – 166.
- Robert-Baldo, G. L., Morris, M. J., and Byrne, R. H. 1985. Spectrophotometric determination of seawater pH using phenol red. *Anal. Chem.*, 57: 2564-2567.
- Robertson, J. E. and Watson, A. J. 1992. Thermal skin effect of the surface ocean and its implications for CO₂ uptake. *Nature*, 358, 734-740.
- Rowe, G.T., Theroux, R., Phoel W., Quinby H., Wilke R., Koschoreck D., Whitledge T.E., Falkowski P.G., and Fray C. 1988. Bnetic carbon budgets for the continental shelf south of New England. *Contin. Shelf. Res.* 8:511:527.

- Sabine, C. L. and Key, R. M. 1998. Controls on $f\text{CO}_2$ in the South Pacific. *Mar. Chem.* 60:960-110.
- Saito, H., Tamura, N., Kitano, H., Mito, A., Takahashi, C., Suzuki, A., and Kayanne, H. 1995. A compact seawater $p\text{CO}_2$ measurement system with membrane equilibrator and nondispersive infrared gas analyzer. *Deep-Sea Res.*, 42: 2025-2033.
- Sarmiento, J. L. and Gruber, N. 2002. Sinks for anthropogenic carbon. *Physics Today*, 55: 30-36.
- Sarmiento, J. L. and Sundquist, E. T. 1992. Revised budget for the oceanic uptake of anthropogenic carbon dioxide. *Nature*, 356: 589-593.
- Sarmiento, J. L., Monfray, P., Reimer, E. M., Aumont, O., and Murnane, R. J. 2000. Sea-air CO_2 fluxes and carbon transport: a comparison of three ocean general circulation models.
- Sarmiento, J.L. 1993. Ocean carbon cycle. *Chem. Engineering News*. May 31, 1993, pp.31-43.
- Schluessel, P., Emerry, W. J., Grasil, H., and Mammen, T. 1990. On the bulk-skin temperature difference and its impact on satellite remote sensing of sea surface temperature. *J. Geophys. Res.* 95, 13,341-13,356.
- Shi, W., Sun M., Molina M, and Hodson B. 2001. Variability in the distribution of lipids biomarkers and their molecular isotopic composition in Altamaha estuarine sediments: implications for the relative contribution of organic matter from various sources. *Organic Geochem.* 32:453-467.
- Skirrow, G. 1975. The dissolved gases: carbon dioxide. In J. P. Riley and G. Skirrow (editors), *Chemical Oceanography*, vol. 2, pp 1-192. Academic Press.
- Smith, S. V. and Hollibaugh, J. T. 1993. Coastal metabolism and the oceanic organic carbon balance. *Rev. Geophys.* 31:75-89.
- Smith, K. L. Jr., Baldwin, R. J., and Williams, P. M. 1992. Reconciling particulate organic carbon flux and sediment community oxygen consumption in the deep North Pacific. *Nature*, 359:313-316.
- Smith, S. V. and Hollibaugh, J. T. 1997. Annual cycle and interannual variability of ecosystem metabolism in a temperate climate embayment. *Ecol. Monogr.*, 67: 509-533.
- Smith, S. V., Hollibaugh, J. T., Dollar, S. J., and Vink, S. 1991. Tomales Bay metabolism: C-N-P stoichiometry and ecosystem heterotrophy at the land-sea interface. *Estuarine, Coastal and Shelf Sciences*, 33:223-257.

- Steimle, E. T., Kaltenbacher, E. A., Byrne, R. H., 2002. In situ nitrite measurements using a compact spectrophotometric analysis system. *Mar. Chem.*, 77: 255-262.
- Stephens, M., Samuels, G., Olson, D., and Fine, R. 1995. Sea-air flux of CO₂ in the North Pacific using shipboard and satellite data. *J. Geophys. Res.* 100, 13571-13583.
- Tabacco, M. B., Uttamlal, M., McAllister, M., and Walt, D. R. 1999. An autonomous sensor and telemetry system for low-level pCO₂ measurements in seawater. *Anal. Chem.*, 71: 154-161.
- Takahashi, T., Olafsson, J., Goddard, J. G., Chipman, D. W., and Sutherland, S. C. 1993. Seasonal variation of CO₂ and nutrients in the high-latitude surface oceans: a comparative study. *Global Biogeochemical Cycles*, 7: 843-878.
- Tans, P. P., Fung, I. Y., and Takahashi, T. 1990. Observational constraints on the global atmospheric CO₂ budget. *Science*, 247: 1431-1438.
- Tapp, M., Hunter, K., Currie, K., and Mackaskill, B. 2000. Apparatus for continuous-flow underway spectrophotometric measurement of surface water pH. *Mar. Chem.*, 72, 193-202.
- Teal, J. M. 1962. Energy flows in the salt marsh ecosystem of Georgia. *Ecology* 43: 614-624.
- Ternon, J. F., Oudot, C., Dessier, A., and Diverres, D. 2000. A seasonal tropical sink for atmospheric CO₂ in the Atlantic ocean: the role of the Amazon River discharge. *Mar. Chem.* 68, 183-201.
- Thomas, H. and Schneider B. 1999. The seasonal cycle of carbon dioxide in Baltic Sea waters. *J. Mar. Syst.* 22:53-67.
- Tsunogai, S., Watanabe, S., and Sato, T. 1999. Is there a “continental shelf pump” for the absorption of atmospheric CO₂? *Tellus*, 51B:701-712.
- Tsunogai, S., Watanabe, S., Nakamura, J., Ono, T., and Sato, T. 1997. A preliminary study of carbon system in the East China Sea. *J. Oceanogr.*, 53: 9-17.
- Van Green, A., Takesue R.K., Goddard, J., Takahashi, T., Barth, J. A. and Smith R. L. 2000. Carbon and nutrient dynamics during coastal upwelling off Cape Blanco, Oregon. *Deep-Sea Res. II.* 47:975-1002.
- Verhagen, F. J. M. and Laanbroek, H. J. 1991. Competition for NH₄⁺ between nitrifying and heterotrophic bacteria in dual energy-limiting chemostats. *Applied and Environ. Microbio.* 57: 3255-3263.
- Verity, P. G., Yoder, J. A., Bishop, S. S., Nelson, J. R., Carven, D. B., Blanton, J. O., Robertson, C. Y., and Tronzo, C. R. 1993. Composition, productivity and nutrient

- chemistry of a coastal ocean planktonic food web. *Continental Shelf Research*, 13: 741-776.
- Walsh, J. J. (ed) 1988. On the nature of continental shelves. Academic Press, San Diego, CA (USA), 528 pp.
- Walsh, J. J. 1981. Biological export of shelf carbon is a sink of the global CO₂ cycle. *Nature*, 291: 196-201.
- Walsh, J. J. 1991. Importance of continental margins in the marine biological cycling of carbon and nitrogen. *Nature*, 350: 53-55.
- Walt, D. R., Gabor, G., and Goyet, C. 1993. Multiple-indicator fiber-optic sensor for high-resolution *p*CO₂ seawater measurements. *Anal. Chim. Acta*, 274: 47-52.
- Wang S.-L., Chen, C.-T.A., Hong, G.-H., and Chung, C.-S. 2000. Carbon dioxide and related parameters in the East China Sea. *Continental Shelf Res.*, 20:525-544.
- Wang, Z. A., Wang, Y. C., Cai, W.-J., and Liu, S. Y. 2002a. A long pathlength spectrophotometric *p*CO₂ sensor using a gas-permeable liquid-core waveguide. *Talanta*, 57: 69-80.
- Wang, Z. A., Wang, Y. C., Cai, W.-J., and Upchurch, B. 2002b. A Long Pathlength Liquid-Core Waveguide Sensor for real-time *p*CO₂ measurements at sea. Submitted to *Marine Chemistry*.
- Wanninkhof, R. 1992. Relationship between wind speed and gas exchange over the ocean. *J. Geophys. Res.*, 97: 7373-7382.
- Wanninkhof, R. and Thoning, K. 1993. Measurement of fugacity of CO₂ in surface water using continuous and discrete sampling methods. *Mar. Chem.*, 44: 189-204.
- Ward, B. B. 1985. Light and substrate concentration relationships with marine NH₄⁺ assimilation and oxidation rates. *Mar. Chem.* 16: 301-316.
- Waterbury, R. D., Yao, W., and Byrne, R. H. 1997. Long pathlength absorbance spectroscopy: trace analysis of Fe (II) using a 4.5 m liquid core waveguide. *Anal. Chim. Acta*, 357: 99-102.
- Weiss, R. F. 1974. Carbon dioxide in water and seawater: the solubility of a non-ideal gas. *Mar. Chem.*, 2: 203-215.
- Wiegert, R. G., Alber, M., Alexander, C., Blanton, J., Chalmers, A., Hodson, R., Moran, M. A., Pomeroy, L., and Wiebe, W. 1999. The Georgia Rivers LMER Program: A comparative study of five coastal rivers. *Limnologica*, 29: 286-292.

- Wiegert, R. G., Chalmers, A. G., and Randerson, P. F. 1983. Productivity gradients in salt marshes: the responses of *Spartina alterniflora* to experimentally manipulated soil water movement. *Oikos*, 43: 1-6.
- Wiegert, R. G., Christian, R. R., and Wetzel, R. L. 1981. A model view of the marsh, p. 183-218. In L. R. Pomeroy and R. G. Wiegert [eds], *The ecology of a salt marsh*. Springer.
- Williams, P. J. LeB. and Robertson, J. E. 1991. Overall planktonic oxygen and carbon dioxide metabolism: the problem of reconciling observations and calculations of photosynthetic quotients. *J. Plankton Res.*, 13 (suppl.): 153-169.
- Windom, H. L., Dunstan, W. M., and Gardner, W. S. 1975. River input of inorganic phosphorous and nitrogen to the southeastern salt marsh estuarine environment. p. 309-311. In F. G. Howell, J. B. Gentry, and M. H. Smith [eds]. *Mineral cycling in southeaster ecosystems*. (CONF-740513) ERDA Symposium Series.
- Winter, P. E. D., Schlacher, T. A., and Baird, D. 1996. Carbon flux between estuary and the ocean: a case for outwelling. *Hydrobiologia*, 337: 123-132.
- Wollast, R. 1993. Interactions of carbon and nitrogen cycles in the coast zone, in *Interactions of C, N, P, and S Biogeochemical Cycles and Global Change* (ed. Wollast R, F.T. Mackenzie, and L. Chou). NATO ASI Series, Vol. 14, Springer-Verlag Berlin Heidelberg.
- Yao, W. and Byrne, R. H. 1999. Determination of trace chromium (VI) and molybdenum (VI) in natural and bottled mineral waters using long pathlength absorbance spectroscopy (LPAS). *Talanta*, 48: 277-282.
- Yoder, J. A., Atkinson, L. P., Bishop, S. S., Blanton J. O., Lee T. N., and Pietrafesa L. J. 1985. Phytoplankton dynamics within Gulf Stream intrusion on the southeastern United States continental shelf. *Cont. Shelf. Res.* 4:611-635.
- Yool, A. and Fasham J.R. 2001. An examination of the "continental shelf pump" in an open ocean general circulation model. *Global Biogeochem. Cycles*, 15:831-844.
- Zhang, J. Z., 2000. Shipboard automated determination of trace concentrations of nitrite and nitrate in oligotrophic water by gas-segmented continuous flow analysis with a liquid waveguide capillary flow cell. *Deep-sea Res. I*, 47: 1157-1171.
- Zhao, P. and Cai, W. J. 1997. An improved potentiometric $p\text{CO}_2$ microelectrode. *Anal. Chem.*, 69: 5052-5058.
- Zuev, B. K., Chudinova, V. V., Kovalenko, V. V., and Yagov, V. V. 2001. The conditions of formation of the chemical composition of the sea surface microlayer and techniques for studying organic matter in it. *Geochem. International*, 39, 702-710.